2021

JPSS

SCIENCE SEMINAR ANNUAL DIGEST

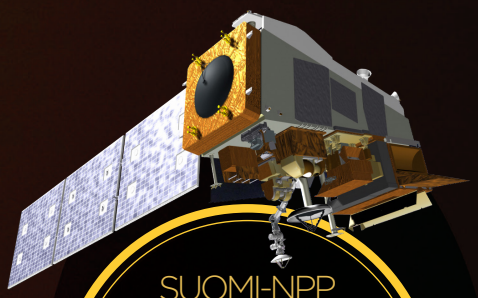

SUOMI-NPP 10 YEAR ANNIVERSARY

ARTICLES + FEATURES

from the new generation polar-orbiting operational environmental satellite system

2021

JPSS SCIENCE SEMINAR ANNUAL DIGEST

CONTENTS

FEATURED ARTICLES

WEB FEATURES

2021 JPSS Science Seminar Annual Digest Contributors

Program Director: Greg Mandt

Program Scientist: Dr. Satya Kalluri

Science Writers: Julie Price[1], ASRC Federal Space and Defense (AS&D) contractor to NESDIS (feature stories), Jenny Marder, Telophase Corporation contractor to JPSS (news articles and highlights)

Editors: Bill Sjoberg, Global Science and Technology (GST), Inc. contractor to JPSS, Julie Price (AS&D)

Graphic Designer: Joshua Brady, GAMA-1 Technologies contractor to JPSS

Strategic Communications and STEM Engagement: Michelle Birdsall, ASRC Federal System Solutions contractor to JPSS

We wish to acknowledge the contributions of all the JPSS seminar speakers. We thank the following contributors and advisers for generously sharing: their research and associated materials, valuable comments and feedback, as well as their time from busy schedules and other commitments.

Dr. Anthony Wimmers, *Cooperative Institute for Meteorological Satellite Studies (CIMSS), University of Wisconsin-Madison*

Dr. Greg Frost, N*OAA/Chemical Sciences Laboratory*

Dr. Hun Meng, *NOAA/NESDIS Center for Satellite Applications and Research (STAR)*

Eric Stevens, *Alaska Interagency Coordination Center (AICC)*

Dr. Alex Gilerson, *NOAA Center for Earth System Sciences and Remote Sensing Technologies (CESSRST), City College New York (CCNY)*

Dr. Huilin Gao, *Texas A&M University*

Dr. Curtis Seaman, *Cooperative Institute for Research in the Atmosphere (CIRA), Colorado State University*

Dr. Pingping Xie, *NOAA Climate Prediction Center (CPC)*

Dr. Lawrence Flynn, *NOAA/NESDIS Center for Satellite Applications and Research (STAR)*

Dr. Cheng-Zhi Zou, *NOAA/NESDIS Center for Satellite Applications and Research (STAR)*

[1]Formerly Science and Technology (STC) contractor to JPSS.

FROM THE PROGRAM DIRECTOR

It is with many mixed emotions that I write this year's Science Digest message. On December 31, 2021, I will retire after 47 years of Federal service. I was in the U.S. Air Force for 18 years, many of those years in the Defense Meteorological Satellite Program. I then spent 29 years with NOAA, 10 years with the National Weather Service, and 19 years with NESDIS. You could say that weather satellites have been in my blood. During these years, I have had the honor of leading both of our nation's premier satellite programs, as well as being part of the user community that leveraged these geostationary and low-Earth orbiting satellite data and products to help save lives and property. I could not be more proud of the work done by the satellite developers, our NOAA corporate partners, and our national and international stakeholders. The success of these satellite programs is a direct result of their extensive collaboration. Let me summarize, for one last time, the impact and importance of the JPSS Program.

In 2021, JPSS continued to rise to challenges and provide life-saving data and valuable products to users in a year marked by significant tornadoes, hurricanes, droughts, floods, fires, and record heat waves. As the COVID-19 pandemic affected a second year, the communication and work structure we put in place in 2020 helped JPSS persevere and continue its outstanding service to its user community. In October 2021, the Suomi National Polar-orbiting Partnership (Suomi NPP) celebrated its 10th year of operations, and a month later NOAA-20 completed its fourth year in orbit. While the JPSS Program and its partners have kept these satellites operating smoothly, they also prepared for the launch of JPSS-2 (NOAA-21) planned for September 30, 2022. Our JPSS-3 and -4 hardware is progressing well, with launch readiness expected for 2027 and 2032. This year, we have also taken the initial steps in LEO planning to adapt to "new space" with a much larger commercial component. As we begin working on new approaches for future missions, we have initiated a small sat microwave sounding mission with a three-year development timeline.

As we move forward, JPSS continues to emphasize global collaboration. The program maintains important relationships with international partners, such as the European Organisation for the Exploitation of Meteorological Satellites (EUMETSAT) and the Japan Aerospace Exploration Agency (JAXA), which enable the international satellite community to leverage existing and planned capabilities from other research and operational satellite programs to deliver more capabilities to their service areas and stakeholders. Advances in the future of our LEO satellite constellation and our international partnerships expand the capabilities of our data and modeling, which are vitally important for ongoing weather prediction and environmental monitoring as we experience and prepare for extreme weather patterns.

Every day seemed to bring another news headline highlighting the need for these critical partnerships. The Western United States suffered another record fire season, damaging wide areas of virgin forests, cities and towns, and producing a saddening loss of life. Once again our GOES and JPSS satellites teamed together to help identify the early stages of these wildfires and their growth and eventual demise. The use of fire radiative power products in the NOAA smoke models helped prepare first responders on the fire lines as well as the populace hundreds of miles away for the impact of the smoke and its hazardous components. The 2021 Hurricane Season produced 21 named storms, including seven hurricanes (winds of 74 mph or greater) of which four were major hurricanes (winds of 111 mph or greater). "NOAA provided the science and services necessary to protect life and property before, during and after storms all season long," said NOAA Administrator,

Rick Spinrad, Ph.D. “From essential observations to advanced warnings to critical response actions, NOAA supports communities so they are ready, responsive and resilient to the impact of tropical cyclones each and every hurricane season.” The JPSS program can take great pride in doing its part helping in the response to these storms. These are just a few examples of the daily impact our JPSS program has had in helping NOAA meet its operational missions in 2021.

Looking back on my time as the JPSS Program Director, I want to provide some additional highlights. We have accomplished so much together, across all aspects. We celebrated a successful JPSS-1 launch. We transitioned level 1 of our operational data processing ground system to cloud computing, a first for NOAA. We integrated next generation EUMETSAT operations into ground data relay from McMurdo and integrated next generation GCOM operations into ground data relay from Svalbard. We prepared for the future, leading NESDIS LEO strategic planning.

It is always difficult to leave a wonderful organization. Thank you to the many contributors to this Science Digest, and to our JPSS science team and community for their outstanding contributions to the program. This Science Digest joins the other Digests dating back to 2014 in documenting the successful research and operational applications of our JPSS capabilities. Thank you to Satya Kalluri, JPSS program scientist, for his leadership. JPSS is producing well and will continue to do so.

It has been my honor serving JPSS these last five years. I look forward to seeing what comes next for JPSS and future LEO satellite constellations.

Greg Mandt
Joint Polar Satellite System (JPSS)
Satellite and Information Services
National Oceanic and Atmospheric Administration (NOAA)
U.S. Department of Commerce

FROM THE SENIOR PROGRAM SCIENTIST

October 28, 2021 marked the successful 10th anniversary of the Suomi NPP (SNPP) satellite, a critical risk reduction and preparatory mission for the Joint Polar Satellite System (JPSS). SNPP carried the new generation Earth-observing sensors that are significantly more advanced and capable than their predecessors onboard NOAA's Polar Orbiting Environmental Satellites (POES). The Visible Infrared Imaging Radiometer Suite (VIIRS), the Cross-track Infrared Sounder (CrIS), the Advanced Technology Microwave Sounder (ATMS), the Ozone Mapping and Profiler Suite (OMPS), and the Earth's Radiant Energy System (CERES), observe a large part of the electromagnetic spectrum from the UV region to the microwave region. These measurements are critical to understanding the Earth and its atmosphere for not only meteorological applications but also for creating climate records.

A critical part of the JPSS mission is to work closely with the end users to enable full use and exploitation of the data to maximize the benefits of the mission to NOAA, our nation and society. The Proving Ground and Risk Reduction (PGRR) activities are an integral part of this mission. They are enabled through periodic call-for-proposals (CFPs), where the program competitively selects proposals from NOAA line offices and the cooperative institutes that have enabled infusion of JPSS data and products into applications, models and decision aids to support NOAA service areas. Since its inception in 2012 after SNPP became operational, the JPSS PGRR program has funded nearly 200 proposals and can claim several successes in promoting new applications into operation. This includes the VIIRS fire radiative power (FRP) product in National Weather Service's (NWS's) AWIPS system and the FRP as initial conditions in the High-Resolution Rapid Refresh (HRRR) Smoke Model. Collaborative work between developers and NWS River Forecast Centers led to the creation of satellite flood products that are used around the world including via the international disaster charter. As applications of the VIIRS unique day-night band (DNB) capability continue to diversify, its utility has exploded. VIIRS is used in the northern latitudes during winter months, and it has become a staple of FEMA for tracking power outages and recovery in remote areas due to damage from land-falling hurricanes. VIIRS Neural Network retrievals of harmful algal blooms (HABs) has progressed from research toward practical operations. Better knowledge of HABs can lead to the identification of areas that might grow out of control, producing toxic or harmful effects on people, fish, shellfish, marine mammals, and birds, which has a huge impact on local economies.

In addition to guiding PGRR activities, the CFPs help the JPSS Program communicate to its stakeholders and the scientific and operational communities the current areas of satellite emphasis. The latest CFP was in 2021 and covered 13 initiatives in ocean, land, atmosphere, and NWP applications as well as training. It produced 94 proposals, from which an independent panel of 63 experts selected 44 proposals for funding. The recipients of these awards will be working on a variety of JPSS applications over the next three years so that we continue to innovate.

In 2021, we experienced several significant events including tornadoes, hurricanes, droughts, floods and fires. While the western US was reeling from one of the worst droughts and fires in recent years, a heat dome engulfed the Pacific northwest, causing a record heat wave. JPSS sensors provided vital information to forecasters around the world to enable early warning and to track these events as they evolved. At the end of October 2021, atmospheric rivers, which are bands of atmospheric moisture that travel across the Pacific Ocean toward North America brought record precipitation over parts of California, Oregon and Washington state. The article by Tony Wimmers in this year's digest describes very nicely how microwave soundings from sensors such as ATMS are used to measure

Total Precipitable Water (TPW) in the atmosphere, a key ingredient of atmospheric rivers. ATMS radiances are also vital for estimation of Snow Fall Rate (SFR), and the NOAA Climate Prediction Center's Morphing technique, which combines infrared measurements from geostationary satellites and microwave data from polar satellites to provide global precipitation estimation. The articles by Huan Meng and Pingping Xie describe these applications of microwave soundings in precipitation.

Profiles of temperature in the troposphere, stratosphere and temperature of deep atmospheric layers are among Essential Climate Variables in the upper atmosphere. Observations from the satellite microwave sounders, especially AMSU and ATMS onboard NOAA, NASA, and EUMETSAT satellites provide global atmospheric temperature observations for long-term climate change monitoring. Temperature time series developed from such observations have been extensively used in global warming investigations as well as for verifying climate model simulations of climate change in the past, providing confidence in using climate models to project future climate change. As our concern for climate change grows, these satellite measurements are becoming increasingly important and relevant. The article by Cheng-Zhi Zou describes how the microwave soundings help reconstruct the temperature record.

The applications of VIIRS are numerous and the benefits are enormous since it covers a large range of the electromagnetic spectrum from visible to thermal infrared including the unique Day-Night band that is sensitive to faint light signals at night. It provides not only true-color images similar to what we see with our naked eye, but also science data that has applications in ocean, land and atmosphere remote sensing of quantitative variables such as ocean chlorophyll concentration, and measurements of fire radiative power. The articles by Curtis Seaman, Eric Stevens, Alex Gilerson and Huilin Gao highlight the use of VIIRS for meteorology, fire detection, ocean color and hydrology respectively.

The air we breathe has several trace gases, chemicals and aerosols that are affected by a variety of natural, as well as anthropogenic factors, such as emissions from wildfires, volcanic eruptions, combustion of fossil fuels and dust blowing from the deserts. Manmade chemicals are also known to destroy the ozone in the upper atmosphere, the "ozone layer," where it is beneficial in blocking harmful ultraviolet radiation. The articles by Greg Frost and Larry Flynn highlight how measurements by CrIS and OMPS contribute to our understanding of atmospheric chemistry.

We also held two highly successful workshops around microwave and infrared sounding in low-Earth orbiting satellites from sensors such as ATMS and CrIS. These workshops were intended to not only convey how data from sounders are used, but also to solicit feedback from users on what improvements they would like to see in future generations of sensors. As NESDIS plans to manage these backbone observations in an enterprise way, these workshops are vital to hear from the community. We heard a strong reaffirmation about the significant impacts of JPSS sensors on climate, weather, Earth system modeling and other vital applications. About 150 people attended each workshop including users from numerical weather prediction centers, forecasters, scientists, and engineers who make these sensors.

2021 marks my second year as the JPSS program scientist and I am grateful to all the scientists, users and my staff who continue to expand and extend the uses of JPSS data in ways that were never imagined. With the planned launch of the JPSS-2 satellite in 2022, we expect to have an unprecedented amount of global observations with the new, and current satellite constellation. I am excited about the future of the program!

Warm regards,
Satya Kalluri

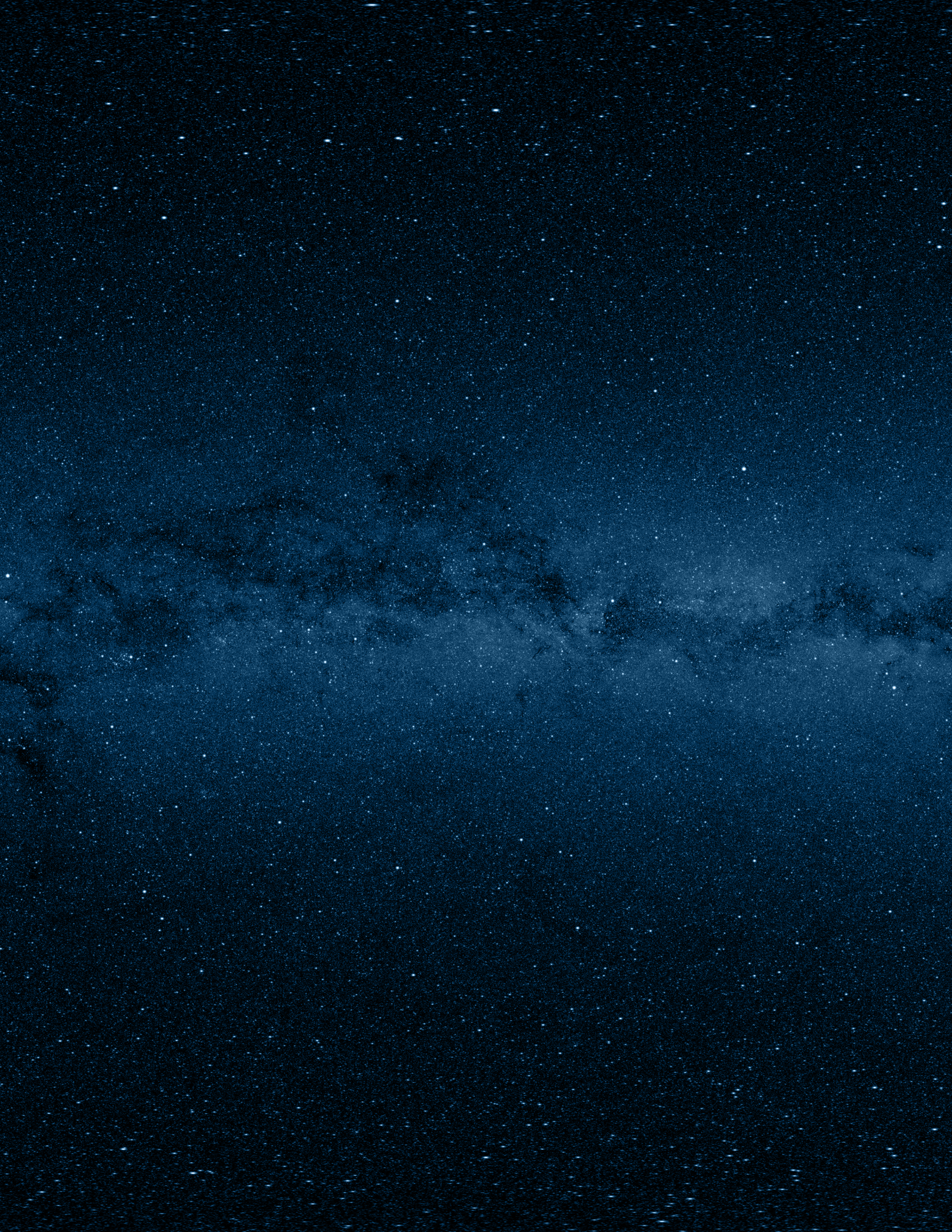

FEATURED ARTICLES

THE ADVANTAGES OF MERGED JPSS OBSERVATIONS:

MID-LATITUDE AND TROPICAL WEATHER APPLICATIONS

The information in this article is based, in part, on the October 19, 2020, JPSS science seminar presented by Anthony Wimmers, Cooperative Institute for Meteorological Satellite Studies (CIMSS), University of Wisconsin-Madison. With contributions from Derrick Herndon, CIMSS; John Forsythe, Cooperative Institute for Research in the Atmosphere, Colorado State University; and Josh Cossuth, Office of Naval Research.

Photo by John Fowler on Unsplash (https://unsplash.com/?utm_source=unsplash&utm_medium=referral&utm_content=creditCopyText)

The atmosphere contains a substantial amount of moisture that circulates around the globe in various forms including water vapor, liquid water, and ice. The moisture in the atmosphere is a principal agent in weather systems. It is the fuel for many precipitation-related weather events, which are especially important for meteorologists.

Gaseous water, or water vapor is a long-lived tracer, which usually stays in the atmosphere for at least 12 hours—just enough time to be observed by polar-orbiting satellites, which view most locations on Earth twice a day; once in daylight and once at night—except for the poles which receive frequent coverage. Global vertical profiles of water vapor can be derived from several satellite instruments including microwave sounders on polar-orbiting satellites, for example the Advanced Technology Microwave Sounder (ATMS) on the NOAA-20 and Suomi National Polar-orbiting Partnership (Suomi NPP) satellites.

"The longevity of water vapor and observational capability of polar-orbiting satellites offer the means and opportunity for optimal sampling frequency to do image morphing," said Dr. Anthony Wimmers, an Associate Scientist at Cooperative Institute for Meteorological Satellite Studies (CIMSS) at the University of Wisconsin-Madison.

On October 19, 2020, Dr. Wimmers presented a talk about the use of blended observations from various sensors/satellites in weather forecast applications of midlatitude and tropical weather. His talk focused on the Morphed, Integrated Microwave Imagery at CIMSS—Total Precipitable Water (MIMIC-TPW), which is a technique that creates near-seamless hourly imagery of TPW by blending separate swaths of microwave observations from polar-orbiting satellites; the Automated Rotational Center Hurricane Eye Retrieval (ARCHER) algorithm for identifying centers of tropical cyclones; and the Satellite Consensus (SATCON) algorithm for estimating the intensity of tropical cyclones.

TPW is one of several ways to measure and express the amount of moisture content in the atmosphere. It is a retrieved quantity that

plays an important role in forecasting because it shows the potential for precipitation, heavy rainfall, and other severe weather.

WHAT IS TOTAL PRECIPITABLE WATER?

TPW, as Wimmers describes, is:

The condensed depth of water from the surface to space. This quantity is also referred by several other names, including Precipitable Water (PWAT), Total Column Water Vapor (TCWV), Integrated Precipitable Water (IPW), and Integrated Water Vapor (IWV).

Put differently, "if you were to take all the water vapor and turn it into liquid, its depth expressed in millimeters tells you the amount of water vapor that you are measuring," Wimmers said.

WAYS TO VISUALIZE TPW

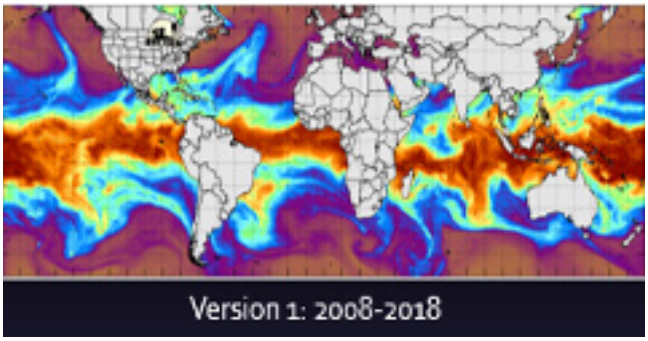

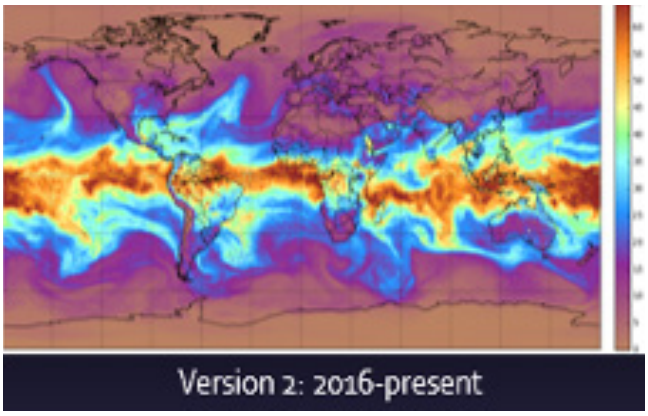

In 2008, Wimmers and Chris Velden, a Tropical Cyclone scientist, and a colleague at CIMSS, developed the MIMIC-TPW. This form of MIMIC-TPW existed until 2018. In 2016, the second and currently deployed version was developed. The version used MiRS water vapor retrievals from the NOAA-19, NOAA-20, Suomi NPP, and Meteorological Operational satellites (MetOp)-A, -B satellites. By using NOAA's MiRS algorithm, the newer version takes advantage of the wider range of channels on the Joint Polar Satellite System (JPSS) platform in order to retrieve TPW over land and ice as well. ATMS combines the capabilities and channels of its predecessors, the Advanced Microwave Sounding Unit-A (AMSU-A) and AMSU-B1 or Microwave Humidity Sounder (MHS) into a single sensor (Kim et al., 2014). In addition, ATMS has a wider swath that enables improved vertical sampling of the precipitation layer and minimizes surface affects.

MIMIC-TPW METHOD

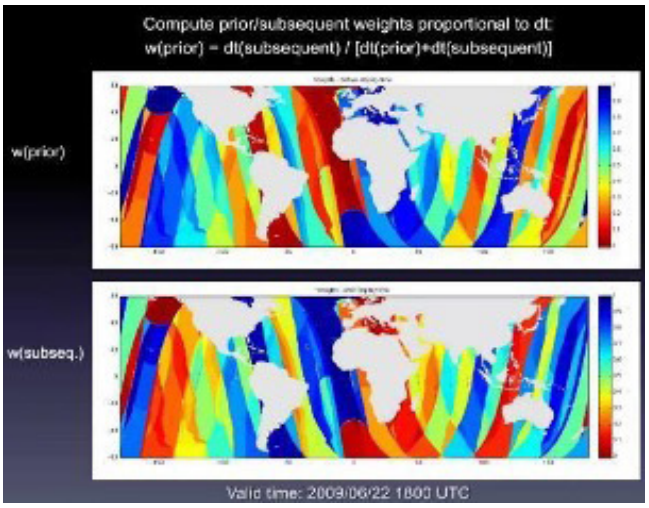

The MIMIC-TPW technique relies on knowledge of a background wind field that is most relevant to the subject water vapor, which enables one to advect or push a single satellite swath of TPW forward or backward in time. This advection of data forward or backward in time makes an observation taken one area sound over a 12-hour period. This type of manipulation can be applied to various observations from many different satellite platforms including NOAA-19, NOAA-20, Suomi NPP, MetOp-A, and MetOp-B. These observations combined with other information such as: footprint size and the time away from the valid time, are computed with weighting functions to produce a fluid/seamless impression of water vapor, as shown in the figure on the right. The correct weighting function enables the synthesis of any observation that was pushed forward or backward.

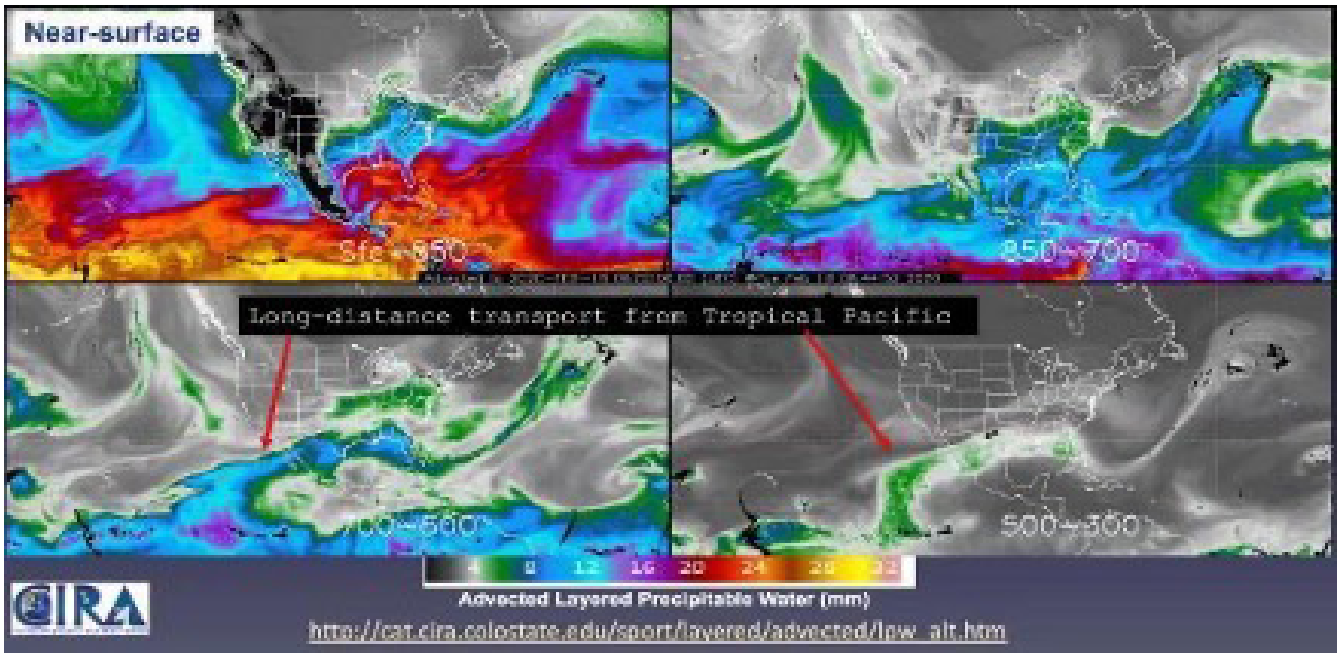

Advected Layered Precipitable Water

TPW can also be viewed in different layers of the atmosphere. The capability, which is referred to as advected layered precipitable water (ALPW), was developed by the Cooperative Institute for Research in the Atmosphere (CIRA), under a JPSS Proving Ground and Risk Reduction (PGRR) project. The ALPW product allows forecasters to see the vertical distribution of water vapor in near real time at four distinct levels of the atmosphere (surface–850, 850–700, 700–500, 500–300 mb). The ALPW allows forecasters to track individual layers of moisture and easily identify areas of "regular" and "very eventful" precipitation. For example, in February 2020, the ALPW product showed a stream of moisture that was only evident in the 700–500 mb layer, and led to significant weather in Texas and other areas along the Gulf coast.

IMPACT ON WEATHER FORECASTING APPLICATIONS

Spaceborne microwave sounders provide various global observations, including atmospheric temperature and water vapor measurements. They are notable for their ability to pierce through deep, non-precipitating clouds, which enables them to collect data in all weather conditions, during both daytime and nighttime. Their observations provide a means, at times the only one, to forecast weather in locations that have a sparse network of surface and upper-air observations. Examples of how this plays out and the kind of impact they have on weather forecast applications are provided in this section. On a global scale, ground-based radar has coverage gaps over land and only a little or no coverage over open ocean waters. Where this is the case, satellite-derived TPW products are a particularly useful tool for forecasters. The first example demonstrates the usefulness of TPW in an area with poor radar coverage.

POOR RADAR COVERAGE

American Samoa: September 2020

American Samoa is a group of islands in the South Pacific Ocean. It is the only U.S. territory south of the equator. The outline map on the left shows Tutuila and Aunu'u, the major islands of American Samoa, as well as an inset of the smaller islands Ofu, Olosega, and Ta'u, and two remote coral atolls, Swains Island along with the uninhabited wildlife refuge, Rose Atoll. Image credit https://www.cia.gov/the-world-factbook/countries/american-samoa/map.

With a total land area of 76.83 square miles (199 square kilometers), American Samoa is roughly

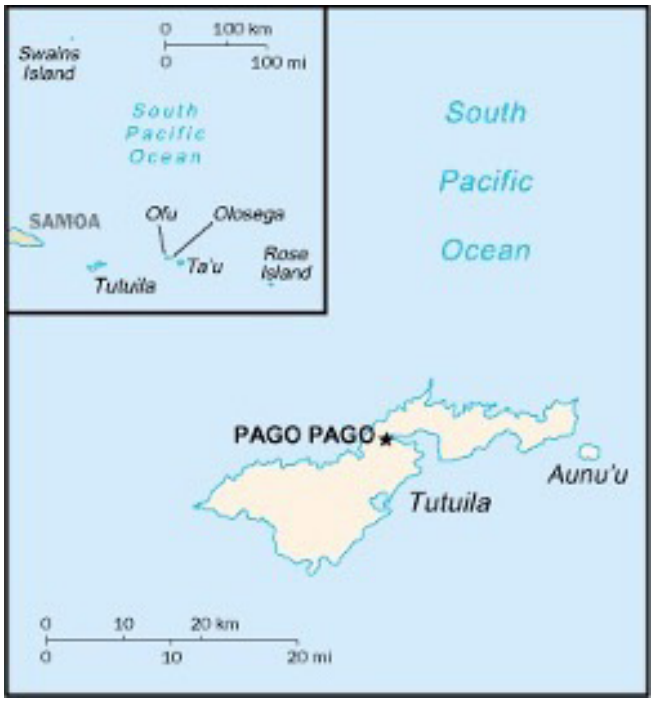

13 times smaller in size than the smallest U.S. state of Rhode Island.

American Samoa is one of several areas of responsibility for the U.S. National Weather Service (NWS) in the Pacific, which has long been recognized as a data-sparse region. The important role satellite observations play in the data-sparse region are presented in the screen capture shown below.

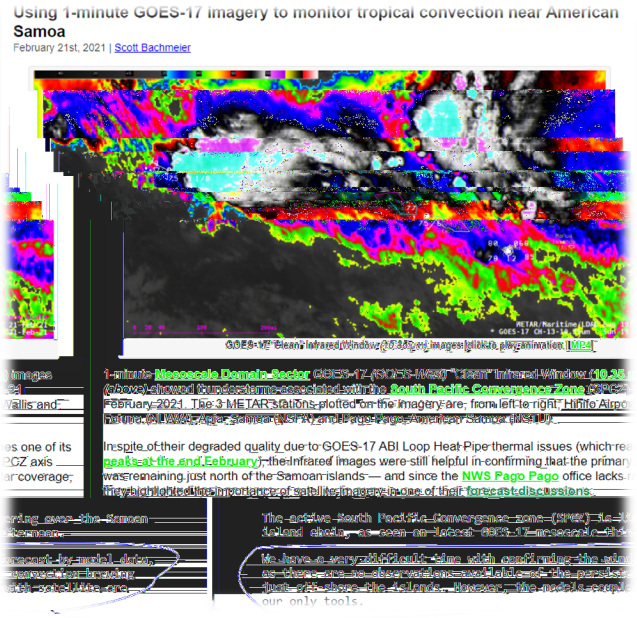

Screenshot of 1-minute GOES-17 (GOES-West) imagery by Scott Bachmeier, Cooperative Institute for Meteorological Satellite Studies (CIMSS), CIMSS Satellite Blog. https://cimss.ssec.wisc.edu/satellite-blog/archives/40019.

Over a period of twelve days in the month of September, precipitation and moisture events propelled by the Inter-Tropical Convergence Zone (ITCZ) came in waves, one at a time from the north and the south, and brought heavy rain over American Samoa. According to meteorological records, September is typically one of the drier months in American Samoa. Yet the region received almost five inches of precipitation on the first day of this 10-day event.

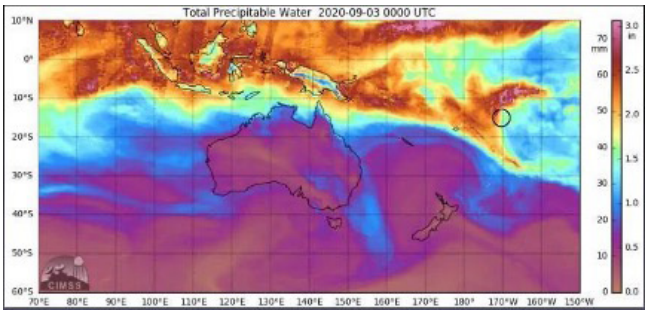

The observation of TPW showed the precise boundaries of the high-moisture patterns as they encountered the island, and the continuity of those patterns allowed a heavy precipitation advance warning of many hours.

A TROPICAL EVENT IN ALASKA?

Area flooding in Seward Alaska

> "For flood forecasting Alaska, so many times it is not the first or second, but most likely the third and fourth round of precipitation which causes flooding. Being able to look at the last few days of TPW history is a quick and accurate way of understanding both antecedent conditions and TPW which is still over the Gulf of Alaska and headed our way...Preliminary estimates are that this event cost $250,000 in flood fighting alone. This is exactly the type of event for which we lean on TPW heavily."
>
> –Celine van Breukelen, Senior Service Hydrologist, WFO Anchorage

Landslide on Lowell Point Road

Near washout of Alaska Railroad

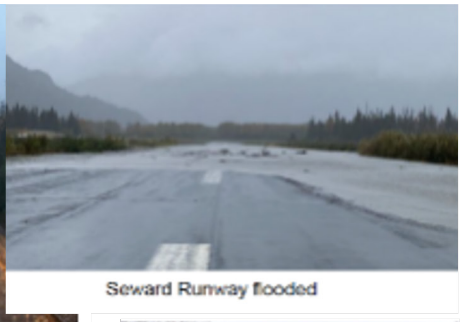

Seward Runway flooded

Dieckgraeff Rd impassable

Images from Seward Area Flooding Summary, David Kochevar (September 26–October 3, 2020)

In late September/early October heavy rain and high winds caused severe flooding in areas of Seward Alaska. This event caused infrastructure damage, induced landslides, and also left some communities surrounded by water and cut off from the outside world.

The event, which was visualized in the TPW product (below), showed a set of atmospheric rivers of high moisture drawn up from the tropics by a series of slow-moving low pressure systems. The eight-day event impacted several areas in the region, with some areas accumulating over 9 inches of rain.

IMPROVEMENTS AHEAD

The Automated Rotational Center Hurricane Eye Retrieval (ARCHER)

One of the most recognizable features of a tropical cyclone is the eye—a central area around which the entire storm rotates. Its structure typically indicates a tropical cyclone's strength. Locating the eye is critical for forecasting and analysis. It is generally done manually by experienced forecasters. Locating the eye can be a challenge due to the forecaster dealing with a lot of data, from many disparate

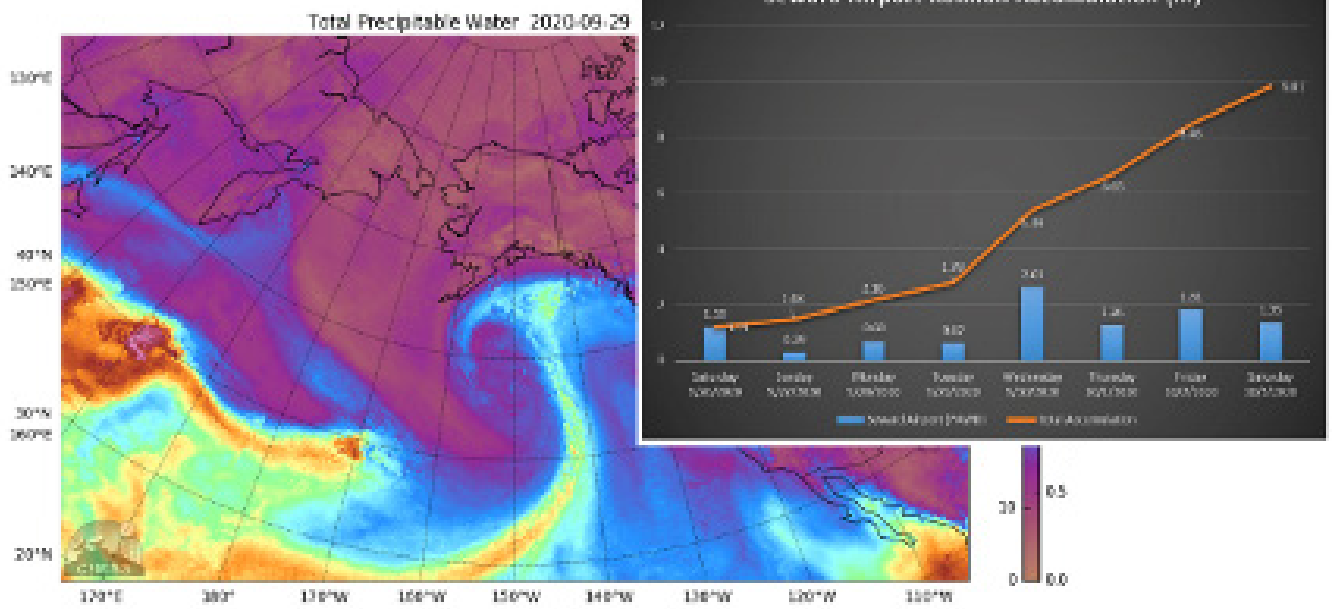

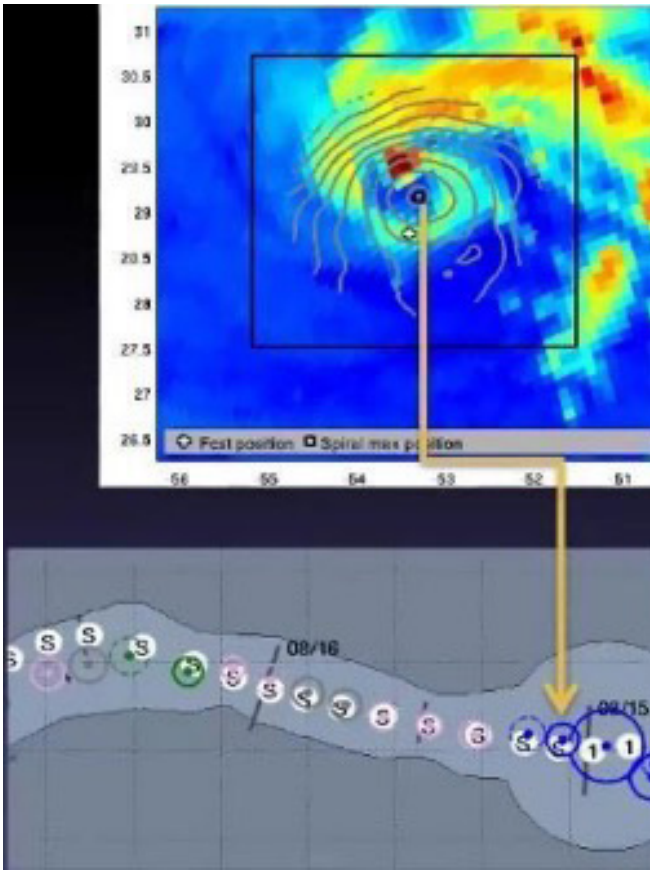

sources which could include near-infrared, far-infrared, visible, microwave, and scatterometer satellite observations, as well as non-satellite sources. A forecaster has to examine the data from all these sources in order to resolve a tropical cyclone's 24-hour path.

In 2010, Wimmers developed a technique to help reduce the time-load for forecasters by automatically processing all the satellite data available. The ARCHER algorithm performs image analysis of features such as the center of a tropical cyclone and eye size. The algorithm also incorporates all the data available from various sources to generate user-friendly storm track as well as eye wall trends.

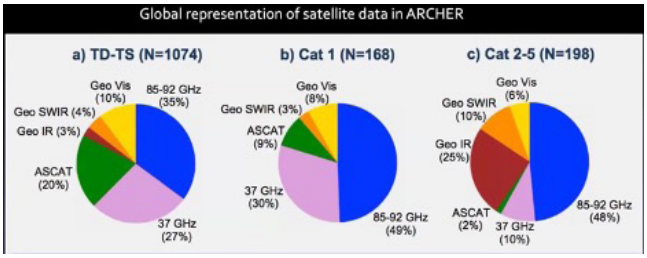

A SATellite CONsensus (SATCON) Method

Knowing a tropical cyclone's current intensity is vital to the forecast process. A manual process can take considerable time to sift through and gather data from multiple sources. The SATCON method is another approach that leverages data from multiple satellite instruments. SATCON produces unanimous estimates of a tropical cyclone's intensity by combining infrared and microwave-based satellite data. The idea is that such an estimate is more skillful than a simple average as well as estimates from individual data sources.

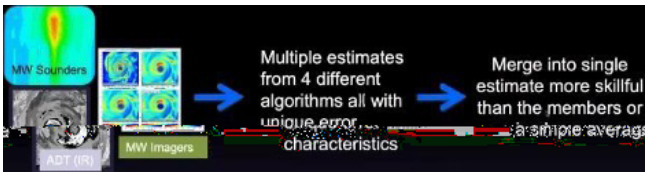

The Advanced Technology Microwave Sounder (ATMS) instrument is very sensitive to warm-core heating in the middle and upper troposphere. This warm core is directly related to the surface pressure anomaly, a measure of tropical cyclone intensity, through hydrostatic balance.

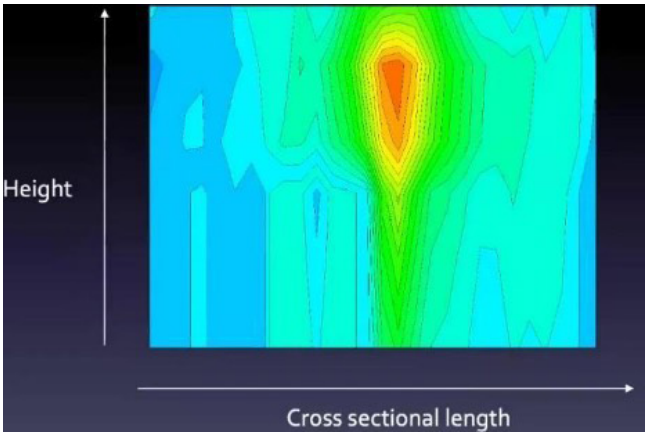

The ATMS instrument provides higher spatial coverage and its higher spatial resolution has greatly enhanced tropical cyclone analysis.

ARCHER and SATCON are in various stages of deployment onto the community development platform GitHub. Both are being incorporated into the Naval Research Laboratory's satellite analysis and display package GeoIPS, to be used

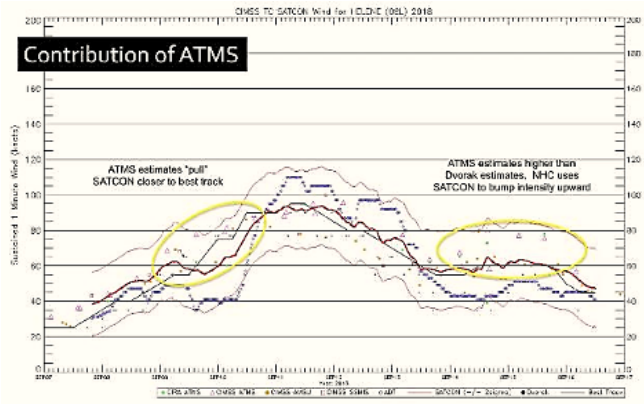

at various tropical weather forecasting offices in the U.S. GeoIPS will be a vital tool for applying JPSS data into rapid, actionable information for severe weather forecasting.

SUMMARY AND FUTURE WORK

Microwave sensors such as the JPSS instrument, ATMS, offer more channels, better resolution, and a wider swath that allows for improved vertical sampling. These adaptations have enabled fluid global visualizations of TPW that were heretofore available over land only.

This global-scale meteorological awareness is complemented by smaller-scale retrievals as well, through algorithms such as ARCHER and SATCON, which assimilate the multichannel, multispectral information from JPSS to give precise information of the hazardous conditions of tropical cyclones. Still more work lies ahead to incorporate new technologies such as the GeoIPS platform and to apply new forms of multispectral analysis, in order to translate this imagery into more and more actionable information for weather readiness.

Of note, satellite data play a pivotal role in operational forecasting in data-sparse regions like the Pacific, where they are, at times, the only source of information on meteorological conditions. ❖

Story Source

Materials obtained from JPSS October 19, 2020 Science Seminar titled "Serving the 50 states and territories with merged JPSS observations of midlatitude and tropical weather: MIMIC-TPW, Blended TPW, ARCHER and SATCON."

Footnotes

[1]In May 2005, the MHS officially replaced AMSU-B with its launch onboard the NOAA-18 satellite.

References

Wimmers, A. J., C. S. Velden, 2011: Seamless Advective Blending of Total Precipitable Water Retrievals from Polar-Orbiting Satellites. J. Appl. Meteor. Climatol., 50, 1024-1036. doi: http://dx.doi.org/10.1175/2010JAMC2589.1.

Kim, E., C.-H. J. Lyu, K. Anderson, R. V. Leslie, and W. J. Blackwell, 2014: S-NPP ATMS instrument prelaunch andon-orbit performance evaluation, J. Geophys. Res. Atmos., 119, 5653–5670,doi:10.1002/2013JD020483.

Knapp, K.R., C.S. Velden, and A.J. Wimmers, 2018: A Global Climatology of Tropical Cyclone Eyes. Mon. Wea. Rev., 146, 2089–2101, https://doi.org/10.1175/MWR-D-17-0343.1.

Zou, C.-Z., M. D. Goldberg, X. Hao, 2018: New generation of U.S. satellite microwave sounder achieves high radiometric stability performance for reliable climate change detection. Sci. Adv. 4, eaau0049.

CHARACTERIZATION AND APPLICATION OF ATMOSPHERIC COMPOSITION PRODUCTS FROM THE JOINT POLAR SATELLITE SYSTEM

The information in this article is based, in part, on the April 22, 2020, JPSS science seminar presented by Greg Frost, Program Manager, Climate Program Office, Silver Spring, MD. Full list of contributors on page 31.

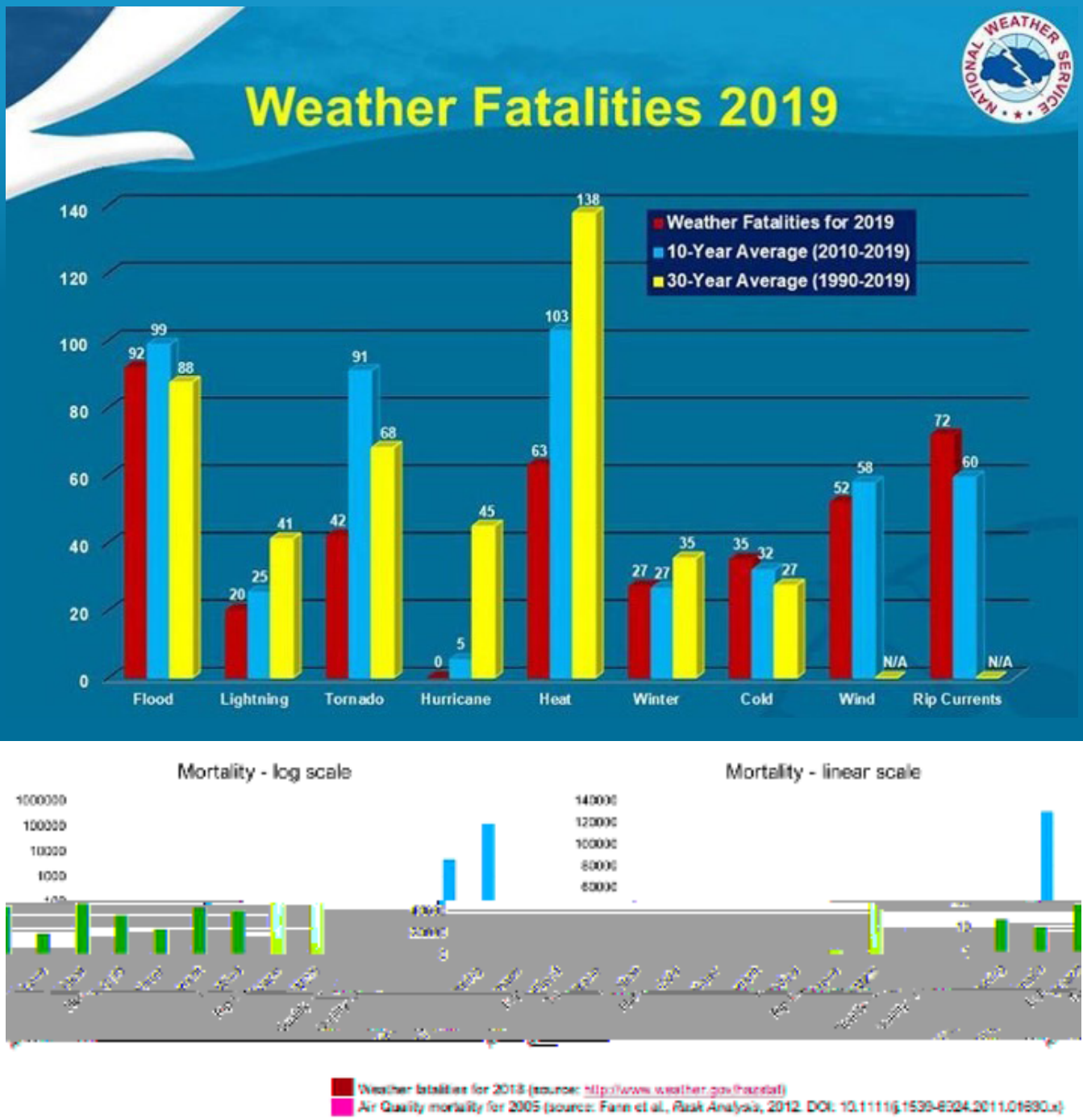

Top figure shows weather-related fatalities in the U.S. in 2019 (red bars), for the past 10 years (blue bars), and for the last 30 years (yellow bars). Credit. U.S. National Weather Service.

Lower figures show Annual mortality in the U.S. due to poor air quality and all weather phenomena. Data gathered from NWS (2020b) and Fann et al. (2012). Credit. Frost et al, 2020.

The atmosphere is composed of a mixture of trace gases and aerosol particles, many of which can be harmful to air quality, human health and the environment. Examples of the harmful effects of poor air quality, according to the United States Environmental Protection Agency (EPA), include asthma and other respiratory issues and cardiovascular diseases, leading to premature mortality. Air pollution can impair visibility, affecting air and ground transportation, and have negative impacts on natural resources such as forests, water quality, and biodiversity.

Every year a report is produced by the National Oceanic and Atmospheric Administration (NOAA) National Centers for Environmental Information (NCEI) on billion-dollar weather and climate disasters in the United States. The latest report, which covers data over a period of four

All Disasters | Drought | Flooding | Freeze | Severe Storm | Tropical Cyclone | Wildfire | Winter Storm

Select Time Period Comparisons of United States Billion-Dollar Disaster Statistics (CPI-Adjusted)

TIME PERIOD	BILLION-DOLLAR DISASTERS	EVENTS/YEAR	COST	PERCENT OF TOTAL COST	COST/YEAR	DEATHS	DEATHS/YEAR
1980s (1980-1989)	29	2.9	$178.1B	9.5%	$17.8B	2,870	287
1990s (1990-1999)	53	5.3	$274.0B	14.6%	$27.4B	3,045	305
2000s (2000-2009)	62	6.2	$519.0B	27.7%	$51.9B	3,091	309
2010s (2010-2019)	119	11.9	$810.5B	43.2%	$81.1B	5,217	522
Last 5 Years (2016-2020)	81	16.2	$606.9B	32.3%	$121.4B	3,969	794
Last 3 Years (2018-2020)	50	16.7	$234.3B	12.5%	$78.1B	553	184
Last Year (2020)	22	22.0	$95.0B	5.1%	$95.0B	262	262
All Years (1980-2020)	**285**	**7.0**	**$1,876.6B**	**100.0%**	**$45.8B**	**14,485**	**353**

decades (1980–2020), identified an average of 353 deaths yearly from severe weather events (NCEI, 2021). In 2020, these disasters accounted for 262 deaths (see top figure on the next page). Still, these numbers pale in comparison to those attributed to poor air quality—roughly 100,000 premature deaths every year (see figure on previous page on the right).

"The magnitude of issues around air quality are part of the reason why NOAA has a robust capability for observing and predicting air quality and atmospheric composition," says Dr. Gregory Frost, a research chemist at the NOAA Office of Oceanic and Atmospheric Research (OAR), Chemical Sciences Laboratory (CSL) in Boulder, Colorado. The type of information provided by NOAA's observing and prediction systems helps scientists like Frost and his team at the CSL study atmospheric composition, in order to better understand the origin of gases and aerosols found in the atmosphere and to discover what happens to them once they get there.

METHODS USED TO PROBE THE COMPOSITION OF THE ATMOSPHERE

Information on the composition of the atmosphere comes from various sources including aircraft, ground-based in-situ and remote-sensing instruments, and Earth-observation satellites. "Observations from polar-orbiting satellites provide the input needed to monitor and understand the atmosphere, make predictions, and design climate change mitigation and adaptation strategies," Frost says.

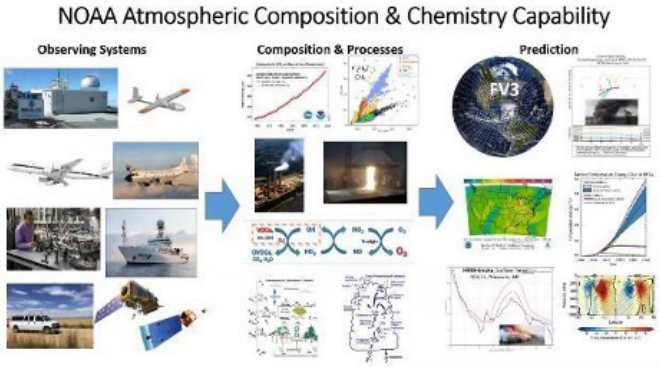

Aircraft field campaigns, such as the field research studies carried out by NOAA and NASA, provide opportunities to sample different geographic regions on a repeat basis. These studies provide high accuracy and precision and resolve fine-scale horizontal and vertical distributions of atmospheric constituents. One example of these campaigns is the Southeast Nexus (SENEX) study that NOAA carried out in 2013, whose flight tracks are shown at the top of the next page. SENEX focused on understanding the mix of natural processes and human-made pollution sources impacting the air quality across the Southeast and Midwest U.S. Over the past several decades, NOAA and NASA have carried out many other field campaigns, providing a rich dataset that allows better characterization of satellite observations.

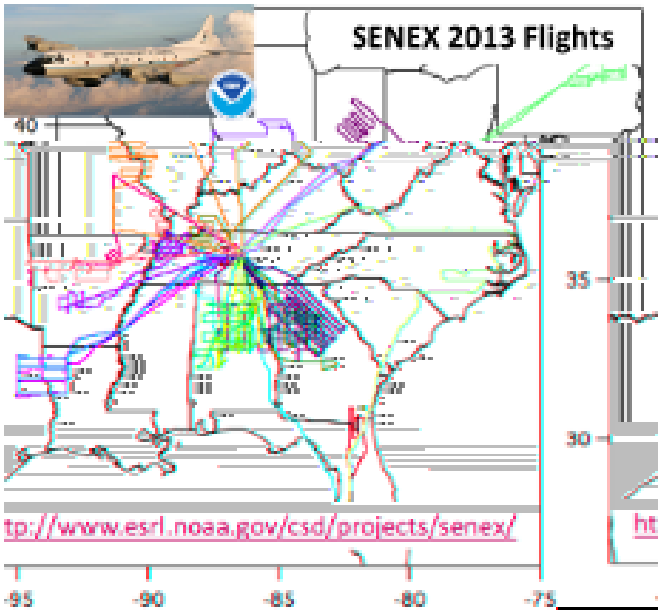

However, "these field studies are episodic," Frost says, which limits their ability to produce a continuous dataset. To construct a longer and more spatially representative time series that covers parts of the atmosphere outside the reach of aircraft, the CSL uses atmospheric chemical-transport models, such as the Weather Research and Forecasting with Chemistry (WRF-Chem) model shown below. These models are first validated using aircraft data and then used to provide more continuous datasets that can be compared with satellite observations.

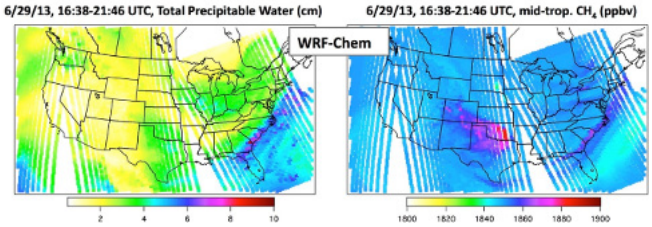

OPTIMIZING CAPABILITIES

In addition to his roles as a research chemist and a program manager for NOAA's Climate Program Office, Frost serves as the OAR liaison for atmospheric composition and chemistry, where he's been working to "facilitate the connections between OAR's laboratories and programs and also between different line offices of NOAA," Frost says. One example, Frost says, "is the Joint Polar Satellite System (JPSS) Proving Ground and Risk Reduction (PGRR) program," where he and his team are investigating atmospheric composition products from instruments on the NOAA-20 and the NOAA/NASA Suomi National Polar-orbiting Partnership (Suomi NPP) spacecraft.

The Cross-track Infrared Sounder (CrIS) instrument onboard the Suomi NPP and NOAA-20 satellites can quantify the distributions of trace gases in the atmosphere, such as Water Vapor (H_2O), Ozone (O_3) and Carbon Monoxide (CO). Frost and his team are investigating CrIS retrievals produced by the NOAA Unique Combined Atmospheric Processing System (NUCAPS) of tropospheric CO, Methane (CH_4), O_3, and other gases. As part of their JPSS PGRR efforts, Dr. Frost's team is conducting evaluations of aerosol optical depth (AOD) from the Visible Infrared Imaging Radiometer Suite (VIIRS) and retrievals of Nitrogen Dioxide (NO_2), O_3, and Formaldehyde (HCHO) from the Ozone Mapping and Profiler Suite (OMPS). These capabilities make JPSS "a foundational piece in NOAA's suite of atmospheric composition observing systems, and developing a better understanding of JPSS products is a key part of making better predictions with NOAA systems," Frost says.

"Our PGRR work with JPSS products," Frost says, "is to assess spatial averaging, characterize vertical profiles, and evaluate the accuracy of the tropospheric columns that are retrieved." Frost and his team have used these products in field mission planning and analysis, along with evaluating model predictions. Their goal is to advance the retrieval algorithms for JPSS atmospheric composition data and to help demonstrate the usefulness of these JPSS data in improving NOAA's operational forecasts.

ASSESSING CrIS SPATIAL AVERAGING

Frost and his colleagues examined the spatial averaging of CrIS data needed to produce meaningful signals in the trace gas data from the instrument. To visualize this method, consider a time series of observations made by aircraft or simulated by a model along the aircraft's

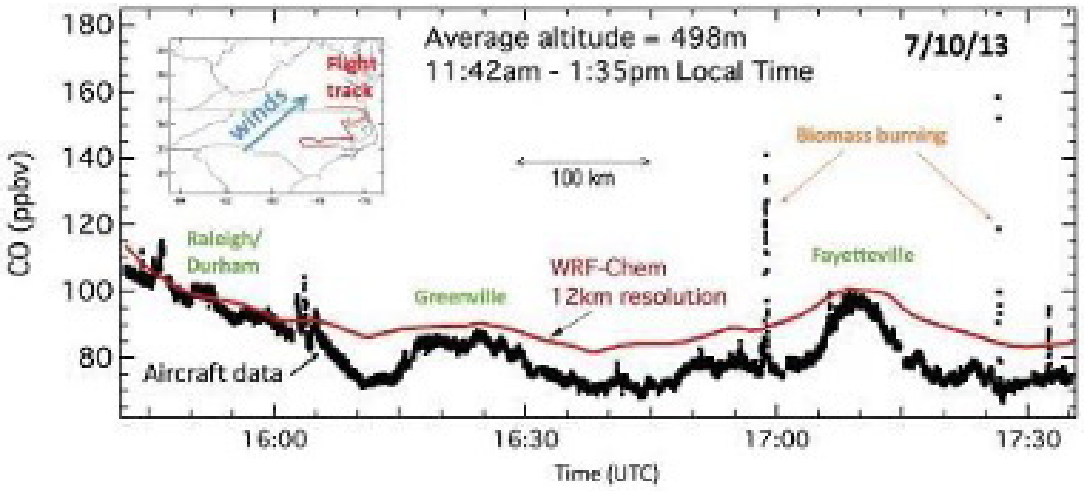

Time series of aircraft data and model output

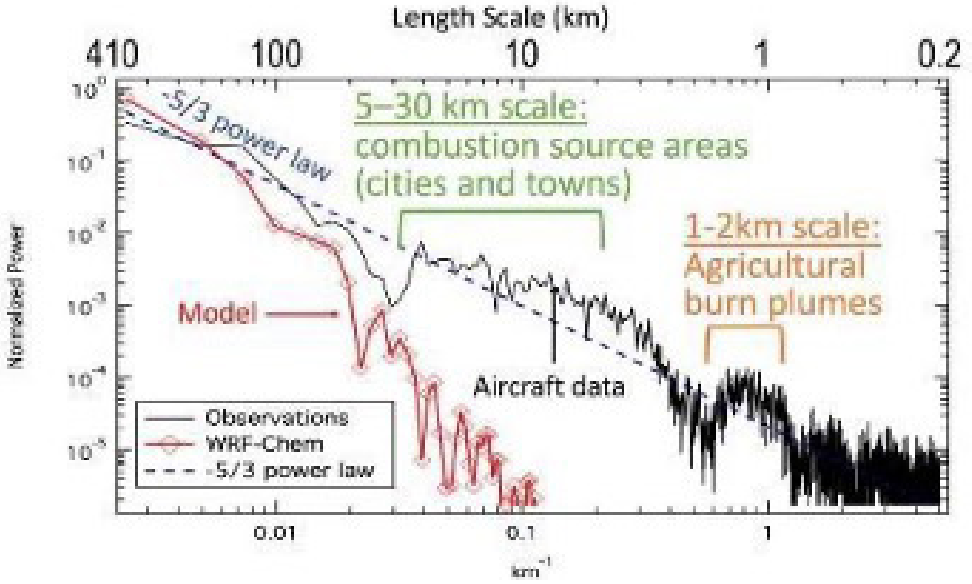

Power spectra of aircraft data and model output

flight track. For example, the amount of carbon monoxide (CO) in the atmosphere measured and modeled during a portion of a SENEX 2013 flight is shown in the top figure above. Because the plane is flying across a geographic area at a constant speed, this series of data collected as a function of time represents a distribution of CO present at equal spatial increments across the region in the southeast U.S. The spatial variability of the measured tracer, in this case CO, can be mathematically transformed into a power spectrum, shown in the lower plot below. The power spectrum of a tracer, which is well mixed, or evenly distributed, will look like a straight line with a slope of -5/3. The behavior of the power spectrum is predicted by the theory of atmospheric turbulence, representing an objective way to determine the inherent measurement frequency of the instrument in question. In the example shown below, the aircraft CO data generally follow the -5/3 power law line down to length scales of a few hundred meters, demonstrating that CO is evenly distributed at the high frequency of measurement that the aircraft instrument enables. Peaks in the power spectrum represent local deviations from well mixed behavior, which happens when the aircraft encounters pollution plumes of CO from cities or agricultural fires. When the power spectrum begins to diverge completely from the -5/3 line, the instrument can no longer resolve the behavior of the CO tracer. In the example below, this divergence occurs at length scales of 80–90 km for the model simulation of CO, meaning that the model cannot resolve the spatial variability of CO at spatial scales finer than that.

A similar analysis approach was applied to the data collected by CrIS along each of its cross-track scans as it collected vertical soundings of trace gases like CO and CH_4. A power spectrum analysis of the CrIS trace gas data allowed Frost and his team to diagnose the inherent spatial resolution of tropospheric measurements of gases such as CH_4. They found that CrIS produces meaningful tropospheric measurements of CH_4 at spatial scales of about 200 km or greater, while CrIS tropospheric CH_4 at finer spatial scales will not be reliable for diagnosing CH_4 variability.

EVALUATING CRIS TRACE GAS RETRIEVALS USING AIRCRAFT DATA FROM THE ATMOSPHERIC TOMOGRAPHY MISSION

To make direct comparisons of aircraft-derived atmospheric composition data to satellite derived data, Frost and his colleagues leveraged data from the NASA Atmospheric Tomography Mission (ATom). The NASA DC-8 aircraft, filled with instruments to measure a wide variety of trace gases and aerosols, deployed four different times between 2016 and 2018 in order to sample the remote marine atmosphere in every season. The DC-8 circled the planet, flying southward across the Pacific Ocean and then northward over the Atlantic, and collected vertical profiles of atmospheric gases and aerosols from just above the surface of the Earth up to the tropopause, the top of the troposphere (see figures below).

The ATom aircraft's sampling strategy provides many excellent comparison opportunities for CrIS retrievals of trace gases in the troposphere. CrIS vertical soundings of trace gases such as CO can be directly compared with CO measured during each of the up-and-down vertical profiles made by the DC-8. Examples of these comparisons from three flights during the first ATom deployment in August 2016 are shown in the figures below. The distribution of CO measured by CrIS across the depth of the troposphere as well as over wide swaths of the globe generally match the measurements made onboard the aircraft, providing confidence in the CrIS retrieval of this important trace gas. Differences between the CrIS observations and the aircraft observations indicate where improvements could be made in the CrIS retrieval algorithm and also highlight inherent limitations of the satellite measurement. For example, CrIS does not have much sensitivity in the lowest part of the troposphere, and is much better at measuring gases in the upper part of the troposphere. CrIS may also have difficulty retrieving trace gases under very hazy conditions, like in the plumes of smoke from large tropical forest fires in Africa.

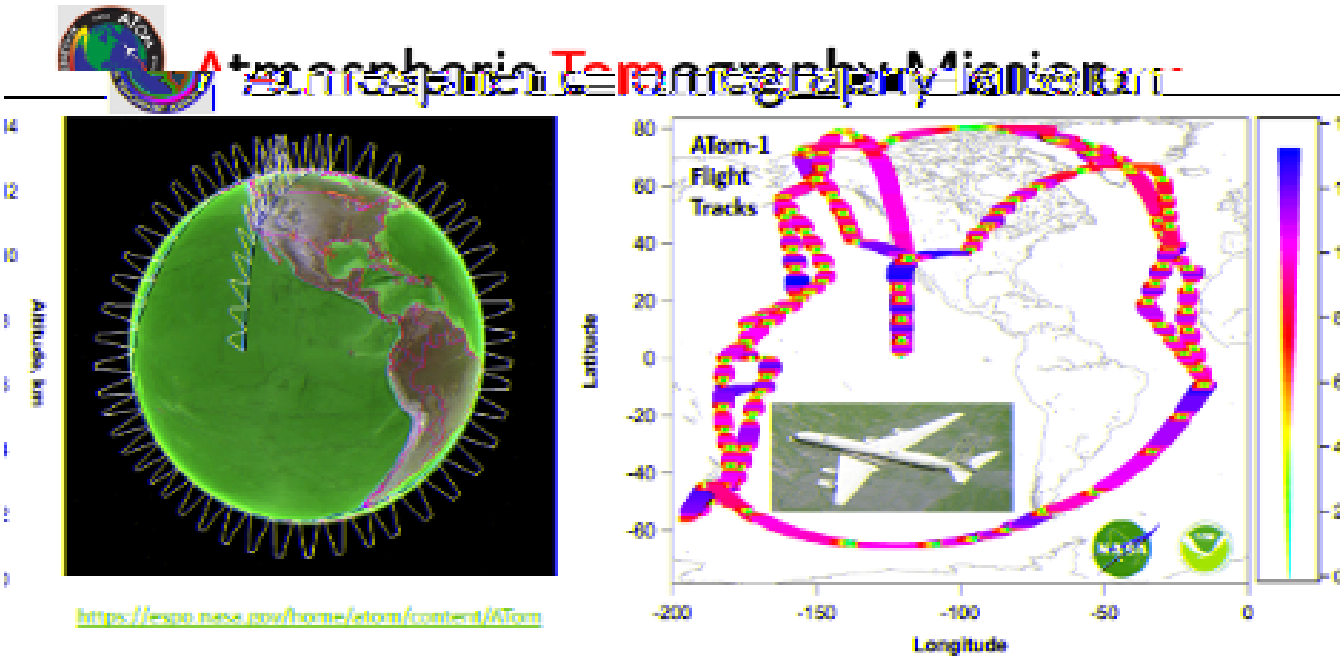

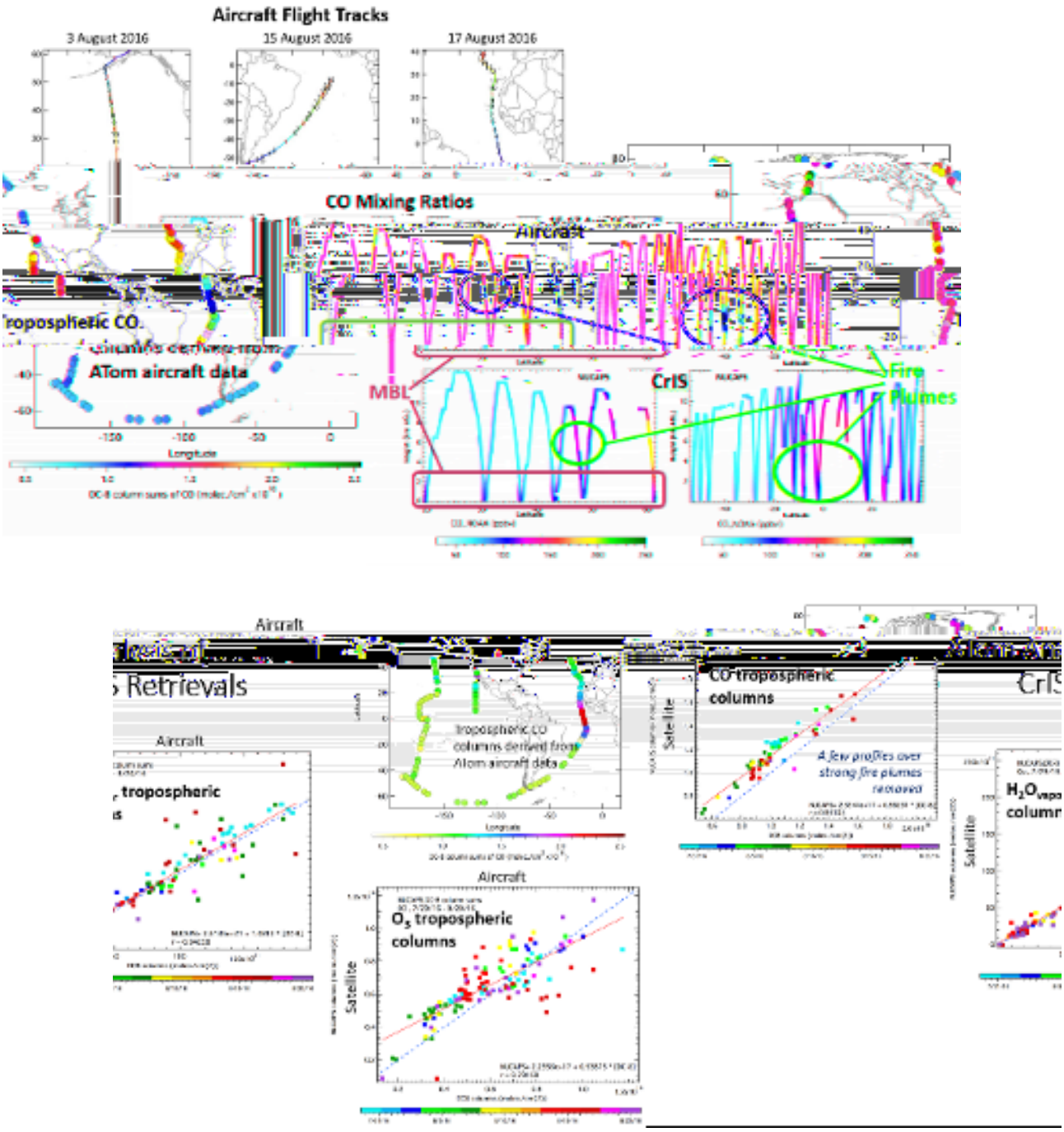

By summing up all of a trace gas, like CO, measured across a CrIS sounding or an aircraft vertical profile, one can calculate the tropospheric column of that gas, which is essentially the amount of the gas that exists from the Earth's surface to the top of the troposphere (i.e., the tropopause). Comparisons of tropospheric columns of CO, water vapor, and ozone measured by CrIS and onboard the DC-8 during the first ATom deployment in 2016 are shown above. These examples demonstrate that CrIS can quite accurately measure the amount of CO and water vapor in the troposphere, while the satellite instrument is less skillful at measuring ozone in the troposphere. These results are very encouraging, since they demonstrate that CrIS is a powerful monitor for CO. Since CrIS measures the entire planet every day, CrIS can potentially provide a long-term record of global CO that can be used to provide a reality check on atmospheric models and to understand changes to this important marker of human and natural sources.

ANALYZING VIIRS AEROSOL MEASUREMENTS

Other measurements taken during ATom included the size distributions, chemical composition and optical properties of aerosols. Charles Brock and colleagues at NOAA CSL and elsewhere pieced together the entire size distribution of aerosols measured during the 4 ATom deployments. They combined the size distributions with measurements of the chemical composition and optical properties of these aerosols. Their work enabled them to derive the optical extinction, i.e., the amount of light attenuation, of aerosols at different wavelengths along all of the flight tracks of the DC-8 during the 4 ATom deployments. These aerosol extinction data for one such visible wavelength are shown as a function of latitude and altitude in the plot at right. The manuscript by Brock et al. describing their analysis is soon to be submitted to a peer-reviewed journal.

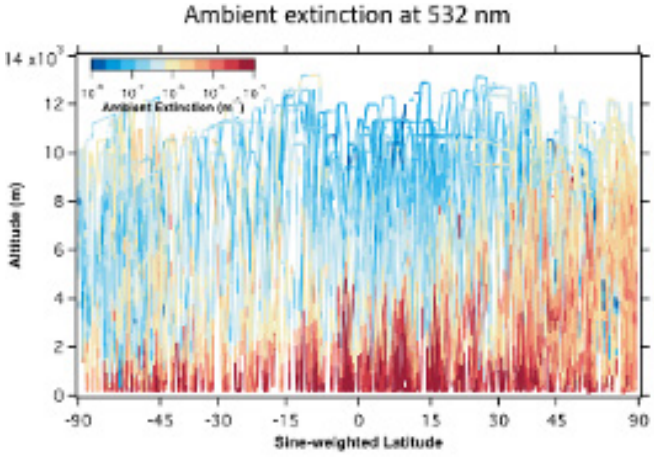

The dataset that this study constructed offers a direct measure to compare with aerosol products derived from the VIIRS instrument. Over the coming months, Frost and his team plan to use the various components of the Brock et al. ATom aerosol extinction dataset to evaluate aerosol optical depth observations by VIIRS on the NOAA-20 and Suomi NPP spacecraft. These ATom aircraft comparisons will help the VIIRS retrieval team led by Shobha Kondragunta to improve their algorithms and to produce more reliable aerosol products for strong sources such as fires and dust storms.

STUDYING WILDFIRES

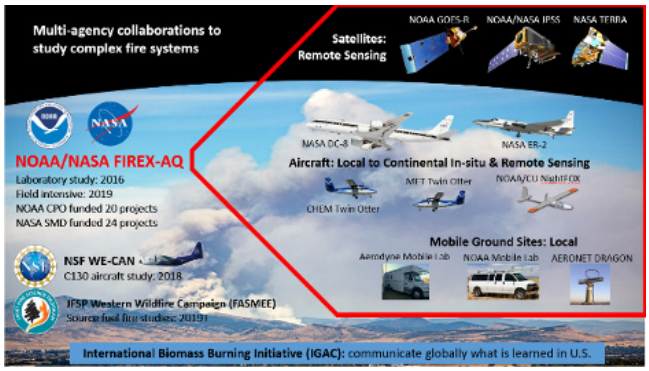

Coordinated recent U.S. Wildfire Research Activities

The Fire Influence on Regional to Global Environments and Air Quality (FIREX-AQ) was a multi-agency research campaign led by NOAA and NASA that included a 2019 intensive deployment of various aircraft, drones, field assets such as mobile laboratories and ground sites, and many available satellite observations. The scope of FIREX-AQ science questions included predicting and tracking the trajectory of wildfire smoke, describing the downwind chemistry in smoke plumes, and understanding the impacts of wildfires on air quality.

The JPSS Program played key roles in the success of FIREX-AQ. JPSS data were made available to FIREX-AQ researchers in near-real-time by the Science & Technology Corporation team of Rebekah Esmaili, Nadia Smith, and Chris Barnet, which has been a long-time recipient of JPSS support. The observations of wildfire plumes by VIIRS and CrIS helped the FIREX-AQ aircraft measurement teams better plan their flights to target a number of fires across the western U.S. during the late summer 2019 field deployment. The JPSS program also provided half of the support needed to deploy the NASA ER-2 aircraft, a former Air Force spy plane converted to scientific use by NASA and its partners. Frost served as the NOAA program scientist for the ER-2's FIREX-AQ deployment in 2019. The ER-2 carried a suite of instruments designed to mimic those on satellites such as the JPSS spacecraft. The ER-2 has the advantage that it could sample any given wildfire source many times, while the satellite instrument only takes measurements when its orbit happens to pass over the fire. Analysis of

the ER-2 measurements collected by each of its instrument teams during FIREX-AQ is ongoing. These studies are already providing a number of opportunities for direct comparison of the aircraft and JPSS instruments, which Frost will be able to show in a future talk. None of this work would have been possible without the generous and strategic support of the JPSS program.

AIR POLLUTION SATELLITES CARRY ON AMID A PANDEMIC: NOAA RESEARCH ON ATMOSPHERIC IMPACTS RELATED TO THE COVID-19 PANDEMIC

In 2020, a novel coronavirus caused a pandemic that led to global economic and social disruption. Restrictions imposed in response to the COVID-19 pandemic threw field research and analysis projects into uncertainty. At the same time, the COVID-19 pandemic created opportunities for researchers to capture the real-world impact of these disruptions on the environment. A number of NOAA research efforts focused on the pandemic's impacts on societal behavior and the resulting changes in emissions and air quality. This research makes use of ground-based, aircraft and satellite atmospheric composition products to capture the state of the atmosphere during the pandemic, to quantify changes to urban emissions resulting from the pandemic's societal restrictions and economic slowdown, and to understand the corresponding impacts on air quality and the Earth's radiative balance.

ON-ROAD EMISSIONS

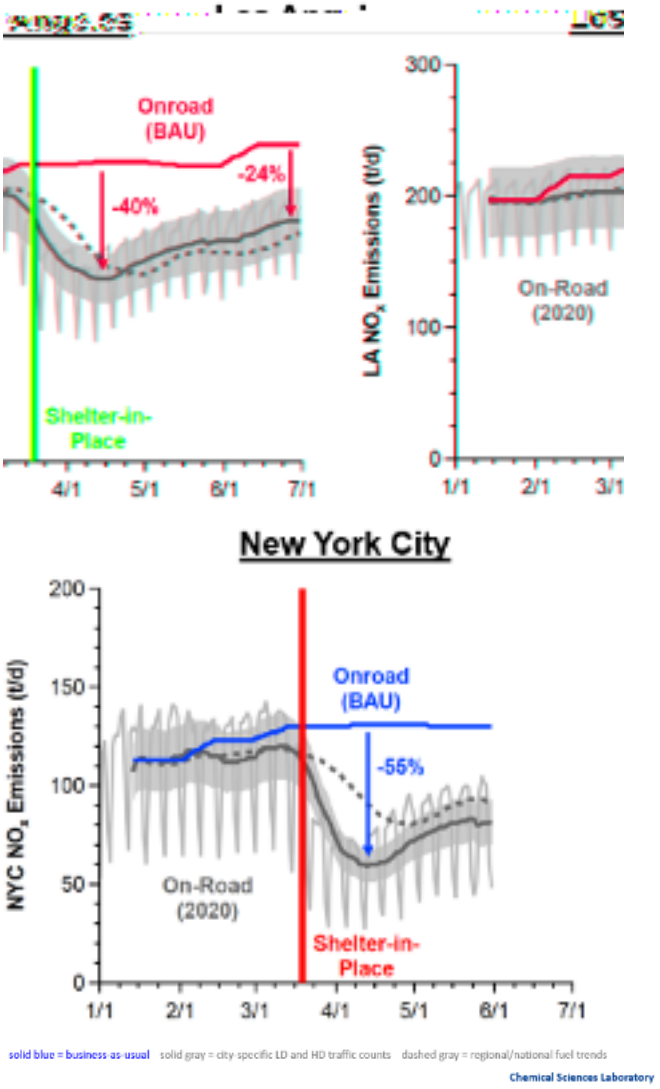

Frost and his CSL colleagues built an emissions inventory from publicly available datasets such as fuel-use statistics and motor vehicle activity in various cities. With the inventory, Frost's group was able to estimate what emissions of pollutants like Nitrogen Oxide (NO_x) are doing in close to real-time in cities across the U.S. (see above). NO_x is one of the ingredients of photochemical smog. Levels of NO_x and of even more harmful pollutants from the atmospheric processing of NO_x, such as ozone and aerosols, are closely regulated by the U.S. Environmental Protection Agency (EPA). Emissions inventories of NO_x are used by the EPA and state and local regulators to set air pollution standards and

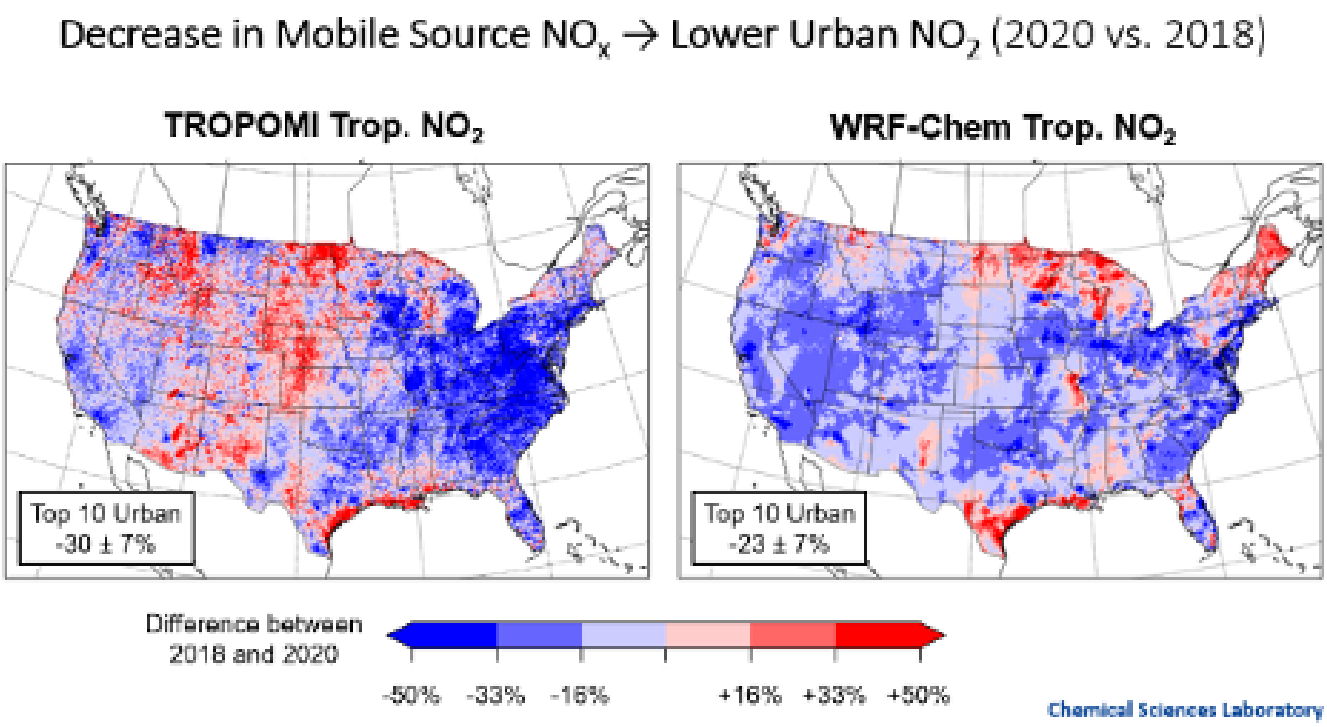

to identify when a region or a state is not in compliance with those standards. Because of the complexity of the EPA's inventory development process, they are only able to produce an updated inventory every three years. The major deviations to "business as usual" emissions that are expected during the COVID-19 pandemic are therefore not captured in EPA's currently available inventories.

Frost's team took advantage of their inherent flexibility to use cutting-edge research methods relying on publicly available datasets and NOAA's atmospheric observations in constructing inventories during the period of pandemic disruptions to transportation networks and economic activity. The team used their emission inventories in atmospheric chemical transport models in order to simulate how much of pollutants like NO_x (represented by one of its components, NO_2) should be in the atmosphere. They then compared the modeled NO_2 to satellite observations of the pollutant in the atmosphere across the U.S. The illustration in the figures above shows the change in the tropospheric column of NO_2 between 2020 and 2018 measured by a European Space Agency (ESA) satellite instrument called TROPOMI (left) and predicted by the NOAA model WRF-Chem (right). The agreement between the satellite and model in most U.S. urban areas and other NOx source regions demonstrates that the inventories produced by Frost's team accurately capture the large changes in this pollutant during the pandemic's period of maximum economic disruption.

The JPSS OMPS instrument on Suomi NPP and NOAA-20 has a number of similarities to the ESA TROPOMI instrument. Like TROPOMI, OMPS can retrieve NO_2 tropospheric columns (see below). As part of its upcoming PGRR-funded work, Frost's team will collaborate with its partners at STAR and the University of Maryland to analyze the ability of OMPS to detect changes in NO_2 resulting from the COVID-19 pandemic's societal disruptions. By providing a quantitative assessment of OMPS NO_2, the team will be able to demonstrate the utility of JPSS in providing near-real-time information that could be used in the future to improve air pollution alerts that help protect vulnerable populations.

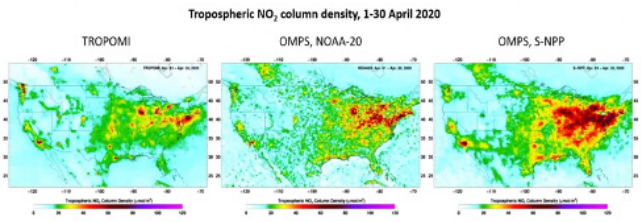

APPLICATIONS OF JPSS DATA TO NOAA UNIFIED FORECAST SYSTEM

Satellite products play a key role in the development of NOAA's air quality and weather forecast models and in assessing the performance of these models. As part of his research, Frost and his colleagues use the data from several JPSS instruments, including VIIRS and CrIS, in the improvement and validation of the modeling systems that are part of NOAA's new Unified Forecast System (UFS). The UFS aims to provide a seamless prediction system ranging from short-term weather and air quality forecasts to climate projections at seasonal, annual, and even longer timescales.

Frost and his team have been working with colleagues from several NOAA Laboratories, NESDIS, and the National Weather Service (NWS) for the past six years on efforts to improve the global forecast of aerosols in the NOAA Global Forecast System (GFS). This cross-NOAA team included realistic representations of aerosol sources from wildfires, dust storms, sea spray, and human sources, such as motor vehicles in the newest version of the GFS. This work culminated in the operational implementation of the GFS with aerosols as one member of the daily Global Ensemble Forecast System (GEFS). The first GEFS-Aerosol operational forecast was released by NWS on September 23, 2020, and GEFS-Aerosol will continue as NOAA's official global aerosol forecast for the next several years.

JPSS observations played a key role in the validation of GEFS-Aerosol's aerosol source descriptions. VIIRS aerosol products observe dust plumes produced by wind storms in the Sahara. In an example shown below, VIIRS shows the plume from an exceptionally large Saharan dust event in the summer of 2020, termed "Dustzilla", which transported this dust plume across the Atlantic and caused hazy skies across the southeast U.S. GEFS-Aerosol accurately quantified the huge Dustzilla plume's source and its westward transit to the U.S.

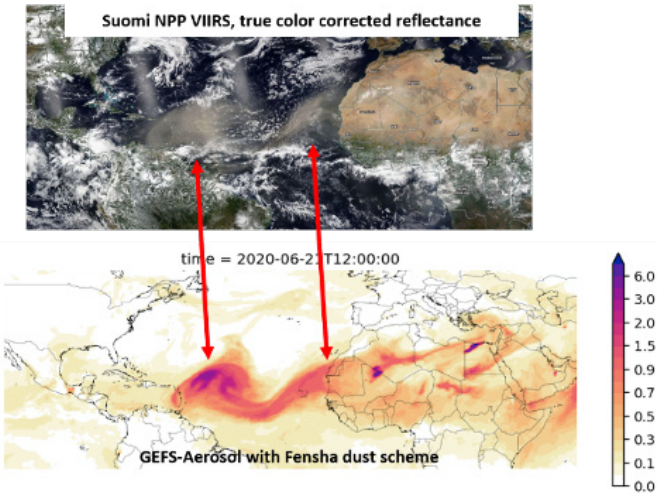

Dust event in June 2020: "Dustzilla". Credit Barry Baker, OAR ARL

VIIRS data also play key roles in quantifying the strength of wildfires in GEFS-Aerosols and in validating the model's transport of smoke plumes. The radiative power contained in fires is one of the products from VIIRS measurements. GEFS-Aerosols uses this fire radiative power product to predict how high a smoke plume is lofted into the atmosphere and to quantify how much and what types of pollutants are produced by the fire. An independent VIIRS product, aerosol optical depth (AOD), is then compared to the model's prediction of this quantity in order to assess the model's performance. In the example below, the AODs measured by VIIRS and simulated by GEFS-Aerosol are compared in smoke plumes from the major fires in southeastern Australia in December 2019 and January 2020. These fires were so large that these smoke plumes could be tracked across the Pacific Ocean and South

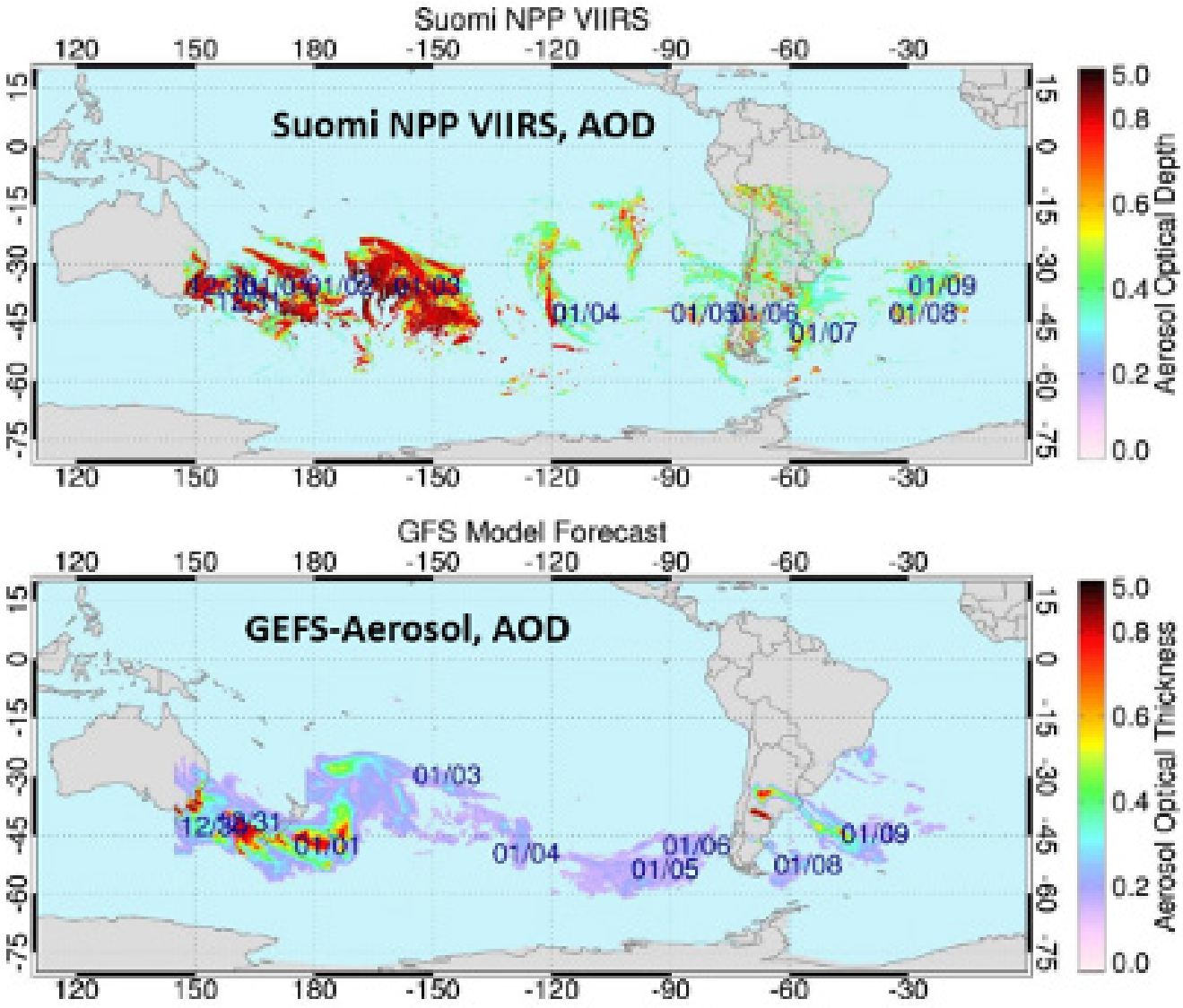

Australian wildfire plumes, December 2019–January 2020. Credit Shobha Kondragunta, NESDIS STAR.

America, where they mixed with smoke from South American fires before moving over the Atlantic Ocean. GEFS-Aerosol was able to simulate the transport of these plumes shown by VIIRS, although the magnitude of AOD predicted by the model differed somewhat from the satellite observation.

AOD data such as these from VIIRS, as well as trace gas products from CrIS, are being used by Frost and his team to further improve UFS model simulations. The team aims to ultimately use VIIRS and CrIS in data assimilation efforts that will help to produce better UFS forecasts in the future.

SUMMARY AND FUTURE WORK

Through its ongoing support of the JPSS PGRR program, Greg Frost and his team are helping to better characterize JPSS trace gases and aerosol products and advancing their applications in Earth system predictions. This reinforces that JPSS is a key component of NOAA's atmospheric composition and chemistry capability. In-situ and remote-sensing atmospheric observations made by NOAA and others provide useful information for characterizing and improving JPSS retrievals. Ambient measurements help to quantify the spatial representativeness and absolute accuracy of JPSS atmospheric composition products,

even in complex environments such as wildfires and dust storms. Continuous, validated, global JPSS atmospheric composition datasets provide complementary information to other observing systems and can help constrain the temporal and spatial variability of atmospheric composition and chemical processes. JPSS products are critical input to, and provide key evaluations of, the constantly evolving atmospheric composition capabilities of NOAA's Unified Forecast System. Finally, Frost and his team have demonstrated that strong connections between JPSS retrieval and evaluation teams lead to improved JPSS products, smooth the path of these products' research-to-operations transitions, and increase awareness of the value of JPSS atmospheric composition products to NOAA and its stakeholders. ❖

Story Source

Materials obtained from JPSS November Science Seminar titled "Characterization and Application of JPSS Atmospheric Composition Products."

References

NOAA National Centers for Environmental Information (NCEI) U.S. Billion-Dollar Weather and Climate Disasters (2021). Accessed January 28, 2021 from https://ww8 0 0 8 72 4i olders. F9ad3002 20031).

ENTERPRISE SNOWFALL RATE AND RADAR-SATELLITE BLENDED SNOWFALL RATE PRODUCTS

The information in this article is based, in part, on the December 15, 2020, JPSS science seminar presented by Huan Meng (NOAA/NESDIS/Center for Satellite Applications and Research (STAR). Full list of contributors on page 42.

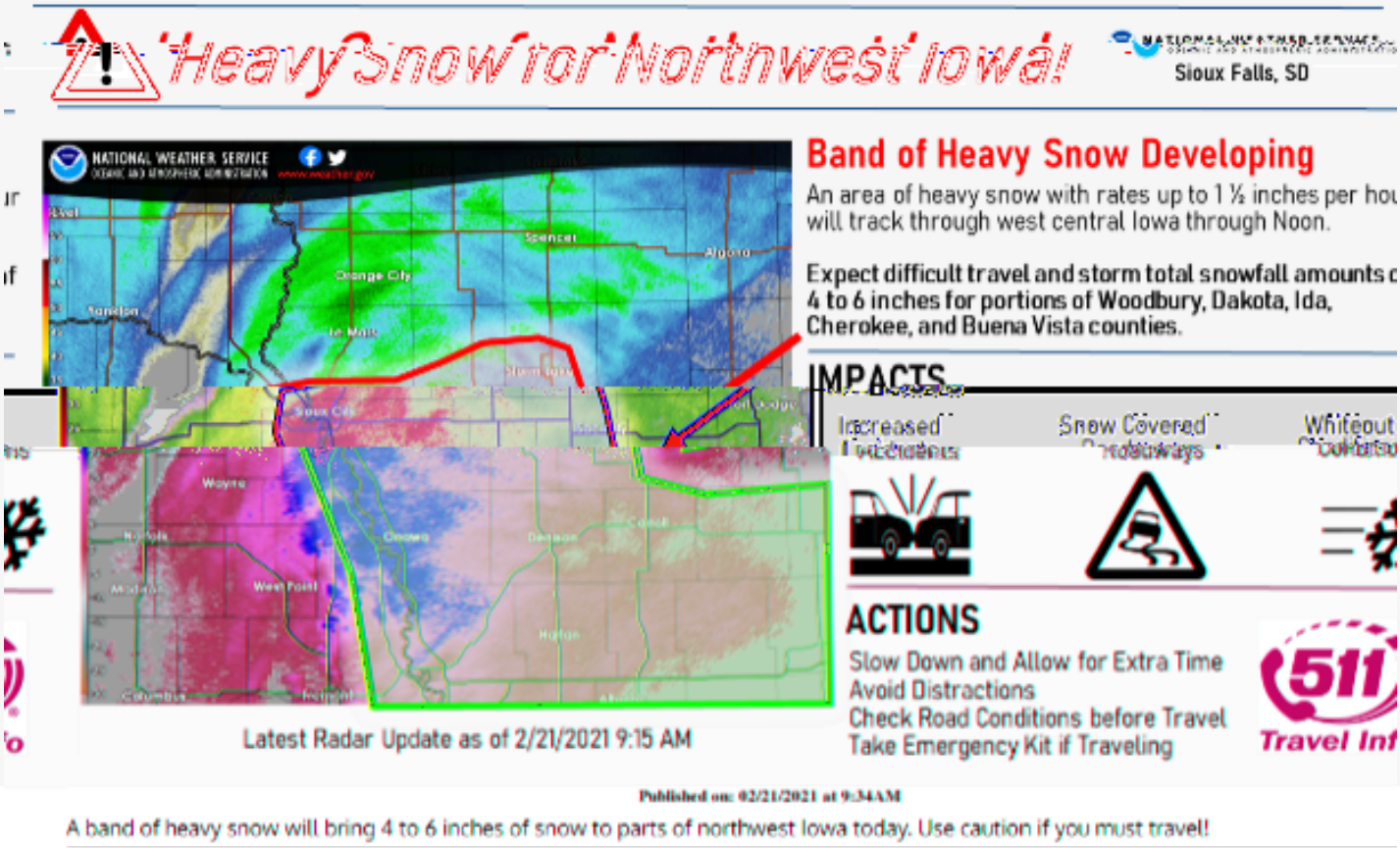

NWS snow forecast for February 21, 2021. https://www.weather.gov/fsd/weatherstory. Accessed 2/21/2021. Credit: National Weather Service, Sioux Falls, South Dakota.

Snow and freezing temperatures are weather events often associated with the winter season. Weather events like major snow storms can create hazardous conditions, which can cause risk to lives and livelihoods. The impacts from such events can last anywhere from a few hours, several days or even months.

There are several tools, including satellites and RAdio Detection And Ranging (radar) that meteorologists use to create short-term forecasts and track winter storm systems. Over land, ground-based observation tools, such as radars, are used to observe precipitation. They provide crucial information such as the structure of a storm as well as its severity. However, there are some areas where ground-based measurements cannot be taken or are missing. For example, the high latitude and mountainous regions across North America, such as Alaska, the northern plains, and the Rockies, which have a little more than a handful of surface weather observations and limited ground radar coverage.

Due, in part, to their capacity for large-scale sampling, satellite observations can fill in gaps where no conventional snowfall data are available to forecasters. Moreover, satellite passive microwave (PMW) instruments are sensitive to the scattering effect of snow particles, and therefore provide an effective way to monitor snowfall with global coverage.

Since 2012, a snowfall rate (SFR) product derived from a suite of passive microwave instruments onboard polar-orbiting satellites has run operationally at the U.S. National Oceanic and Atmospheric Administration (NOAA). The instruments include the Advanced Technology Microwave Sounder (ATMS) on the NOAA/ National Aeronautics and Space Administration (NASA) Suomi National Polar-orbiting Partnership (S-NPP) satellite, and the Advanced Microwave Sounding Unit (AMSU) and Microwave Humidity Sounder (MHS) pair onboard NOAA Polar Operational Environmental Satellites (POES) and European Organisation for the Exploitation

of Meteorological Satellites (EUMETSAT) Meteorological Operational satellite-A, and -B (MetOp).

The SFR product is one of the more prominent efforts of a science team at the NOAA National Environmental Satellite, Data, and Information Service (NESDIS) Center for Satellite Applications and Research (STAR) and the Cooperative Institute for Satellite Earth System Studies (CISESS)/Earth System Science Interdisciplinary Center (ESSIC) at University of Maryland, College Park. The team, led by Dr. Huan Meng, a Physical Scientist at STAR designed, developed and saw the product's implementation in NOAA operations.

Since the first generation SFR product came online, Meng and her colleagues have focused on building a better product. They have introduced several updates aimed at making the user experience better, and "significantly improved product quality," she says. These include a new technique that establishes regression between bias and various variables including 1DVAR-retrievals, satellite measurements, and Numerical Weather Prediction (NWP) data; new missions; machine learning to extend to cold regimes; and snowfall detection over three surface types: ice-free ocean, sea ice, and coast. In addition, Dr. Meng and her colleagues have developed a radar-satellite blended snowfall rate product (mSFR) that combines the National Severe Storms Laboratory (NSSL) Multi-Radar/Multi-Sensor (MRMS) instantaneous precipitation rate with SFR. The mSFR product takes advantage of satellite's broad spatial coverage and provides no-gap snowfall rate estimates within satellite swath. It provides situational awareness for weather forecasting by identifying the extent and intensity of snow in real-time, and tracking storm evolution with its looping capability.

In December 2020, Dr. Meng presented these research and development highlights at the JPSS monthly science seminar.

THERE'S ALWAYS ROOM FOR IMPROVEMENT

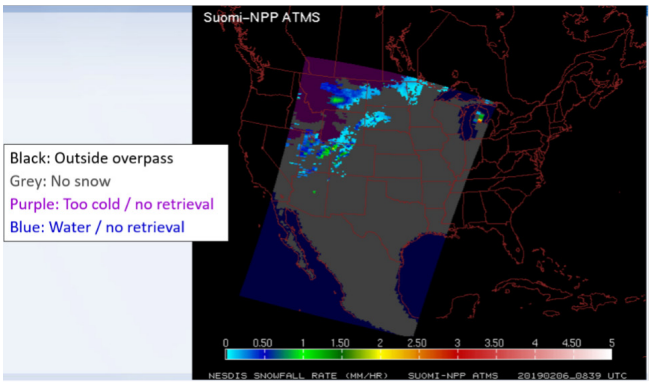

The first-generation product showed promise in detecting snowfall and estimating snowfall rate over global land. However, some of its features limited its application in weather forecasting. For example, the bias correction approach can be ineffective under certain conditions. In addition, the SFR algorithm is only applicable if the two meter temperature is above 7°F.

In cases where it is colder than this temperature, the algorithm is incapable of detecting snowfall. The operational product is also flagged over water because it is a land-only product.

"The lack of coverage over the ocean adversely impacts product applications in weather forecasting," Meng says. To illustrate this point, she gives an example of a snowstorm over the southeastern coast of Alaska, as shown in the image below. In this example, the product fails to detect the portion of the system over the

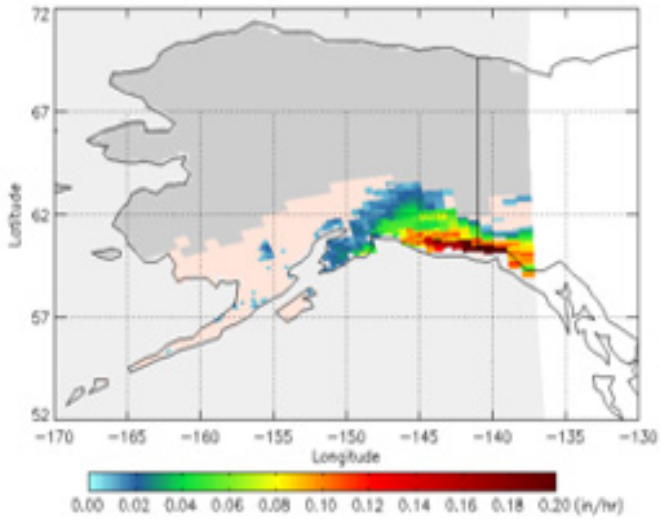

Nathan Eckstein, Alaska Region Headquarters

The extension of the SFR product over ocean areas would be greatly beneficial to NWS Alaska Region in several areas of our operations. Many of our coastal communities can be impacted by heavy snow events, which can include long duration type of events where accumulations over several days presents local challenges such as resource allocation. This kind of product can inform meteorologists of the potential for, and the continuous nature of these events for these communities as these systems transition from offshore to inland. Another benefit of having this product extended over ocean areas is snowfall over sea ice, particularly in the Arctic coast of Alaska. The potential to know more about blowing snow conditions that result from snowfall over these areas can be highly informative to forecasters in their support of activities like USCG search and rescue and other aviation activities along the Arctic coast where visibility forecasts are a primary hazard to operations.

Michael Folmer, Satellite Liaison at Ocean Prediction Center

The extension of the SFR product over ocean areas would greatly benefit the Ocean Prediction Center in a few areas of our operations. Mariners are very concerned with lowered visibilities at sea, which is not always related to fog, but heavy precipitation as well. Determining lowered visibilities associated with heavy snow under cloud would help separate the differences between the two phenomena. Snow over ice would also be very beneficial to mariners when trying to navigate icy passages or even when snow near icebergs creates a common background and subsequent associated hazards.

Gulf of Alaska, leaving coastal communities potentially unaware of and unprepared for offshore snowstorms before they transition to land, or spiraling snow bands that can reach land, an occurrence not uncommon along the East Coast. The idea to overcome this limitation would be an ocean extension, which is now in development. More details are provided in the "updates explained" section. The ocean extension should bring benefits to various stakeholders including product users, coastal communities, and mariners (as shown in the paragraphs reproduced above).

UPDATES EXPLAINED

SFR Bias Correction

Uncertainty may negatively impact the effectiveness and accuracy of results. In the case of the SFR, uncertainties can arise from the radiative transfer model and the various algorithm assumptions. The best strategy is to perform bias correction using high quality "truth" snowfall data. The NOAA Stage IV Next Generation Weather Radar (NEXRAD) and gauge combined hourly precipitation product is the "truth" used for SFR bias correction. Rather than continue with a histogram matching technique used previously, Meng and her colleagues established regression relationships between SFR bias and a selected set of 1DVAR-retrieved parameters, satellite observations, and NWP model predictions. The new technique noticeably outperforms the histogram matching method.

Ocean Extension

As a first step to extending the algorithm over the ocean, Dr. Meng and her colleagues developed snowfall detection (SD) algorithms over ice-free ocean, sea-ice, and coast surface types for the S-NPP and NOAA-20 ATMS instruments, with the ultimate goal of developing snowfall rate algorithms for the three surfaces. While ATMS draws its heritage from the AMSU-A and MHS instruments, it has some improvements

Channel		Frequency (GHz)		NEΔT (K)		Beam Width (deg)		Peak WF (hPa)
ATMS	AMSU	ATMS	AMSU	ATMS	AMSU	ATMS	AMSU	ATMS or AMSU
1		23.8		0.50	0.30	5.2	3.3	Window
3		50.3		0.70	0.40	2.2	3.3	Win
4		51.76		0.50		2.2		95
5	4	52.8		0.50	0.25	2.2	3.3	85
6	5	53.596 ± 0.115		0.50	0.25	2.2	3.3	70
7	6	54.4		0.50	0.25	2.2	3.3	40
8	7	54.94		0.50	0.25	2.2	3.3	25
9	8	55.5		0.50	0.25	2.2	3.3	20
10	9	57.29		0.75	0.25	2.2	3.3	10
11	10	57.29 ± 0.217		1.00	0.40	2.2	3.3	5
13	12	57.29 ± 0.322 ± 0.022		1.25	0.60	2.2	3.3	10
14	13	57.29 ± 0.322 ± 0.010		2.20	0.80	2.2	3.3	5
2	15	57.29 ± 0.322 ± 0.0045		3.60	1.20	2.2	3.3	
Window	16	15	88.2	89.0	0.30	0.50	2.2	3.3
Window		16		89.0	0.60	0.84	1.1	1.1
Window	17	17	165.5	157.0				
800	18	20	183.31 ± 7.0	190.31	0.80	0.84	1.1	1.1
700	19		183.31 ± 4.5		0.80	0.60	1.1	1.1
500	20	19	183.31 ± 3.0		0.80	0.70	1.1	1.1
400	21		183.31 ± 1.8		0.80	1.06	1.1	1.1
300	22	18	183.31 ± 1.0		0.90		1.1	

nted from Table showing channel characteristics of ATMS and AMSU repr
Weng et al. in JGR (2012)

including wider scans with no gaps in between swaths. ATMS also has two water vapor sounding channels (19 at 183.31 ± 4.5 GHz and 21 at 183.31 ± 1.8 GHz) that are not on AMSU, which allow for improved vertical sampling of the precipitation layer and minimizing surface effects.

After reviewing well over 100 candidate predictors including brightness temperatures (TBs) from satellites and model data, the team selected snow detection models with 14–16 predictors for each surface type. These included ATMS TBs, relative humidity profile as well as Total Precipitable Water (TPW) and cloud water from the Global Forecast System (GFS). The team developed a global SD model as well as a set of regional SD models from these predictors.

In their analysis of how the models performed based on the predictors, they found that over all the surface types, a combination of TBs and GFS predictors produced satisfactory SD models with Heidke Skill Score (HSS) from 0.55–0.59, and the possibility of detection (POD) from 0.69–0.74. When using TBs only, the global model performed comparably over the ice-free ocean surface type, but was quite degraded over the sea-ice and coast surface types. They concluded that over the ice-free ocean the algorithm primarily depends on TBs for snowfall detection. However, the GFS predictors are critically important for snowfall detection over sea-ice and coastal regions.

Performance Statistics
(TBs + GFS predictors, Global model)

	POD	FAR	HSS
Ice-free Ocean	0.69	0.15	0.59
Sea-Ice	0.74	0.15	0.55
Coast	0.74	0.15	0.56

Performance Statistics
(TBs Only, Global model)

	POD	FAR	HSS
Ice-free Ocean	0.66	0.15	0.57
Sea-Ice	0.54	0.15	0.34
Coast	0.53	0.15	0.32

A comparison between the global and regional models showed that they were comparable, although the statistics from individual regional models can be much better (e.g., POD > 0.8) over certain regions. The final SD algorithm is an optimal combination of the two models depending on their performance in specific regions.

Case study comparing with GPM KuPR: 01-16-2016

In this case study, the snowfall probability derived from the S-NPP SD model is compared with the snowfall rate product retrieved from NASA Global Precipitation Measurement (GPM) Ku-band precipitation radar (KuPR). The two black lines in the images define the limbs of a KuPR swath. KuPR detected some snowfall in the Labrador Sea between Newfoundland and Labrador, Canada and Greenland. S-NPP snowfall probability is greater than 80% over almost all the areas where KuPR indicates snowfall. The global comparison with KuPR revealed that ATMS detects much more snowfall than KuPR since the SD model is trained using snowfall retrievals from NASA CloudSat Could Profiling Radar (CPR). CPR is a much more sensitive radar than KuPR. It has been found that the latter misses most light snowfall.

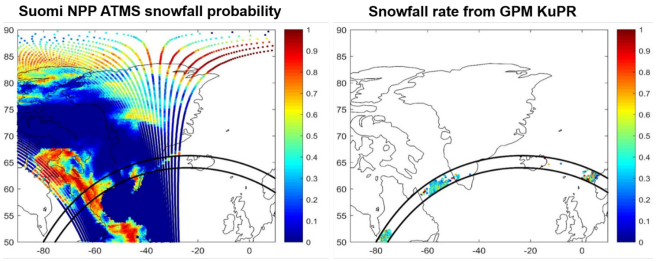

Cold Extension

The current SD algorithm shows a degraded performance when surface temperatures are below ~21°F. Moreover, it is non-applicable in temperatures below ~7°F. Thus there are major obstacles to applications in cold areas where traditional observations are often lacking, e.g. in Alaska and mountainous regions. Meng and her group have created a workaround by developing a cold extension using a neural networks model,

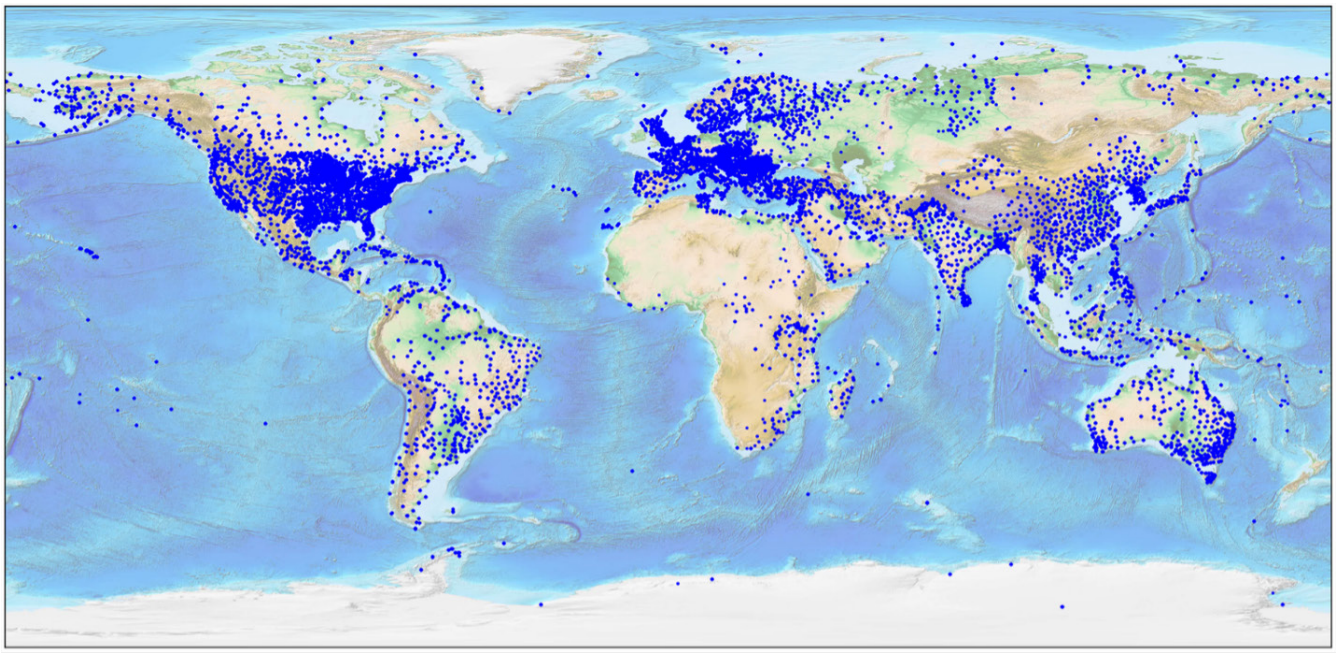

Dark blue spots signify data locations. Majority are based in the U.S. and Europe.

which is a machine learning (ML) technique. They call it the Deep Neural Network (DNN) SD model. As a first step, they built a global training dataset with three collocated sets of data: truth data from NOAA's Integrated Surface Database (ISD) ground observations; satellite measurements from the S-NPP ATMS instrument; and GFS analyses. All of which have led up to a total of 1.3 million data records.

Thus far, Meng and her group have conducted a feature analysis, which has resulted in the identification of 50 features to predict snowfall. The dataset was split into two: 80% of which is the training set and 20% is the testing set. They categorized the data into warm and cold regimes, then applied random sampling and oversampling techniques to ensure an equal number of samples in each regime. Next, they trained a preliminary DNN with 50x25 neurons. So far, their results indicate a considerably improved performance for the neural network when compared to the logistic regression (LR) algorithm under warm conditions (T2m > -15°C). In addition, it has also shown good performance in cold conditions (T2m < -15°C) where the LG algorithm is not applicable.

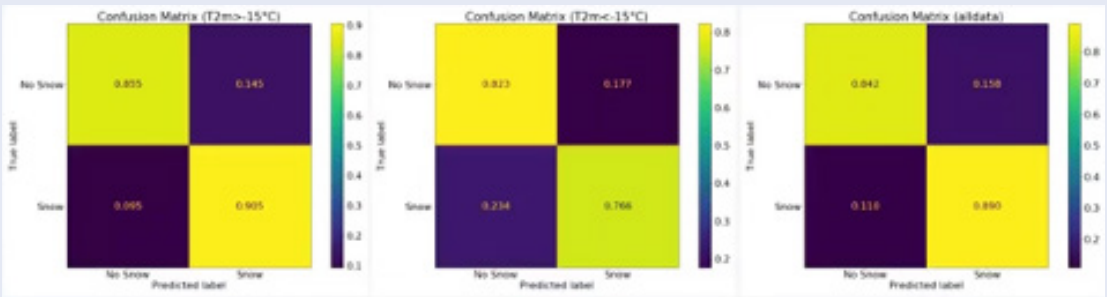

	T2m>-15°C		T2m<-15°C		All Data	
	DNN	LR	DNN	LR	DNN	LR
Probability of Detection	90.5%	80.9%	76.6%	N/A	89.0%	N/A
False Alarm Rate	14.5%	31.4%	17.7%	N/A	15.8%	N/A
Heidke Skill Score	0.754	0.496	0.535	N/A	0.735	N/A

Radar-Satellite Blended Snowfall Rate (mSFR)

Meng and her team have also been working on a radar and satellite blended liquid-equivalent snowfall rate product—a quantitative precipitation estimation (QPE). The product combines the NSSL MRMS instantaneous precipitation product with SFR from seven satellites including NOAA-20 and S-NPP. The MRMS instantaneous QPE provides radar snowfall rate estimates with high spatiotemporal resolutions of 1 km and 2 minutes. However, there are some issues. Among these is coverage in mountainous and remote regions, as well as quality degradation from snowfall.

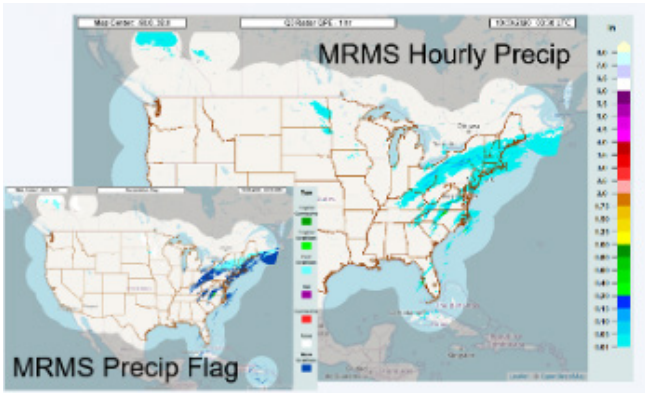

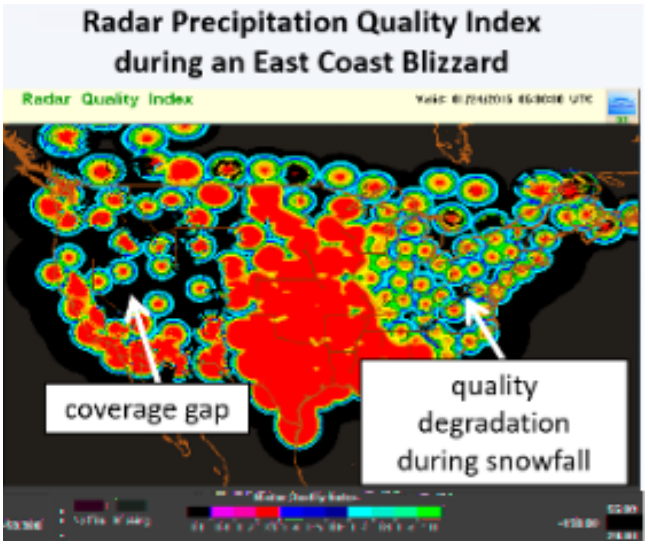

Consequently, these issues, along with a request from forecasters for a looping capability, prompted Meng and her research team to develop a blended product with enhanced spatial coverage and temporal resolution. The result, mSFR, is a blended algorithm generated using SFR retrieved from Direct Broadcast (DB) and MRMS instantaneous precipitation data. The DB capability reduces the product's latency to less than 30 minutes. The DB-based SFR and mSFR products are generated at the University of Maryland (UMD) Cooperative Institute for Satellite Earth System Studies (CISESS). The data are then sent to the NASA Short-term Prediction Research and Transition Center (SPoRT) for AWIPS reformatting and distribution to some weather forecast offices (WFOs) at near real-time. In addition, SFR can be found online at near real-time from the following websites:

- SPoRT mSFR page: https://weather.msfc.nasa.gov/cgi-bin/basicLooper.pl?category=snowfallratemergedconus&loc=conus&regex=conus_msfr&title=NESDIS%20CONUS%20Merged%20Snowfall%20Rate&time_drop=show
- SPoRT SFR page: https://weather.msfc.nasa.gov/cgi-bin/sportPublishData.pl?dataset=snowfallrateconus&product=conus_snowrate
- CISESS-MD mSFR page (with archive): http://cics.umd.edu/~jdong/snow4/image/msfr/
- CISESS-MD SFR page (with archive): http://cics.umd.edu/sfr/

SFR and MRMS data are time lagged by 30 minutes. The explanation, says Meng, is that "satellites are sensitive to snow in the atmosphere." As with all snowfall events, "it takes some time for snow to fall to the surface," Since the SFR product is retrieved from satellites, it typically captures snow events before the MRMS product. The 30-minutes lag is by no means an accident. Meng explains that based on a statistical analysis of their data, it is with this time shift that the two products exhibit the highest correlation (see figure on the top of the next page). The product is available only in the continental U.S. (CONUS) due to the fact that MRMS is CONUS only, every 10 minutes.

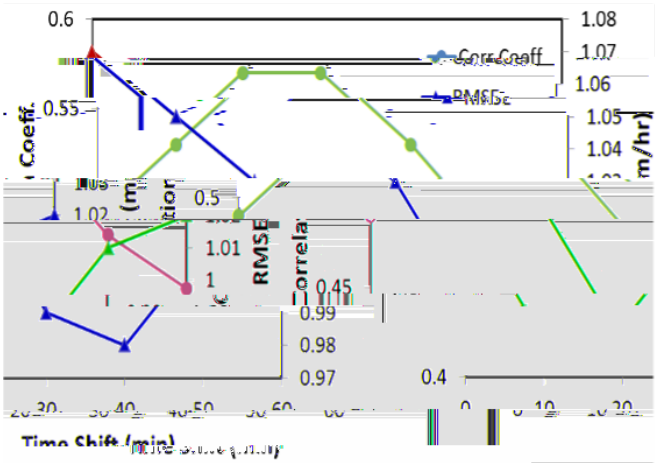

By blending SFR with MRMS, the satellite product fills in the gaps in the radar product and provides no-gap snowfall rate estimates within a satellite swath. The example below demonstrates how SFR fills in the snow (in the magenta oval) missed in MRMS in western Wyoming since the snow fell over a radar gap. The reference image on the right is the hourly snowfall from the snow analyses by the National Operational Hydrologic Remote Sensing Center (NOHRSC).

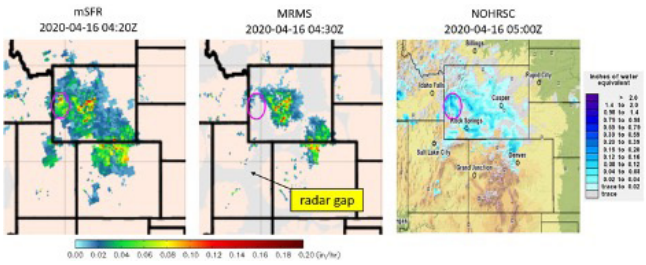

Meng says the mSFR is especially useful for tracking heavy snowfall as shown in the example below from a storm that hit the northern High Plains in October 2019. The mSFR tracked the evolution and movement of the storm every 10 minutes.

Use Case: Northern High Plains, 10/9–11/2019

"What was amazing with this case from 10/9, we were also looking at the Advective Layered PW and we could see the dry layers sfc–850mb and 850mb–700mb approaching the boundary from the N-NW where the mesoscale band of heavy snow was occurring, and then within the next hour or two after the drier air arrived, the snowfall rates rapidly diminished. Both of these products used together provided an advantage for SA and for providing weather and social media updates on the heavy snow band."

-Tom Clemmons, Science and Operations Officer, Glasgow, Montana

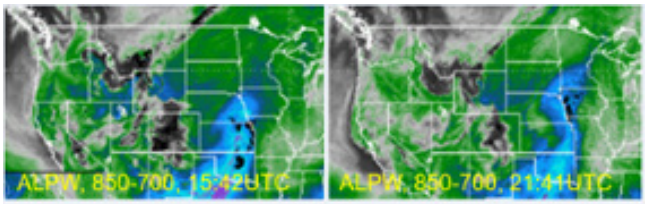

(Courtesy of Sheldon Kusselson)

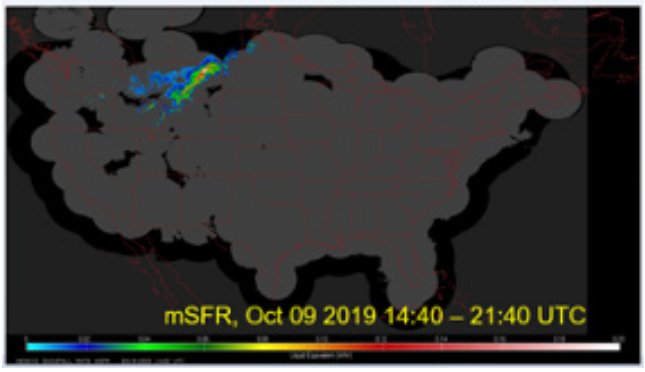

In the mSFR image below, the finer resolution pixels are MRMS and the coarse resolution pixels SFR. Ground observations are in magenta and SN indicates snowfall. As shown by the ground observations, large areas of snowfall not detected by radar were captured by the SFR product including the intense snowfall at the border of North Dakota, Minnesota, and Canada.

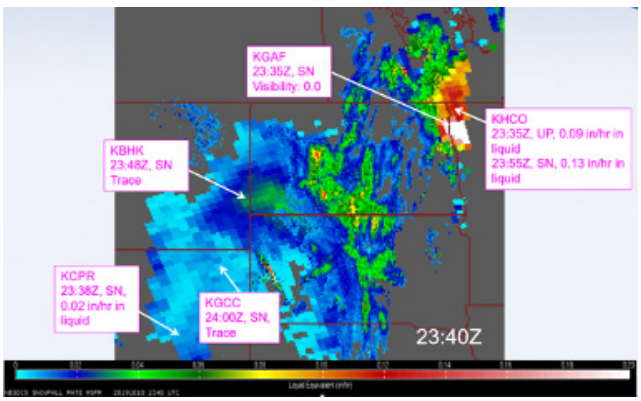

SUMMARY AND FUTURE WORK

Since the first SFR product came online, it has fulfilled its mission to provide much needed gap-filler snowfall measurements in areas with sparse surface weather observations, and/or limited ground radar coverage. While remaining true to its original mission, the SFR product has undergone several evolutions, which have significantly enhanced its quality. What started as a land only product, now—as a result of requests and feedback from user communities—includes a set of experimental ocean extension (over ice-free ocean, sea ice, coast) snowfall detection algorithms for ATMS. The focus of the ongoing research is to develop an ocean snowfall rate algorithm for the ATMS instrument on the S-NPP and NOAA-20 satellites.

In addition, a deep neural network snowfall detection algorithm has been developed. The algorithm, which is derived from ATMS, can detect snowfall in cold regions. Thus far it is showing promise and utility in test runs, and has had good agreement with snowfall analyses.

From that original SFR came several variations and byproducts over the years. For example, the radar-satellite blended product (mSFR)—a byproduct with enhanced spatial coverage and temporal resolution, as well as an additional tool in the weather forecasting toolkit.

And, there's so much more to the SFR as Meng and her colleagues continue to add enhancements. Future efforts include new satellite missions—JPSS-2 in 2022, and MetOp-SG (A1 and B1) and GOSAT-GW in 2023—to the SFR suite and mSFR. The science team is also looking to improve the mSFR blending technique using data fusion, and also making enhancements to spatiotemporal data matching. ❖

Story Source

Materials obtained from JPSS December 2020 Science Seminar titled "Enterprise Snowfall Rate and Radar-Satellite Blended Snowfall Rate Products."

References

Kongoli, C., H. Meng, J. Dong and R. Ferraro, 2020. Ground-based assessment of snowfall detection over land using polarimetric high frequency microwave measurements, Remote Sens. 2020, 12, 3441; doi:10.3390/rs12203441.

Meng, H., C. Kongoli, and R.R. Ferraro, 2020. A 1DVAR-based snowfall rate algorithm for passive microwave radiometers, Satellite Precipitation Measurement, Levizzani, V., C. Kidd, D.B. Kirschbaum, C.D. Kummerow, K. Nakamura, F.J. Turk, Eds. Advances in Global Change Research, 67, Springer Nature, Cham, 297-313, doi: 10.1007/978-3-030-24568-9_17.

You, Y., H. Meng, J. Dong, S. Rudlosky, 2019. Time-lag correlation between passive microwave measurements and surface precipitation and its impact on precipitation retrieval evaluation, Geophys. Res. Letter, 46, 8415-8423, doi: 10.1029/2019GL083426.

Ferraro, R., H. Meng, B. Zavodsky, S. Kusselson, D. Kann, B. Guyer, A. Jacobs, S. Perfater, M. Folmer, J. Dong, C. Kongoli, B. Yan, N. Wang, and L. Zhao, 2018. Snowfall rates from satellite data help weather forecasters, Eos, 99, doi: 10.1029/2018EO096715.

Kongoli, C., H. Meng, J. Dong and R. Ferraro, 2018. A Hybrid snowfall detection method from satellite passive microwave measurements and global weather forecast models, Quarterly Journal of Royal meteorological Society, 144(S1), 120-132, doi:10.2002/qj3270.

Meng, H., J. Dong, R. Ferraro, B. Yan, L. Zhao, C. Kongoli, N. Wang, and B. Zavodsky, 2017. A 1DVAR-based snowfall rate retrieval algorithm for passive microwave radiometers, J. Geophys. Res. Atmos., 122, doi:10.1002/2016JD026325.

Kongoli, C., H. Meng, J. Dong and R. Ferraro, 2015. A Snowfall detection algorithm over land utilizing high-frequency passive microwave measurements—Application to ATMS. J. Geophys. Res. Atmos., 120(5), 1918-1932. doi: 10.1002/2014JD022427.

Weng, F., X. Zou, X. Wang, S. Yang, and M. D. Goldberg, 2012. Introduction to Suomi national polar-orbiting partnership advanced technology microwave sounder for numerical weather prediction and tropical cyclone applications, J. Geophys. Res., 117, D19112, doi:10.1029/2012JD018144

Contributions

The information in this article is based, in part, on the December 15, 2020 JPSS science seminar presented by Huan Meng (NOAA/NESDIS/Center for Satellite Applications and Research (STAR). It also features the research efforts of:

Jun Dong[2], Yongzhen Fan[2], Cezar Kongoli[2], Yalei You[2], Ralph Ferraro[1], Banghua Yan[1], Limin Zhao[3], Kris White[4,5], and Emily Berndt[4]

[1]NOAA/NESDIS/Center for Satellite Applications and Research (STAR)
[2]University of Maryland/ESSIC/Cooperative Institute for Satellite Earth System Studies (CISESS)
[3]NOAA/NESDIS/Office of Systems Architecture and Advanced Planning (OSAAP)
[4]NASA/MSFC/Short-term Prediction Research and Transition Center (SPoRT)
[5]NWS/Huntsville, AL Weather Forecast Office

ADAPTING TO LATITUDES AND ATTITUDES:

AN ALASKAN METEOROLOGIST FORECASTS FIRE WEATHER IN SOUTHERN CALIFORNIA

The information in this article is based, in part, on the February 22, 2021, JPSS science seminar presented by Eric Stevens, Fire Weather Program Manager, Alaska Interagency Coordination Center.

Photograph: Eric Stevens, Alaska Interagency Coordination Center. The image above, taken from a weather station on the morning of December 13, 2020, shows smoke from the Beaumont Fire near Riverside, California as it billows against the rising sun.

ALL HANDS ON DECK

Wildfires can occur anywhere, from remote forested or grassland areas, where they may stay and even remain unnoticed, to woodland settings where people live. Whether natural or man-made, wildfires can have substantial impacts on their surrounding environment and also on social and economic systems. In the United States, as in many parts of the world, every year brings with it new risks of wildfires.

By the beginning of January 2021, Eric Stevens, a Predictive Services meteorologist at the Alaska Interagency Coordination Center (AICC), was nearing the end of a work detail assignment in Riverside, California, outside of Los Angeles where he had been deployed since the middle of September 2020. The AICC is one of 11 Geographical Area Coordination Centers (GACCs) across the country. Ten of these are shown in the map on the right, with the National Interagency Coordination Center housed in Boise, Idaho as well. GACCs are focal points for managing and mobilizing resources (people, aircraft, and ground equipment) during emergency incidents including wildland fires. In a nutshell, you send the fire troops where the fires are.

For example, "in 2019, many crews and managers from the continental United States, or CONUS, were detailed to Alaska to help support wildfire events in a season that saw upwards of two and half million acres burned," he explains. Compared with 2019, Alaska in 2020 had a relatively mild wildfire season. "In 2020, fewer than 200,000 acres burned. As a result many crews and managers from Alaska were detailed to CONUS (especially California) to help," he adds.

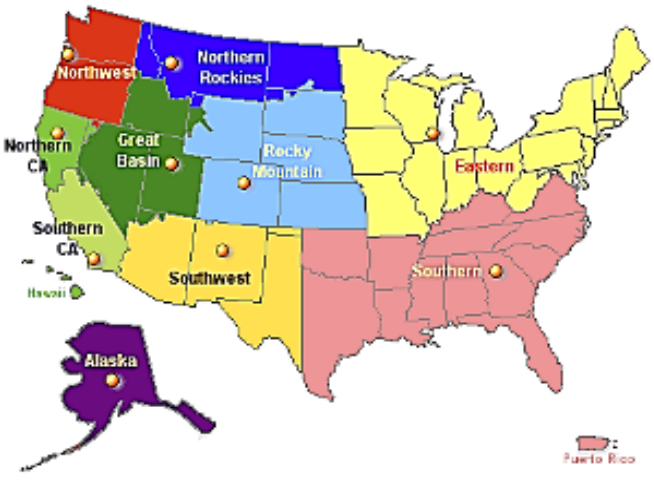

Stevens has been in Alaska since 1993. He says Alaska's nicer winters are what drew him to the area from his native North Dakota. He served as a meteorologist for the National Weather Service (NWS) in Nome, Anchorage, and Fairbanks until 2011. The following year, he joined the Geographic Information Network of Alaska (GINA) where he worked as a Science Liaison for about six years before returning to operational forecasting in 2019 to serve in his current role as the AICC Fire Weather Program Manager. In this role, Stevens provides meteorological decision support to ground crews and wildland fire agencies such as the Alaska Fire Service and the U.S. Department of the Interior. In addition to providing daily briefings and outlooks, this position requires extensive coordination among the various players involved in combating wildland fire in Alaska, including the NWS, wildfire crews and land managers. So, as GACC meteorologists do, Stevens utilizes several datasets relevant to fire behavior, to develop customized analysis and forecasts of weather and the impact of weather on the burnability of the landscape. These datasets include information such as moisture content, fuel combustibility, wind speed and direction, temperature, as well as the impact of terrain on each of these parameters.

ON THE WATCH—24/7

A suite of environmental satellite systems—including some which orbit the Earth just a few hundred miles above its surface, and some which orbit it thousands of miles out in space—keep a constant watch on the planet. In high latitude areas like Alaska and other regions near the poles, imagery from polar orbiting satellites play an outsized role, Stevens says. He explains that polar-orbiting satellites provide more passes per day over Alaska than over the CONUS. Due to the curvature of the Earth, geostationary satellites looking at Alaska suffer from a large viewing angle and associated problems such as parallax and degraded spatial resolution. This combined with a dearth of in-situ observations and radars in Alaska make polar-orbiting satellites a significant source of weather information in Alaska. In fact the Joint Polar Satellite System (JPSS) satellites—NOAA-20 (as primary), and the Suomi National Polar-orbiting Partnership (Suomi NPP) as secondary—constitute the main weather observation satellite system for Alaska and the Polar Regions, where they provide 'nowcasting' capabilities for predicting weather in locations that are not as visible to geostationary satellites. Their datasets are deployed in various applications that run the gamut from weather forecasting, oceanography, coastal erosion, vegetation health, flooding, hydrology, urban growth, to fire weather forecast operations.

NOAA-20 and Suomi NPP are part of a constellation of NOAA and NASA satellites that detect and monitor fires. The pair carry several state-of-the-art instruments including the Visible Infrared Imaging Radiometer Suite (VIIRS) which, Stevens says, "plays so many varied roles vital to supporting fire weather operations." The VIIRS instrument, for example, has the capability to provide the location of fires, as well as an indication of their intensity through the parameter called Fire Radiative Power (FRP). VIIRS also has a Day/Night Band (DNB) that's sensitive to very low levels of visible light at night. It produces a form of visible imagery that makes it possible to track fires at night.

2020: ENTER THE "GIGAFIRE"

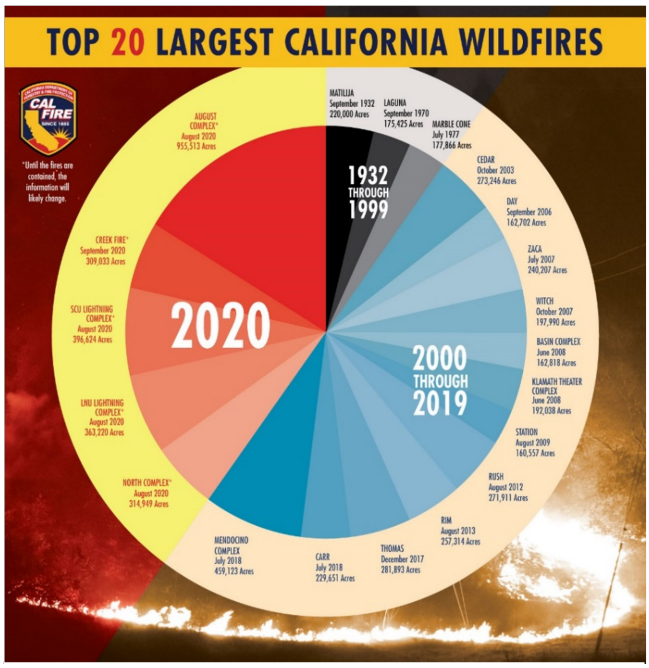

Image credit: CAL FIRE. https://twitter.com/cal_fire/status/1311722710284693505

In 2020, a pandemic upended day-to-day lives across the globe. Activities were marked with and shaped by phrases, words and expressions like "lockdown," "super-spreader event," "community spread," "social distancing," "flatten the curve," and "WFH (work from home)." But it wasn't just the pandemic. There were other notable events that people grappled with, including a record-breaking heatwave in the western U.S. and wildfires in California.

As of the end of the year, more than four million acres of land had burned in California. Wildfires had once again set records. Five of these ended up on the list of largest fires recorded in the state. One would even earn the state its first Gigafire—a designation for fires that consume at least a million acres. It would also be one of many to prompt calls for resources from GACCs across the country to assist in California.

INSIGHTS FROM CALIFORNIA

Stevens' task was to provide fire weather operational forecasting support to the Southern California Geographic Area Coordination Center (OSCC). Here, he would receive firsthand insight to the operational structure, work and

August Complex, September 23, 2020

information flow at the OSCC. He would also encounter different forecast challenges and environmental sensitivities. Stevens says he was also interested to see what the imagery from polar-orbiting satellites was being used for at present and maybe possibilities for the future in the much lower latitudes.

To better understand the forecast challenges and environmental sensitivities, Stevens investigated several environmental factors at play. On his list were typical ones, such as:

The seasonal spring rains, which ended in April;

Dry and hot weather in mid-August;

Consistently dry and occasionally hot weather then continued into the early fall; and

Santa Ana winds became more frequent in the fall and early winter.

And some which he considered "quite unusual" like the significant lightning event on August 15th, including ample dry lightning, which ignited more than 500 individual fires that it was even "described by NWS San Francisco as 'insane'," says Eric. He explains that while there's nothing unusual about the season-ending rains that typically descend southward along the west coast in the fall, this time they "were delayed by the La Niña phase of ENSO."

SEASONAL RAINS

Stevens noted a dry start to the 2020 season in Riverside, California, which picked up in March and continued into April before flatlining for the remainder of the year, albeit with a slight uptick in accumulation towards the end of 2020.

The graph, shown below, of accumulated precipitation at Riverside, California, in 2020 indicates that the normal wet season early in the year did occur, but only yielded roughly half the normal amount of rain. The usual dry season began in the spring and then, unusually, persisted almost uninterrupted until the end of the year. The meager wet season early in the year, combined with a delay in the arrival of seasonal rains late in the year, meant that both live and dead plant matter on the landscape were primed for fire.

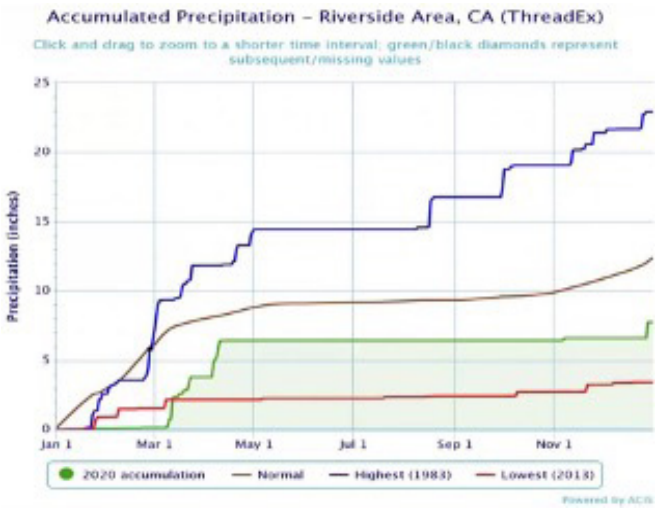

DRY AND HOT WEATHER

According to the National Climate Report (NOAA, 2021), most of the contiguous U.S.

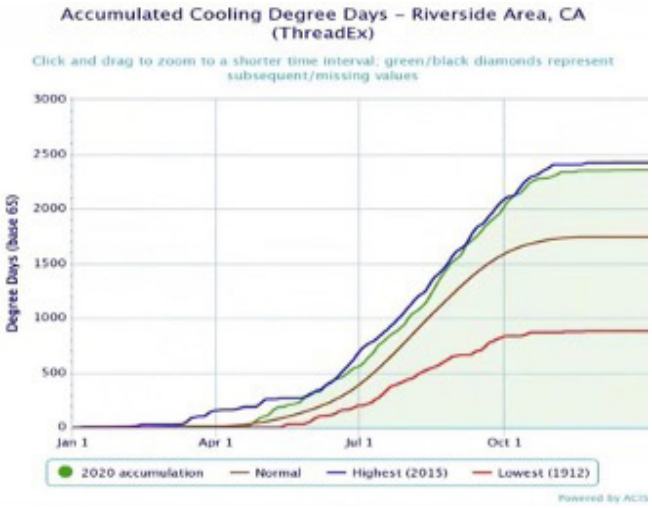

experienced above-average temperatures during 2020. In Riverside, temperatures soared higher than normal for much of the year. The graph (above) depicting the accumulation of "cooling degree days" shows how temperatures in 2020 were almost as warm as in the record year of 2015. The takeaway message from these graphs of precipitation and temperature is that the wildfires in 2020 were facilitated by the long-term drought and heat. As we will see later, with the broad-scale stage thus set, any transitory weather events that included lightning were likely to lead to many new fires.

Hot and dry conditions can increase the probability of wildfires as they dry out trees and vegetation, providing fuel.

LA NIÑA ARRIVES

In addition, in August 2020, NOAA announced that La Niña conditions were present and expected to persist through the winter. La Niña is associated with unusually cold sea surface temperatures in the central and eastern equatorial Pacific. It happens when warm ocean water is pushed westward from South America toward Indonesia. As the warm water moves west, colder water floats to the surface to take its place. La Niña delays the normal movement of the jet stream from north to south through the fall and early winter. Wildfire seasons in California typically end in the fall with the arrival of seasonal rains escorted inland by the jet stream. But in La Niña years, as was the case in 2020, the jet stream stays further north, thereby

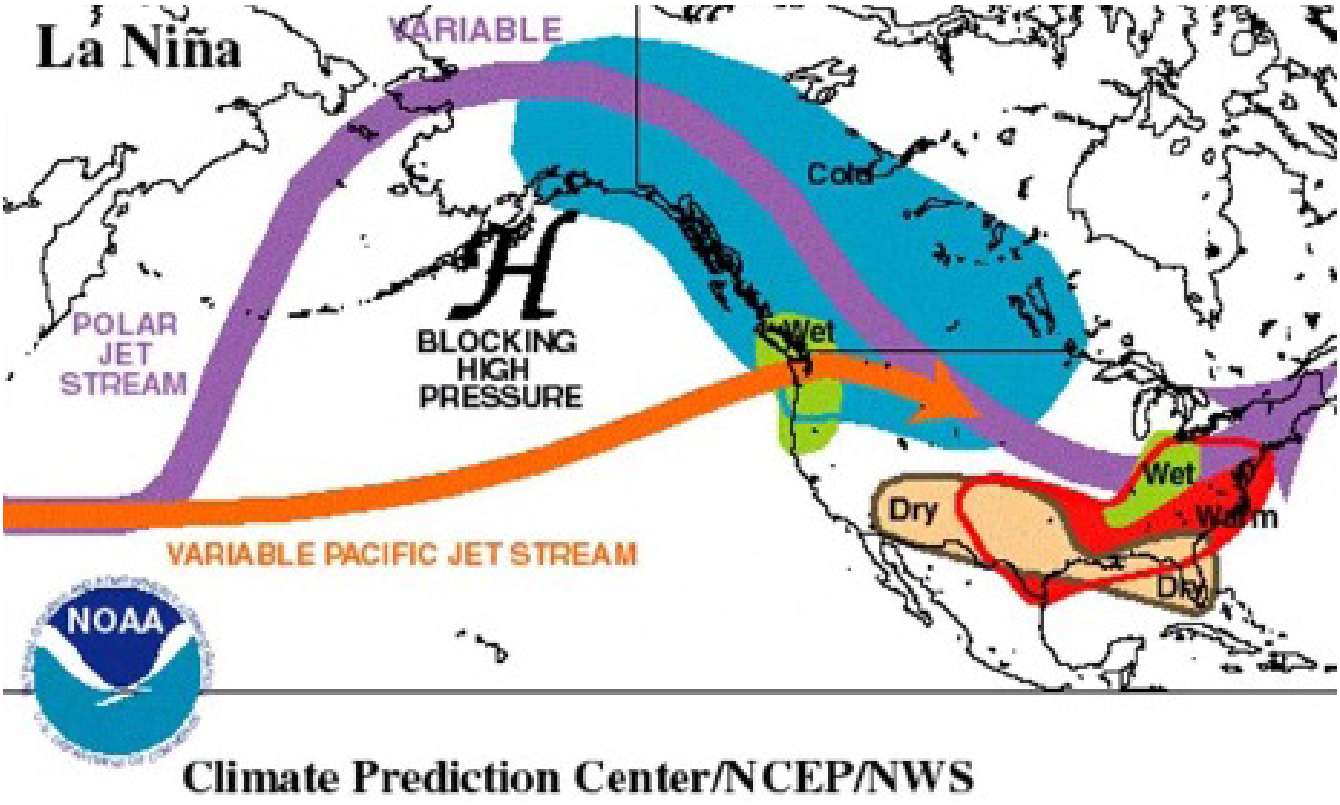

steering moisture into the Pacific Northwest, but leaving the desert southwest and much of California with persistently clear skies.

DRY LIGHTNING OUTBREAK

There's nothing too unusual about lightning igniting a wildfire, unless, of course, it's dry lightning, which is produced by thunderstorms without rain nearby—or at least not to the visible eye. There actually is rain, but it evaporates before hitting the ground.

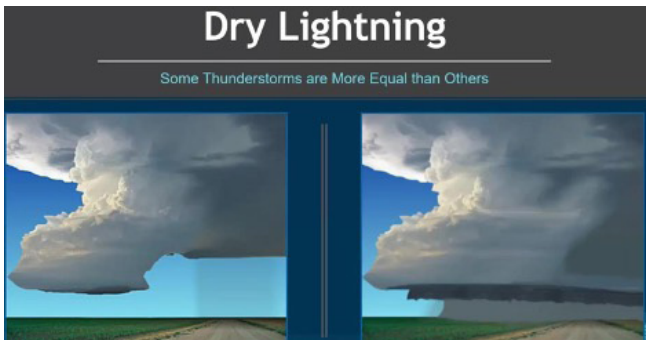

In mid-August, parts of Central and Northern California were burning as a result of dry lightning. The bolts stocked massive wildfires, some of which merged to form record setting wildfires, such as the August Complex.

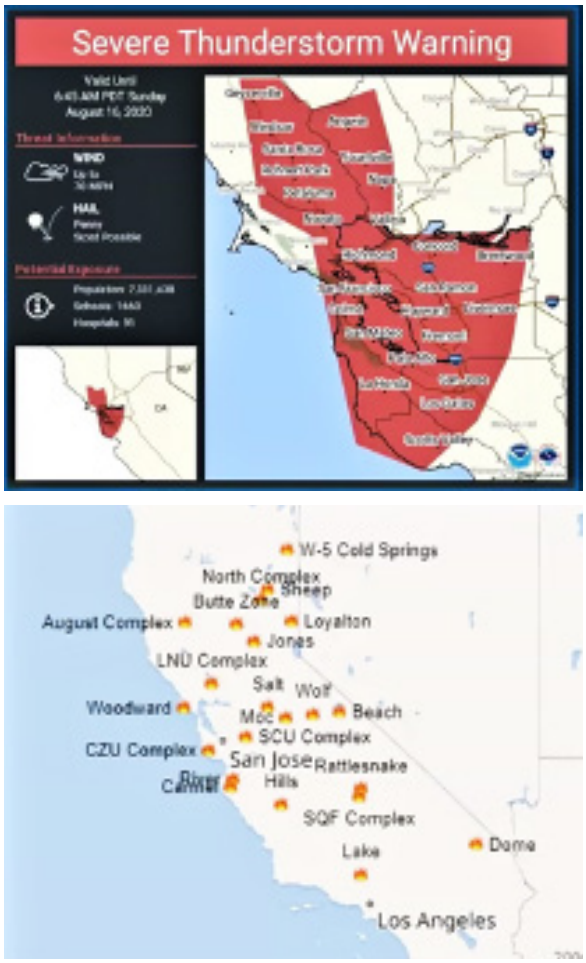

Severe Thunderstorm warning from the NWS, San Francisco (top). Some of the fires started by the mid-August lightning outbreak (bottom).

Stevens says that on occasion the wildfire exhibited “extreme wildfire behavior,” including “plume-dominated” fire behavior in which the enormous amount of heat released by a wildfire enhances the vertical lift over the fire, thereby drawing in more oxygen at the surface and feeding the wildfire even more.

On August 30, the VIIRS instrument captured several heat signatures from blazes still burning across large swaths of the state. It also captured smoke plumes aloft as well as a marine layer just offshore the central and southern coastlines as shown in the image below.

The VIIRS instrument captured the image above on August 30, 2020. It shows heat signatures (red dots) from several fires as well as clouds associated with a cooler marine layer just offshore the central and southern California coastlines.

Wildfires also release harmful pollutants including particulate matter and other toxic gases into the atmosphere. Air pollution from inhalable particles 2.5 micrometers or smaller, or PM2.5, can cause a range of serious health issues, which, according to the Environmental Protection Agency (EPA) include coughing, shortness of breath, decreased lung function and heart attacks.

The JPSS OMPS instrument takes global daily measurements of the distribution of ozone and other constituents in the atmosphere. On August 30, an “aerosol index,” or AI generated from the Suomi NPP OMPS instrument showed the presence of aerosols from the fires. The AI value is related to both the thickness and height of the atmospheric aerosol layer. The scale intervals range from 0.0 (low) to 5.0 (high). Higher concentrations of aerosols can impact visibility or public health. In this case the aerosols found (see figure below) were mostly in the moderate range (yellow) with some higher range areas (red). The AI also helps to identify and track long-range transport of aerosols that move along jet streams.

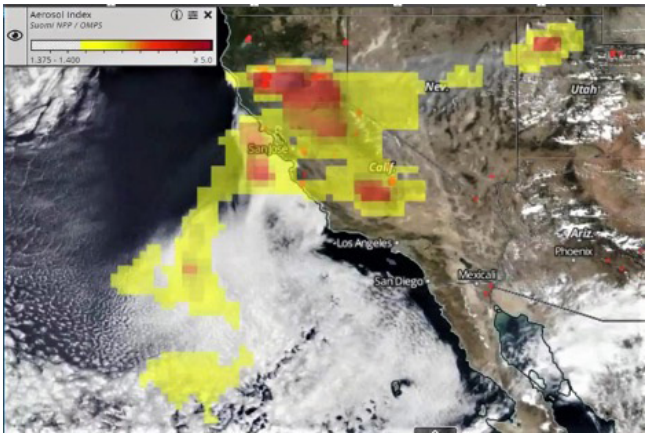

A RESPITE IN JANUARY 2021.

In January 2021, an atmospheric river originating from the subtropical Pacific Ocean brought an end to California’s months-long wildfire events. Measurements from several instruments, including the Advanced Technology Microwave Sounder (ATMS) onboard the NOAA-20 and Suomi NPP satellites, enabled forecasters to observe the atmospheric river that brought record-shattering amounts of precipitation to California.

Atmospheric rivers are long, concentrated moisture rich areas in the atmosphere that stretch over hundreds to thousands of miles. They can be found in any part of the globe. Per NOAA, atmospheric rivers are responsible for most of the horizontal transport of water vapor outside of the tropics. Forecasters use various data, including total precipitable water (TPW), to identify atmospheric rivers. Atmospheric TPW as defined by NOAA Science on a Sphere “is the amount of water that can be obtained from the surface to the “top” of the atmosphere if all of the water and water vapor were condensed to a liquid phase.”

Microwave sensing instruments such as ATMS can see through cloud cover and all but heavy rainfall which allows them to provide information under almost all weather conditions.

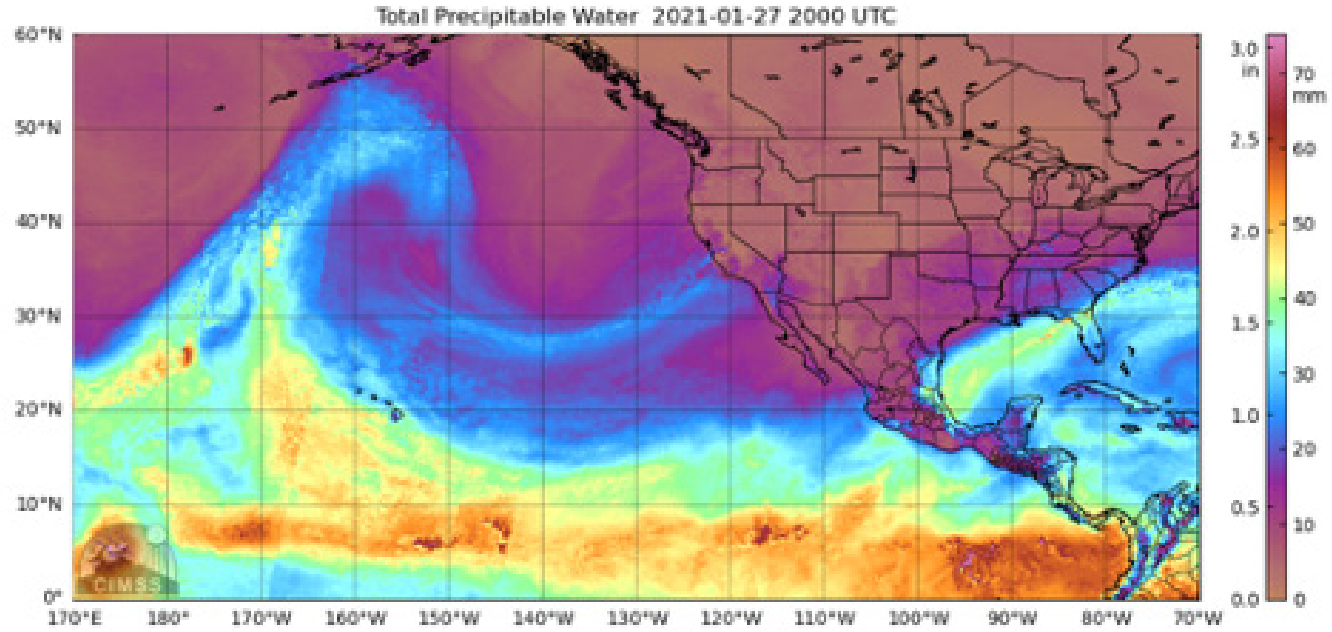

Example of CIMSS MIMIC-TPW product from January 27, 2021, showing rich moisture moving onto the southern California coast. 2000 UTC January 27, 2021. Credit Tony Wimmers, CIMSS

In January 2021, the Morphed Integrated Microwave Imagery at CIMSS–TPW (MIMIC-TPW) showed the atmospheric river of moisture moving over the Pacific Ocean toward the U.S. West Coast. MIMIC–TPW is a satellite derived product from the University of Wisconsin–Madison Cooperative Institute for Meteorological Satellite Studies (CIMSS), which uses retrievals of TPW over the ocean, from multiple microwave sensors. The stripe of blue extending from northeast of Hawaii into Southern California in the MIMIC-TPW image below represents a high moisture content overlapping with the jet stream. Such an arrangement can bring long-lasting heavy rains where the atmospheric river makes landfall.

THERE'S ALWAYS MORE TO EXPLORE WITH JPSS

Severe wind events known as breaking mountain waves typically occur in Alaska's mountainous areas, especially in the winter season. Stevens said that breaking mountain waves, "need a critical layer at the elevation of the terrain crest, and along with it, a mid and upper level flow that's perpendicular to the mountain barrier. They also require a temperature inversion as well as a maximum in wind speed at the elevation of the mountain tops. And a temperature inversion at the elevation of the mountain tops, especially on the upstream side of the barrier."

"Are mountain wave mechanisms present during strong Santa Ana events?" he said. "And can temperature profiles from the NOAA Unique Combined Atmospheric Processing System (NUCAPS) help identify this critical layer? And, maybe help us identify it earlier than we would otherwise be able to do with conventional radiosondes, which are typically only taken at 00Z and 12Z at nearby sites including the Vandenberg Air Force Base and the San Diego NWS," he adds. NUCAPS retrieves profiles of atmospheric temperature and moisture as well as trace gases from microwave and hyperspectral infrared sounders. He notes that while "NUCAPS cannot observe winds, it can see inversions and tell you how high they are off the ground." A downside however is that "the vertical resolution of NUCAPS might not be fine enough to detect subtle inversions. We will need to investigate a few events to learn the answer. He adds that in his experience, "the quality of NUCAPS profiles is marginal down in the boundary layer near the surface of the Earth, but in the case of Santa Ana winds the hoped for temperature inversion is elevated well above the noisy boundary layer. We also have the advantage of a couple of nearby conventional

radiosonde sites that can be used as truth against which to verify the NUCAPS profiles."

THE LOOK AHEAD

For the future, Stevens is looking for an opportunity to explore whether NUCAPS may provide insights during stronger Santa Ana wind events by identifying elevated temperature inversions over complex terrain. In addition to studying events during 2020 in hindsight, events yet to occur in 2021 could be considered in real time with an eye toward investigating the applicability of NUCAPS. And who knows, perhaps such learning could yield techniques applicable in Alaska. ❖

Story Source

Materials obtained from JPSS February Science Seminar titled "JPSS and the 2020 Wildfire Season in California."

References

NOAA National Centers for Environmental Information, State of the Climate: National Climate Report for Annual 2020, published online January 2021, retrieved on February 24, 2021 from https://www.ncdc.noaa.gov/sotc/national/202013.

NOAA. 2015. What are atmospheric rivers? https://www.noaa.gov/stories/what-are-atmospheric-rivers. Accessed February 25, 2021.

DETECTION OF ALGAL BLOOMS IN CHALLENGING CONDITIONS

The information in this article is based, in part, on the April 26, 2021, JPSS science seminar presented by Alex Gilerson, NOAA CESSRST, City College New York (CCNY). It features work being done at Optical Remote Sensing Laboratory, City College of the City University of NY together with Sam Ahmed and Mateusz Malinowski, Ahmed El-Habashi, NRL-DC, Vincent Lovko, Mote Marine Laboratories, Sarasota FL, Dr. Richard P. Stumpf and Michelle C. Tomlinson, NOAA National Centers for Coastal Ocean Science, Silver Spring, MD.

Dead fish on beach near Sarasota, Florida, killed by toxins from a 2018 red tide. Credit: NOAA National Centers for Coastal Ocean Science. https://scijinks.gov/red-tide/

According to the National Ocean Service (NOS) the ocean produces roughly 50–80% of the world's oxygen and absorbs 50 times more carbon dioxide than our atmosphere. The largest contributors to these processes, according to the NOS, are "oceanic plankton—drifting plants, algae, and some bacteria that can photosynthesize." They form the base of the marine food chain. Phytoplankton are microscopic algae, which, similar to land plants, use chlorophyll to photosynthesize.

When phytoplankton or algal blooms grow uncontrollably, they can produce toxins, which can be harmful to humans, marine life, and other animals that depend on marine life. These events are referred to as Harmful Algal Blooms (HABs). The overgrowth of algae can also deplete oxygen and block light from underwater plants and animals.

According to the Woods Hole Oceanographic Institution (WHOI) U.S. National Office for Harmful Algal Blooms, virtually every coastal country in the world is susceptible to HABs. In the last few decades, a number of factors including rising ocean surface temperatures and anthropogenic factors, have led to an increase in the frequency and severity of HABs across the globe, scientists say. HABs can hurt coastal economies that are based on healthy marine and freshwater environments. For example, the NOS estimates roughly $82 million in annual economic losses to the seafood, restaurant, and tourism industries because of HABs. As a result, harmful algal blooms are considered major events, and are closely monitored with the goal to mitigate their impact on ocean life, economy, and recreational activities.

SATELLITE CAPABILITIES FOR SENSING TOXIC TIDES

Satellite ocean color data provides important information on chlorophyll, including the

variability in the distribution and concentration of phytoplankton and other oceanic particles. Algal blooms are often associated with the changes of water color, which depends on the type of phytoplankton species causing blooms and corresponding absorption and scattering features of phytoplankton particles. Ocean Color (OC) satellite sensors measure the spectra of light from the ocean, providing important information about water composition.

On the West Florida Shelf (WSF) harmful blooms, due to the increased amount of *Karenia Brevis (KB)* species, are a frequent occurrence. Even at relatively low chlorophyll concentrations [Chl], typically below 10 mg/m^3, these toxic blooms can lead to grave consequential problems, including the deaths of marine mammals and fish (as shown in the image above), respiratory irritation in humans, and even beach closures.

For many years, the NASA Moderate Resolution Imaging Spectroradiometer (MODIS) sensor on the Aqua satellite has delivered OC data for ocean monitoring. Now, after almost two decades of producing scientifically sound data, the sensor, which has far exceeded its six-year mission life span, is beginning to show signs of degradation. Even so, the capabilities for ocean monitoring have significantly expanded following several launches of a new generation of instruments. These include the National Oceanic and Atmospheric Administration (NOAA) operated Visible Infrared Imaging Radiometer Suite (VIIRS) sensors in 2011 on the Suomi National Polar-orbiting Partnership (Suomi NPP) and in 2017 on the NOAA-20 satellite platforms and Ocean and Land Colour Instrument (OLCI) sensors on Sentinel-3A and B satellites, which are operated by the European Space Agency. In April 2021, Alex Gilerson, a professor in the Electrical Engineering department at the City College of the City University of New York (CCNY), gave a presentation on a collaborative effort between researchers from CCNY and MOTE Marine Laboratory to develop detection techniques for KB blooms based on the VIIRS sensors.

RESEARCH AND INNOVATION: NO FLUORESCENCE CHANNELS? NO PROBLEM! THERE'S A NEURAL NETWORK FOR THAT.

It takes relatively low chlorophyll concentrations [Chl] for KB toxic blooms to wreak havoc including the deaths of marine mammals and fish, respiratory irritation in humans, and beach closures.

–Alex Gilerson, City College of the City University of New York, 2021

Various means are used to detect, quantify and track KB HABs. Among these are normalized fluorescence height (nFLH) and Red Band Difference (RBD) techniques, which rely on "a fluorescence band near 680 nanometers (nm), which is available on MODIS (678 nm) and OLCI (681 nm) but not available on VIIRS," Gilerson says. With more planned launches of the VIIRS sensors on JPSS platforms, VIIRS and OLCI sensors are expected to be the main workhorses in OC.

Given the expected transition to VIIRS data over time, the CCNY team devised a neural network (NN) algorithm, which uses 486, 551 and 671 nm bands. The figure on the right shows that the algorithm performs very similar to the VIIRS [Chl] OC3V algorithm with [Chl] < 10–15 mg/m^3 in moderate coastal waters farther from the coast. The NN algorithm is described in several

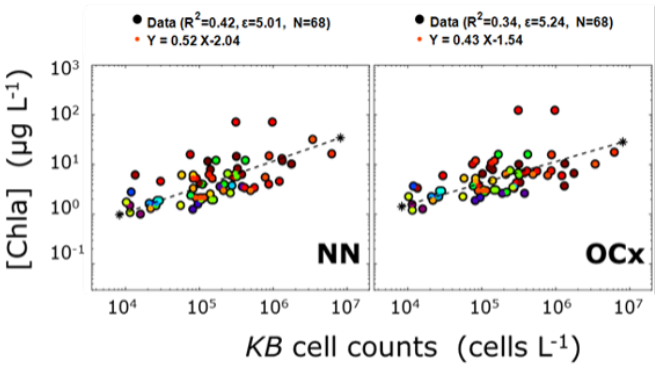

papers including Gilerson et al, 2010, and El-Habashi et al, 2016. In El-Habashi et al, 2019, the algorithm tested well on satellite and field data and demonstrated several advantages over the standard VIIRS [Chl] algorithm, especially near the coast (see figures on the right).

In addition, robust algorithms for the monitoring of ocean features for these sensors have been developed or are in progress. What's more, some of the algorithms are taking advantage of different spatial and temporal resolutions and band sets of VIIRS and OLCI. This will lead to further algorithm multi-platform integration and improvement of observation frequency.

DETECTION OF HABS IN THE CHESAPEAKE BAY AND LONG ISLAND SOUND

In the Chesapeake Bay—the largest productive estuary on the U.S. East Coast with strong spatial and temporal gradients in water quality and composition—HAB events have been known to adversely impact fish and oyster. There is often occurrence of HABs in the Bay, which affect water quality at [Chl] greater than 30–40 mg/m^3 and often as high as 200 mg/m^3 and more. VIIRS OC3V and NN algorithms typically underestimate [Chl] in such conditions. Detection in such conditions, as has been done using the NIR band at 709 nm on the OLCI sensor, is possible with algorithms that use remote sensing reflectance at NIR/Red band. The National Centers for Coastal Ocean Science (NCCOS) have developed a set of bloom detection products based on these bands to support state agencies in MD and VA along the Chesapeake Bay. The products, which include a special atmospheric correction for bands unique to the OLCI sensor, are routinely available from NOAA's CoastWatch Program.

In addition to the narrow bands in the visible spectrum (412, 443, 486, 551 and 671 nm), VIIRS has an imaging band, which covers a range of wavelengths from 600–680 nm, and according to Gilerson, "opens additional possibilities." The band has an almost rectangular spectral transmission function with the center at 638 nm.

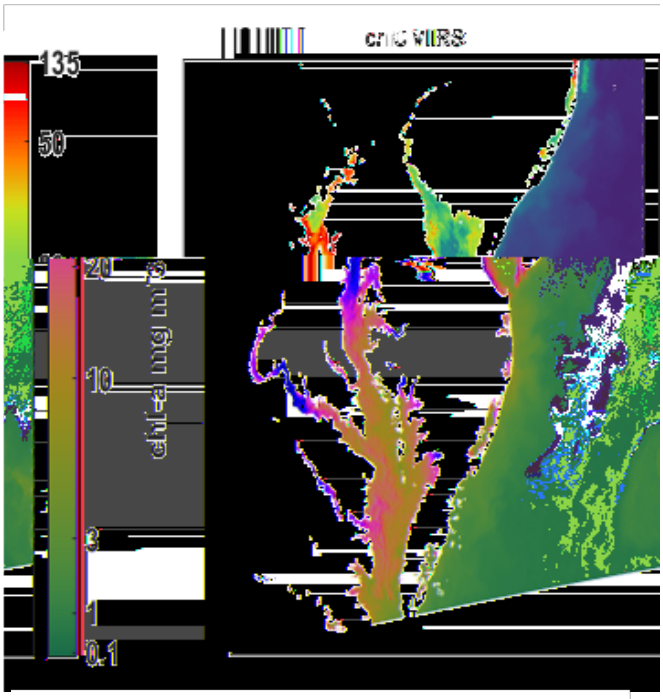

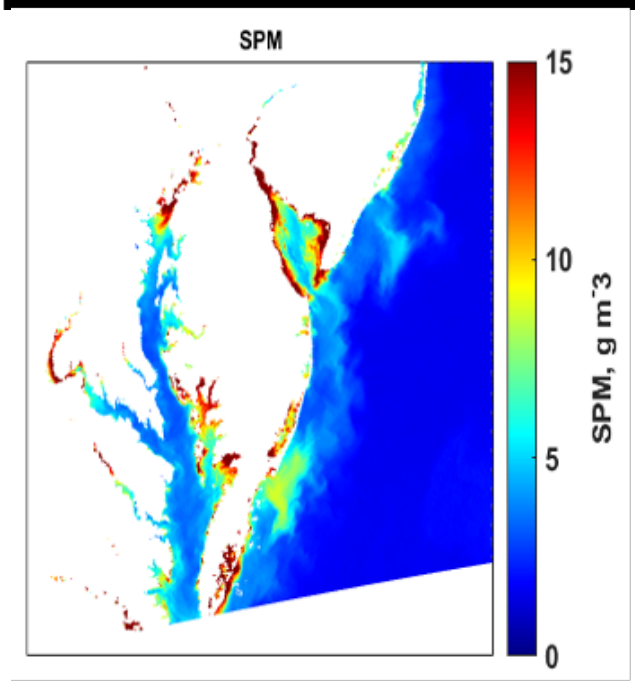

In this case, "the 600–680 nm band radiance covers features related to the increase of specific phytoplankton absorption from very small values at 600 nm to high ones at 675 nm and thus can be sensitive to high [Chl]," Gilerson says. Data for this band at 638_ag (aggregated to 750 m spatial resolution as for other narrow bands) was recently added to the VIIRS images at NOAA CoastWatch. First simple ratio tests for Long Island Sound (LIS) data with water parameters similar to the Chesapeake Bay proved the band's utility in detecting higher concentrations of [Chl] values.

OLCI

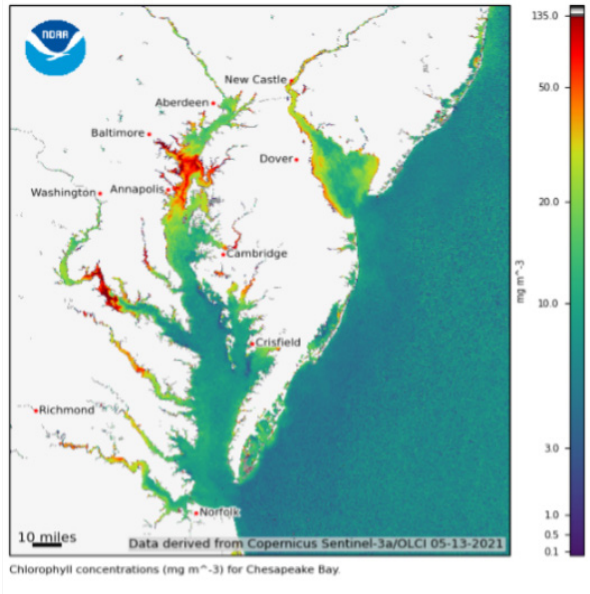

Chlorophyll concentrations (mg m^-3) for Chesapeake Bay

VIIRS

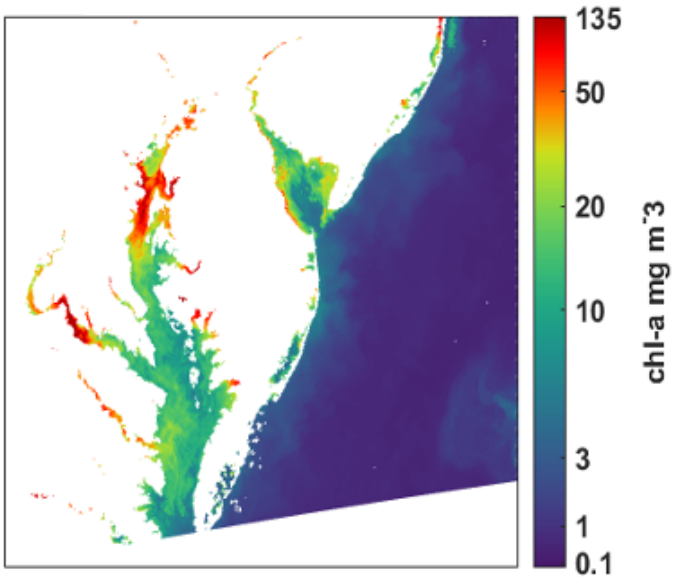

A new algorithm was developed using available band ratios, which include the VIIRS I1 band. The first version of the algorithm with the VIIRS I1 band was calibrated on the field data. In its first application it showed a strong dependence of the estimated [Chl] on the concentration of suspended particulate matter (SPM) as illustrated in the figures above, which show similar [Chl] and SPM distributions. Sediment concentrations were estimated based on the values of remote sensing reflectance at 671 nm.

In the next iteration of the algorithm, the research team corrected for the impact of SPM concentration. They found that the algorithm often underestimates [Chl] at [Chl] < 10–15 mg/m^3, which led them to combine it with the standard OC3V algorithm at [Chl] ≤10 mg/m^3.

Shown above are two images of blooms in the Chesapeake Bay, which were acquired on May 13, 2021. On the left is an OLCI-generated image, which was processed by NCCOS, and on the right is a VIIRS generated image, which was processed with a new algorithm. Two bloom areas are visible: in the Upper Bay to the north and south to Annapolis and in the Potomac River with [Ch] = 50 mg/m^3 (point 'x' and 42 mg/m^3 (point '+'), respectively. Despite the different spatial resolutions (300 m for OLCI and 750 m for VIIRS), "the images are congruent and such similarity was consistent for many other days," says Gilerson.

The algorithm was also validated using VIIRS-in situ matchups within a 10-hour differential and smaller than 0.4 km distance difference between satellite pixels and in-situ points. According to preliminary team results, the time difference has not shown any significant impact on the analysis in the Chesapeake Bay. However, they add that accurate estimation of [Chl] in specific areas requires additional calibration on the algorithm. Something that can only be done when the data on satellite-in situ matchups become available.

The new algorithm was also used in Long Island Sound (LIS) where blooms often occur in February–March in the western parts. In bloom detection tests near the Long Island Sound Coastal Observatory (LISCO) VIIRS imagery processed with the new algorithm showed significantly higher [Chl] values compared to those processed with OC3V (images on next page) with the former confirmed by the field measurements from the LISCO platform.

And there's more to come. In part, due to the complexity of absorption and backscattering spectra of water components variability of CDOM and mineral concentrations in various areas. According to Gilerson, this challenge signifies that the algorithm will probably need to be implemented in a NN format as a modification to the present algorithm.

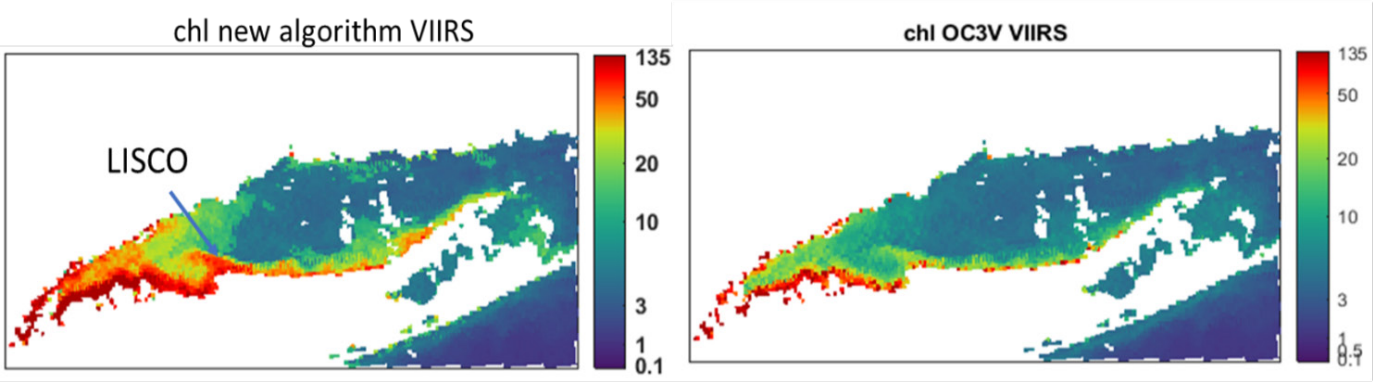

SUMMARY AND THE LANDSCAPE AHEAD

Satellite ocean color data provides important information on chlorophyll including the variability in the distribution and concentration of phytoplankton and other oceanic particles. Ocean color data from instruments such as MODIS, VIIRS, and OLCI provide a way for NOAA scientists to identify, monitor and forecast the location of algal blooms. For many years now, the MODIS instruments have provided OC observations which scientists have used in many applications, including to detect and track HABs on the West Florida Shelf, and in particular KB, which is a dominant species that has been known to wreak ecological and economic havoc in the region.

Having lasted upwards of 18 years, the MODIS era is nearing a close. But its data records, as well as those from previous generations of satellite sensors, will be continued by VIIRS and future satellite sensors. While MODIS has a 678 nm fluorescence channel that is used to detect [Chla] and hence KB HAB retrievals, VIIRS does not. However, innovative techniques such as the neural network approach, which utilizes three existing channels in the visible band, are showing VIIRS to be just as impactful as its peers with fluorescence channels at detecting HABs. In some cases, the NN approach is turning out to be more favorable because it utilizes relatively long wavelengths that are not heavily affected by atmospheric correction. The improvements continue. More recently, a novel [Chla] estimation algorithm for HAB detection at high [Chla] greater than 30–40 mg/m^3, as is often the case in the Upper Chesapeake Bay, was developed utilizing the VIIRS I1 band which covers the 600–680 nm range. Thus far the algorithm provides similar [Chla] distributions as NIR/red algorithm from the OLCI sensor processed by NCCOS.

The OLCI and VIIRS sensors have different temporal and spatial resolutions, something which Gilerson and his team are looking to leverage on the landscape ahead. Their plans include combining data from both sensors with the idea that it will help improve the coverage of HABs from space. ❖

Story Source

Materials obtained from JPSS April Science Seminar titled “Detection of Algal Blooms in Challenging Conditions.”

References

NOAA. How do we forecast harmful algal blooms? National Ocean Service website, https://oceanservice.noaa.gov/facts/hab-forecast.html, 02/26/21.

NOAA. Are all algal blooms harmful? National Ocean Service website, https://oceanservice.noaa.gov/facts/eutrophication.html, 02/26/21.

Alexander Gilerson et al., “ Multi-band algorithms for the estimation of chlorophyll concentration in the Chesapeake Bay “, Proc. SPIE 9638, Remote Sensing of the Ocean, Sea Ice, Coastal Waters, and Large Water Regions 2015, 96380A (October 14, 2015).

El-Habashi, Ahmed et al. “Satellite Retrievals of Karenia Brevis Harmful Algal Blooms in the West Florida Shelf Using Neural Networks and Comparisons with Other Techniques.” Remote Sensing 8.5 (2016): 377.

El-Habashi, Ahmed, Claudia M. Duran, Vincent Lovko, Michelle C. Tomlinson, Richard P. Stumpf, Sam Ahmed, “Satellite retrievals of Karenia brevis harmful algal blooms in the West Florida Shelf using neural networks and impacts of temporal variabilities,” J. Appl. Remote Sens. 11(3), 032408 (2017).

El-Habashi, Ahmed, Sam Ahmed, Michael Ondrusek, Vincent Lovko, “Analyses of satellite ocean color retrievals show advantage of neural network approaches and algorithms that avoid deep blue bands,” Journal of Applied Remote Sensing, 13 (2019).

Wolny, Jennifer L., Michelle C. Tomlinson, Stephanie Schollaert Uz, Todd A. Egerton, John R. McKay, Andrew Meredith, Kimberly S. Reece, Gail P. Scott and Richard P. Stumpf, “Current and Future Remote Sensing of Harmful Algal Blooms in the Chesapeake Bay to Support the Shellfish Industry,” Front. Mar. Sci (2020).

Gilerson, A.A., A. A. Gitelson, J. Zhou, D. Gurlin, W. Moses, I. Ioannou, S. A. Ahmed “Algorithms for remote estimation of chlorophyll-a in coastal and inland waters using red and near infrared bands,” Optics Express,18 (2010).

A. Gilerson, M. Malinowski, E. Herrera, M. Tomlinson, R. Stumpf, M. Ondrusek, “Estimation of chlorophyll-a concentration in complex coastal waters from satellite imagery,” Proc. of SPIE 11752, Ocean Sensing and Monitoring XIII, 2021.

Office of Water. (2013). Impacts of Climate Change on the Occurrence of Harmful Algal Blooms [Fact sheet]. U.S. Environmental Protection Agency. https://www.epa.gov/sites/production/files/documents/climatehabs.pdf

SURFACE WATER RESERVOIR PRODUCT SUITE FROM MODERATE RESOLUTION REMOTE SENSING DATA

The information in this article is based, in part, on the May 17, 2021, JPSS science seminar presented by Huilin Gao, Texas A&M University, with contributions from Gang Zhao, Yao Li, and Deep Shah.

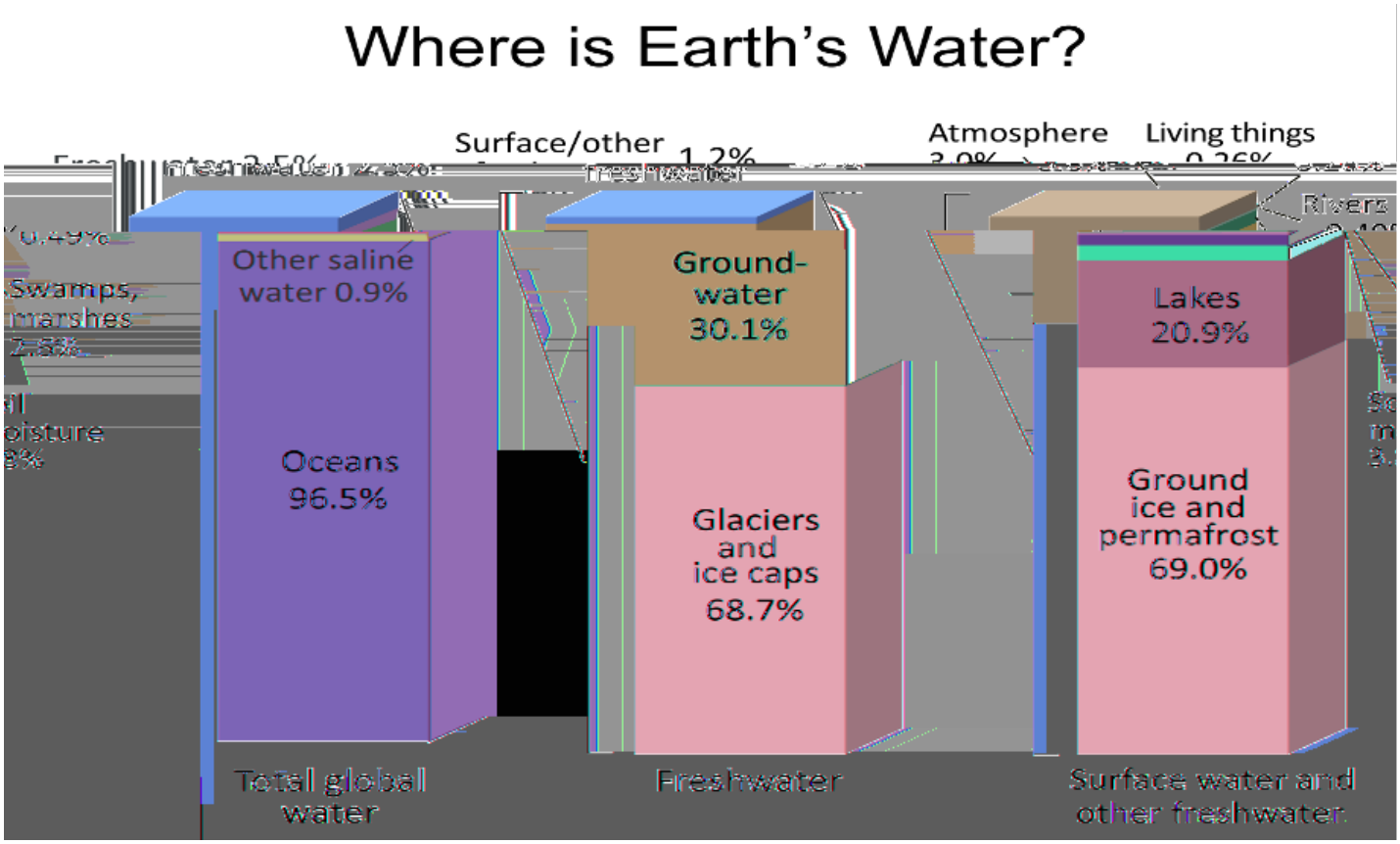

Credit: U.S. Geological Survey, Water Science School. https://www.usgs.gov/special-topic/water-science-school. Data source: Igor Shiklomanov's chapter "World fresh water resources" in Peter H. Gleick (editor), 1993, Water in Crisis: A Guide to the World's Fresh Water Resources. (Numbers are rounded).

Figure showing the distribution of the Earth's water obtained 6/4/2021 from https://www.usgs.gov/media/images/distribution-water-and-above-earth-0

Water covers nearly three-quarters of the Earth's surface. Over 97% of these areas are saline ocean waters, which are not fit for many uses—including irrigation and consumption (by humans and most other living things). The rest—an estimated three percent—is freshwater. However, a significant portion of Earth's fresh water—roughly two percent, according to the U.S. Geological Survey, Water Science School (see bar chart above)—is inaccessible for direct use. The water is either permanent snow or locked away (in glaciers and other ice, underground, in the soil, and/or in the atmosphere). What's left—to meet the world's daily water supply needs—is a little more than one percent of Earth's freshwater, including that coming from the thousands of manmade lakes throughout the world.

Reservoirs—manmade lakes created using barriers or dams across rivers or streams—represent the largest human intervention of freshwater resources. With a global capacity of 7,000–8,300 km^3, they provide many essential

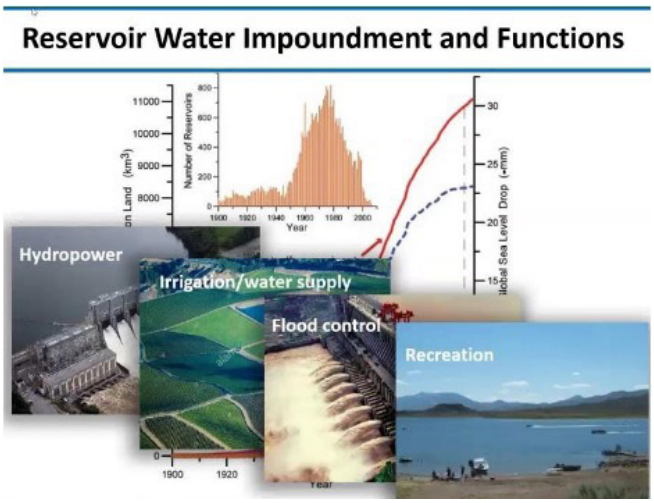

services around the world. These include hydropower generation, irrigation, domestic/industrial water supply, flood control functions, ecosystem services, and recreation. While these freshwater sources constitute only a small fraction of our planet, they play a large and critical role in the planet's ecosystems and economies.

A reservoir receives water from upstream inflow and local precipitation, and it loses water through releases, evaporation, and seepage (relatively small). The balance of these terms determines the reservoir storage. For most functions (except for flood control), the larger the storage volume the more effective the reservoir. Therefore, the loss of surface freshwater creates an important problem—especially in arid and semi-arid regions, which (in addition to having scarce water resources) are prone to high evaporation losses.

WHY DOES THIS MATTER?

"Reservoir evaporation accounts for a significant amount of the losses of the supply of water that is available," says Dr. Huilin Gao, an associate professor in Civil Engineering at Texas A&M University. In a paper titled "NASA's MODIS/VIIRS GlobalWater Reservoir Product Suite from Moderate Resolution Remote Sensing Data," Dr. Gao and her colleagues write that reservoir evaporation losses are critical for water budgeting. Studies have estimated evaporative losses from selected reservoirs and overall regions. For instance, the evaporation volume of Lake Tahoe was found to be larger than the reservoir outflow. The annual evaporation rate of Lake Mead is more than 30 times larger than the surrounding evapotranspiration rate. In Texas, the combined evaporative losses from 200 reservoirs account for 20% of their active storage value. Still, there is a dearth of "reliable evaporation information," due to limited capabilities to monitor reservoir evaporation. These limitations include measurement imperfections, as have been documented from commonly used methods such as pan evaporation. Gao and her coauthors write that only a few (pan evaporation sensors) are sufficiently placed near dams to estimate reservoir evaporation. As a result, this method tends to be imprecise. Other approaches, such as the eddy covariance method are too expensive to use extensively. Further, there is also a lack of knowledge about reservoir storage in some regions (e.g. data-sparse regions or in areas where it is difficult to gather data, such as regions under conflict), and the rules of operation tend to be site-specific (and are typically not shared). The need for real-time global scale data drove Gao and her team to pursue remote sensing as an alternative for filling in such reservoir data gaps. Remote sensing helps minimize the shortcomings of traditional in situ methods. Remote sensing has the ability to continuously monitor the Earth at various temporal and spatial scales. In particular, it provides "long-term, near real-time, global scale capabilities for reservoir monitoring."

ESTIMATING RESERVOIR EVAPORATION LOSSES FROM SPACE

Dr. Gao integrates satellite data in hydrology to study storage variations and evaporation losses over global lakes and reservoirs. Her current research includes a NASA-funded project in which she, Dr. Gang Zhao (Carnegie Institution for Science), and Dr. Yao Li (Texas A&M University), have developed a global water reservoir product suite. They use data from the Moderate Resolution Imaging Spectroradiometer (MODIS) on the National Aeronautics and Space Administration's (NASA) Aqua and Terra satellites, and from the Joint Polar Satellite System (JPSS) Visible Infrared Imaging Radiometer Suite (VIIRS).

Information on the water levels of large lakes and reservoirs is available from several other sources too. Among these are satellite radar altimeters—non-imaging radar sensors, which, over the last three decades have provided data on the world's oceans and seas, rivers, large lakes, and reservoirs. A couple of key benefits of satellite radar altimeters are that they are not dependent on weather conditions, and they provide close to global coverage. However, their small swath widths create revisit time of days instead of hours making them ill-suited for the monitoring of surface water evaporation.

Separate from altimeters, optical remote sensing tools are also being utilized to monitor inland water bodies such as rivers, large lakes, and reservoirs. They provide critical data

Remote Sensing of Reservoir Elevation, Area, and Storage

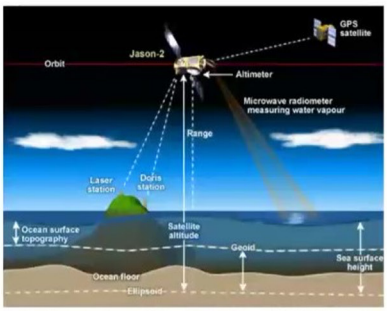

https://www.star.nesdis.noaa.gov/socd/lsa/AltBathy/

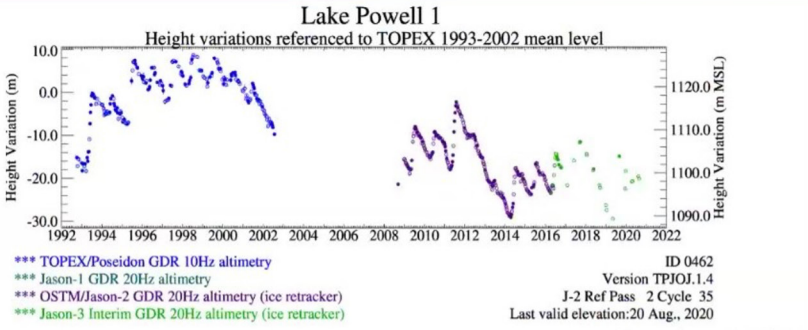

Figure from G-REALM

The water level or height is calculated using a radar signal's round-trip time from the satellite to the surface of the water body.

for global water detection, estimation of reservoir storage, as well as the more unique contribution of Land Surface Temperature (LST) datasets (which scientists use to quantify lake evaporation). While they are mostly limited to daytime viewing (and their field of view is easily hindered by clouds contamination), optical sensors are very advantageous in terms of spatial/temporal resolution, spatial coverage, and long-term data acquisition. Thus, they have been the most commonly used tools for mapping the surface areas of lakes and reservoirs (by classifying optical or near-infrared reflectance data). Satellite instruments providing these data include MODIS, VIIRS, the USGS Landsat series, the European Space Agency's Sentinel-2, and many others. In addition, several global databases (e.g., G-REALM and Hydroweb) are dedicated to monitoring the elevation changes of hundreds of lakes and reservoirs. Since such databases rely on data collected by different sensors, the temporal resolutions, record lengths, and accuracy vary significantly by location.

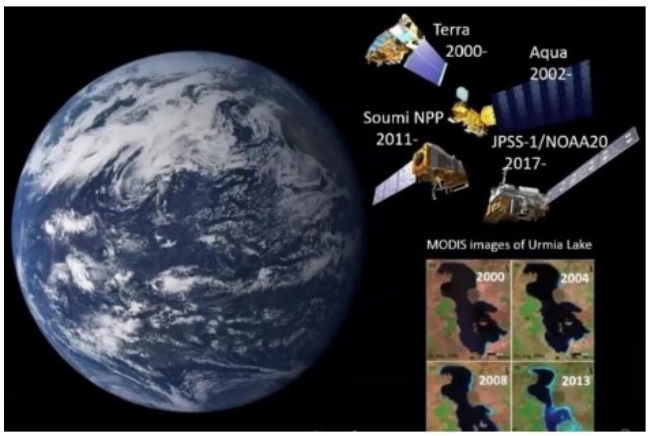

MORE DETAILS ABOUT THE MODIS/VIIRS GLOBAL WATER RESERVOIR PRODUCT SUITE

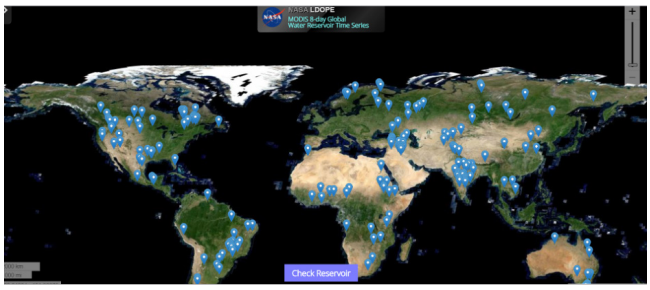

The MODIS/VIIRS product suite was created out of a need for "consistent, comprehensive, long-term, and operationally monitored global scale reservoir products," Gao says. It provides storage and evaporation measurements in two products, eight-day or monthly. It represents the first time that reservoir evaporation has been monitored globally in an operational manner. The image above shows the eight-day MODIS reservoir area time series real monitoring website. https://landweb.modaps.eosdis.nasa.gov/cgi-bin/QS/lake/index.cgi.

Sensor	Product	Measured Parameters	Temporal Resolution	Time Span
MODIS	MxD28C2	Area, elevation, storage	8-day	2000 to present
MODIS	MxD28C3	Area, elevation, storage, evaporation rate and volume	Monthly	2000 to present
VIIRS	VNP28C2	Area, elevation, storage	8-day	2012 to present
VIIRS	VNP28C3	Area, elevation, storage, evaporation rate and volume	Monthly	2012 to present

The product's measurement suite includes area, elevation, storage, and evaporation loss values for 164 reservoirs with a combined area of over 25 square kilometers. This group of reservoirs (locations are shown in the figure on previous page) was selected from the Global Reservoir Bathymetry Dataset. It includes 151 human-made reservoirs (red and blue dots), whose combined storage volume at capacity is roughly 2672 cubic-kilometers (km^3), and 13 regulated natural lakes (yellow dots), whose combined storage volume at capacity is roughly 23,811 cubic-kilometers (km^3). Together they represent 46% of the global capacity. The technique is based on Area–Elevation (A–E) relationships for the identified reservoirs derived by combining altimetry data from multiple satellites with Landsat imagery data.

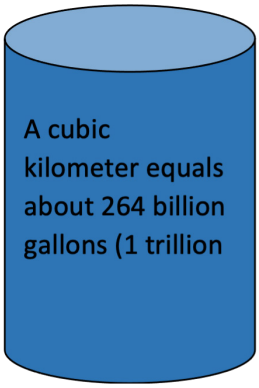

Despite the similarities to traditional radar altimetry products, the MODIS/VIIRS product differs in two important ways compared to RADAR altimetry products alone: First, it can provide reservoir water elevations at an eight-day temporal resolution. Second, it is characterized by a set of continuous and consistent records since 2000 for each of the 164 reservoirs.

Lake Mead

Leading up to the summer of 2021, reports from multiple media outlets and from the U.S. Bureau of Reclamation cited historic drops in the lake's water levels not seen since its creation. Lake Mead, the nation's largest reservoir, was created in the 1930s by the construction of the Hoover Dam. It is a significant economic, social, and ecological resource for millions of people across the Southwest. The lake serves multiple states including Arizona, Nevada, and California.

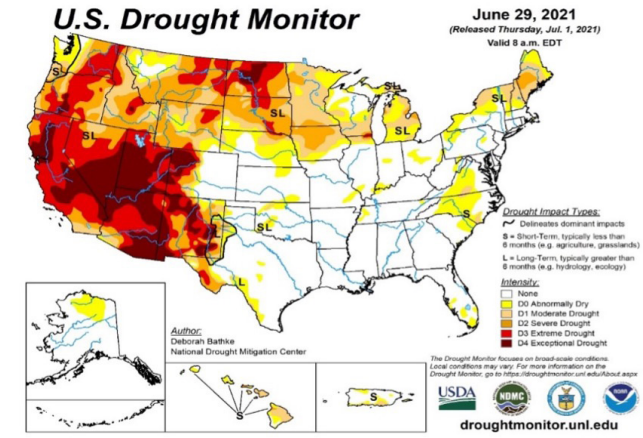

Map showing the extent and intensity of drought conditions across the nation. Source: the U.S. Drought Monitor. https://droughtmonitor.unl.edu/data/jpg/20210629/20210629_usdm.jpg

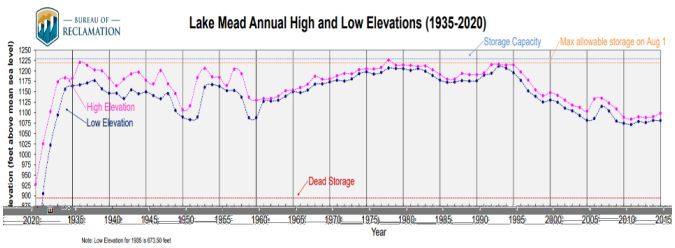

Lake Mead High/Low Elevation Graph. Credit U.S. Bureau of Reclamation, https://www.usbr.gov/lc/region/g4000/lakemead_line.pdf

Lake Mead's elevation at capacity is 1,229 feet, but it is considered "full" when the water level gets to 1,221.4 feet. At this point, it contains enough to hold the Colorado River's entire average annual flow for two years, according to the U.S. Bureau of Reclamation.

According to the June 29, 2021, U.S. Drought Monitor, unprecedented heat and dry weather resulted in extreme and exceptional drought conditions across the western U.S. In a statement summarizing the conditions, it was noted that the excess heat intensified evaporation from soils and vegetation, leaving the region excessively dry.

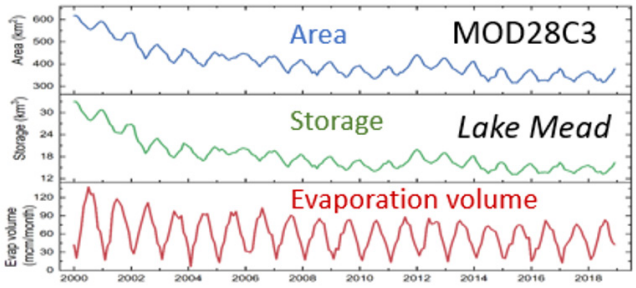

Lake Mead's estimated losses due to evaporation fall roughly between 600,000 acre-feet and 800,000 acre-feet of water yearly. But, on June 9, 2021, the lake's water level dropped to 1,071.56 feet and its storage declined to less than half. The reservoir's previous all-time low was 1,071.6 feet, recorded in July 2016. The time series figure above provides an example of the MODIS/VIIRS product monthly record for Lake Mead from the year 2000 to 2019.

SUMMARY AND FUTURE WORK

Just as other water bodies are subject to water losses by evaporation, so are reservoirs. These losses can be considerable in water deprived areas such as semi-arid and arid lands. Reservoir elevation and storage information can be used to improve the understanding and management of water resources. In addition, it can benefit applications such as flood control, hydropower generation, agricultural irrigation, recreation, and fishery management.

Accurate accounts of evaporation losses from a given reservoir require water surface area and evaporation rate data. While these data can be taken directly from in situ sources or remotely sensed from satellite instruments, high-quality reservoir surface area and evaporation rate data can be difficult to obtain. For example, with in situ sources, several reasons (including costliness, sensor placement, lack of data sharing, and others) lead to gaps in data.

For a few decades now, satellite altimetry has provided many space-based measurements needed to monitor evaporation rates and losses from water supply reservoirs. However, a major challenge associated with them is limited temporal sampling, which also leads to gaps in data.

The MODIS/VIIRS global water reservoir product suite is an example of a satellite-derived product that was created to help bridge the existing data gaps. The product represents the first time that reservoir evaporation has been monitored globally in an operational manner. Gao and her team hope that the product suite will improve the modeling used for hydrological analysis, as well as water management decision-making—particularly during extreme events such as droughts, and/or under climate change. Above all, as these works are in the public domain, Gao and team hope that the product will help to enhance our scientific knowledge of the hydrological cycle, various applications, and other work being performed at many research institutions and national/international agencies. ❖

Story Source

Materials obtained from JPSS June Science Seminar titled "Surface Water Reservoir Product Suite from Moderate Resolution Remote Sensing Data."

References

Li, Y.; Zhao, G.; Shah, D.; Zhao, M.; Sarkar, S.; Devadiga, S.; Zhao, B.; Zhang, S.; Gao, H. NASA's MODIS/VIIRS Global Water Reservoir Product Suite from Moderate Resolution Remote Sensing Data. Remote Sens. 2021, 13, 565. https://doi.org/10.3390/rs13040565

Kohli A and Frenken K 2015 Evaporation from artificial lakes and reservoirs FAO-Aquastat, Rome

National Park Service, U.S. Department of the Interior, Lake Mead's Water Budget, https://www.nps.gov/lake/learn/water-budget.htm, last updated: April 4, 2017. Accessed June 10, 2021.

__ 2021 Storage Capacity of Lake Mead. https://www.nps.gov/lake/learn/nature/storage-capacity-of-lake-mead.htm Accessed June 10, 2016.

U.S. Department of the Interior, Bureau of Reclamation, Lower Colorado Region. 2008. Hoover Dam frequently asked questions and answers: Lake Mead. Online at https://www.usbr.gov/lc/hooverdam/faqs/lakefaqs.html. Accessed July 1, 2021.

Public Domain Content

Distribution of Earth's Water. Provided by the U.S. Geological Survey. Water Science School: Where is Earth's Water? Available at https://www.usgs.gov/media/images/distribution-water-and-above-earth. (Accessed June 4, 2021). Credits: Igor Shiklamonov, 1993, "Water in Crisis: A Guide to the World's Freshwater Resources."

THE VISIBLE INFRARED IMAGING RADIOMETER SUITE:

MAPPING THE EARTH DAY AND NIGHT

The information in this article is based, in part, on the June 21, 2021, JPSS science seminar presented by Curtis Seaman, Colorado State University Cooperative Institute for Research in the Atmosphere (CIRA). With contributions from many, including Steve Miller[1], Carl Dierking[2], Jorel Torres[1], and Bill Line[3].

[1]CIRA/Colorado State University; [2]Geographic Information Network of Alaska (GINA); [3]Center for Satellite Applications and Research (STAR).

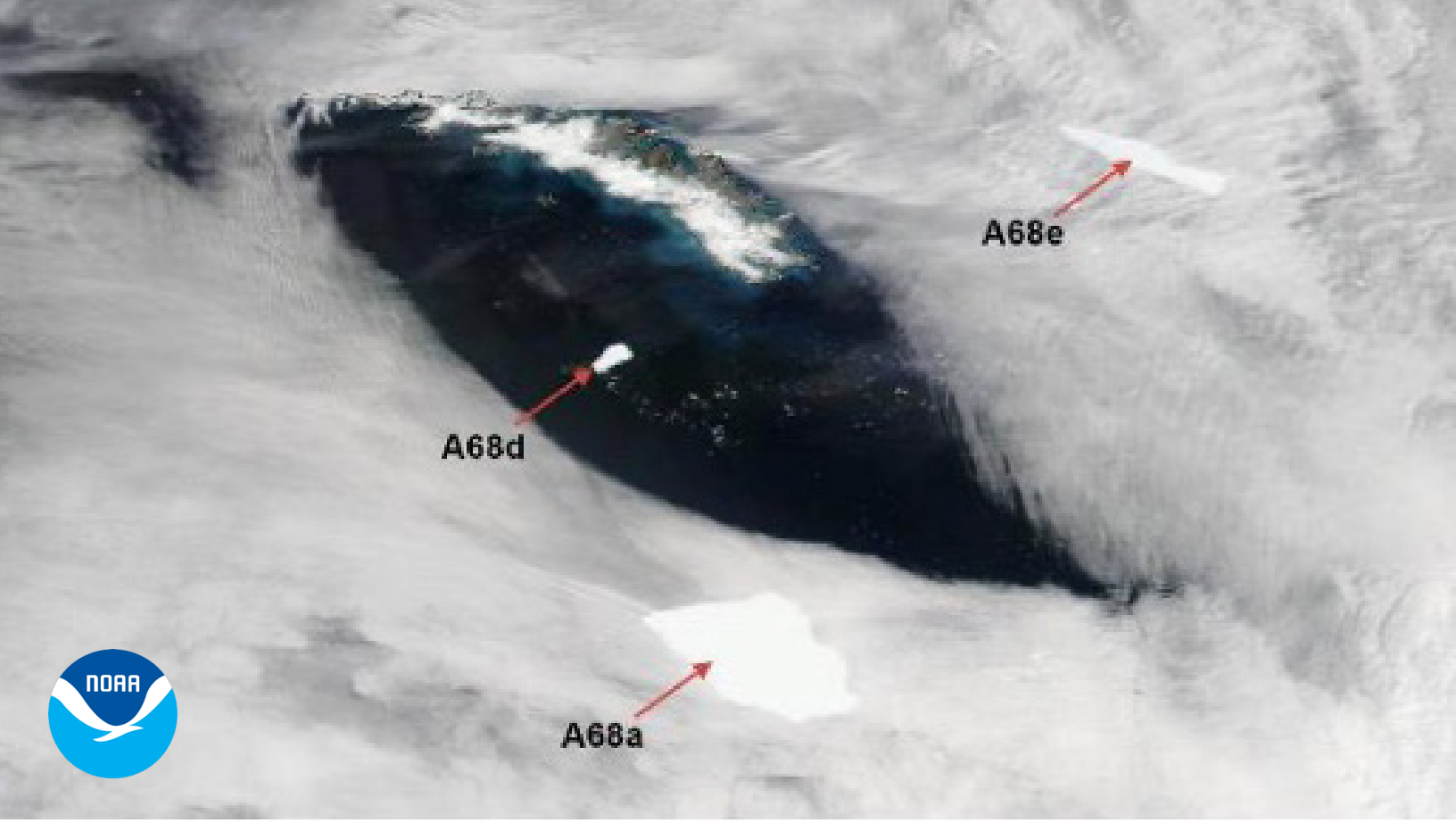

NOAA-20 capture of Icebergs A-68A, A-68D, and A-68E in the Weddell Sea. January 11, 2021. Image credit: NOAA.

According to a popular adage, "a picture is worth a thousand words." But is it? For Dr. Curtis Seaman, an atmospheric scientist at the Colorado State University Cooperative Institute for Research in the Atmosphere (CIRA), and member of the Joint Polar Satellite System (JPSS) Imagery/Visualization team, the answer is "yes!" He explained that pictures "can reveal a lot of information that is not necessarily found in words." The image above serves as an example. It is one of many generated by weather satellites: the sentinels in the sky. Imagery from weather satellites are more than simply pretty three-dimensional environmental observations of the Earth's surface. They serve as specialized mapping and monitoring tools that provide information on places and phenomena on the Earth's surface. They are resources for detecting change in things such as land cover, sea ice, weather patterns, and more. In addition to helping validate quantitative retrievals, satellite imagery provides ways to help inform of evolving conditions, for example, during natural disasters such as wildfires and tropical storms, and therefore can be used to help warn people of hazardous conditions, ultimately helping to save lives and protect property.

As part of his work with the JPSS imagery team, Seaman analyzes and validates imagery from the Visible Infrared Imaging Radiometer Suite (VIIRS) instrument—first on the Suomi National Polar-orbiting Partnership (Suomi NPP) in 2011, followed by NOAA-20 in the Joint Polar Satellite System (JPSS) series of satellites in 2017. Multispectral satellite imagery products are his area of specialty, and he has developed several that forecasters from the National Weather Service (NWS) use to monitor, track, and assess environmental events including wildfires, dust storms, and ice storms.

This article, based in part on his JPSS science seminar in June 2021, aims to illustrate the power of satellite imagery from VIIRS in detecting, monitoring, tracking, and assessing the impacts environmental events such as tropical cyclones, wildfires, smoke and atmospheric aerosols. And, in the year 2020, this list would grow to include the impacts of a global pandemic.

TALES OF THE EARTH TOLD THROUGH IMAGERY

Every day somewhere on the planet, an environmental event occurs. It can be a wildfire ravaging forested areas close to human settlements, or out in the wilderness; a tropical cyclone taking shape in the ocean; a dust plume lifting off desert lands impacting air quality and visibility; a flood event, an iceberg floating or forming in the ocean; and so forth. More often than not, a weather satellite will capture the event. And, in some parts of the world, for example, desolate areas with little to no human footprint, Earth observation satellites are often the only means available to observe these events. Satellite imagery and other remote sensing tools provide valuable information on a wide array of environmental phenomena that cannot be gleaned from conventional sources. Over and above that, "satellite imagery conveys information in ways that words cannot and this is something that one cannot put a price on," Seaman said.

To illustrate this, he refers to the "true-color" image shown below of the region around the Caspian Sea, which was captured by the VIIRS instrument during on overpass from the Suomi-NPP satellite in May 2014. True color imagery is a special form of multispectral imagery that mimics how the world appears in normal human vision.

This single VIIRS image reveals many different features, each with its own story. It provides a near 'real-time' view of the weather where afternoon convection is forming along the Caucasus Mountains and the Alborz Mountain range in Northern Iran. North of the Caucasus Mountains, a plume of dust is visible that extends over the Caspian Sea. "This reveals information about air quality in the region," Seaman said. High concentrations of dust can pose risks for those who are sensitive to air pollution. "Based on the appearance of the dust, one can also infer the wind speed and direction in which the dust is blowing. One can also infer that the soil is dry enough for the wind to loft dust out of it," Seaman added.

And that's not all. In the northern edge of the Caspian Sea, there appears to be a phytoplankton or algae bloom, which can provide some information on the turbidity of the water. While phytoplankton are an important

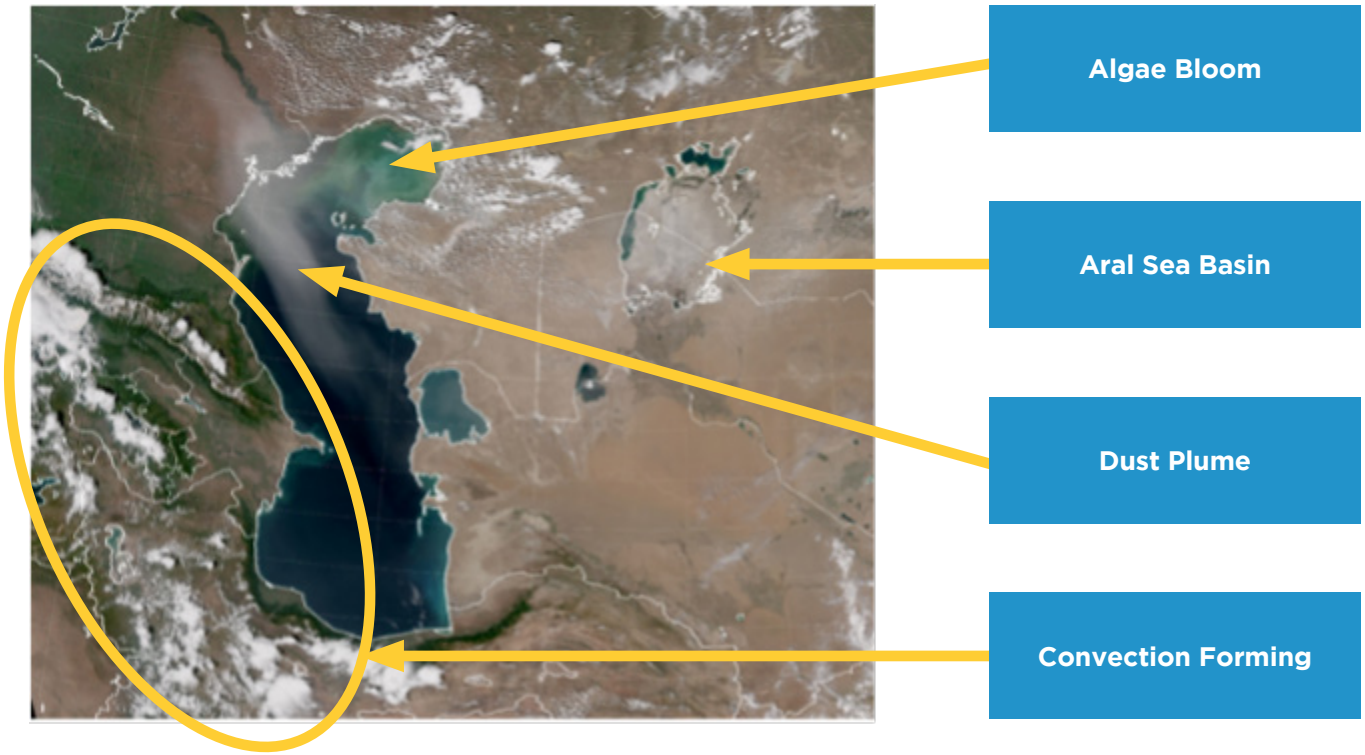

A VIIRS true color image showing dust and algae on the Caspian Sea, May 5, 2014.

food source for marine life, some of their blooms can be harmful to the environment, humans and animals. To the east of the Caspian Sea is an outline of what was once the fourth largest lake in the world, the Aral Sea. The current extent of this body of water tells us something about human activity and the region's climate. Almost four decades ago, a combination of factors, including water diversions and poor agricultural practices, ended up draining the Aral Sea faster than it could be replenished through rainfall.

MERGING SCIENCE AND ART: AN INTRODUCTION TO RGBs

The scenes depicted on the previous page can easily be mistaken for photographs, but they are actually multispectral imagery, which are created using three color channels: red, green and blue—also known as an RGB composite. RGBs are images made from multiple spectral channels designed to enhance one or more specific features. The combination of channels in the blue, green, and red portions of the visible spectrum, generates an intuitive, color realistic image that looks similar to a camera photograph. This is referred to as the "True Color" RGB, which, Seaman said "is useful for identifying features like aerosols, especially in daytime, and others features like fire, dust, snow, ice, clouds, and fog". The history of RGBs is almost as old as that of satellite meteorology. The first appearance of RGB imagery of the Earth was in 1967, from the National Aeronautics and Space Administration's (NASA) Applications Technology Satellite 3 (ATS-3). This was the third in this series of geostationary scientific satellites built for NASA. It was equipped with a single visible band with additional infrared spectral channels (Miller, 2016). While RGB imagery was introduced off of the geostationary platform, its use "beyond true color, was popularized through polar-orbiting satellites," Seaman said.

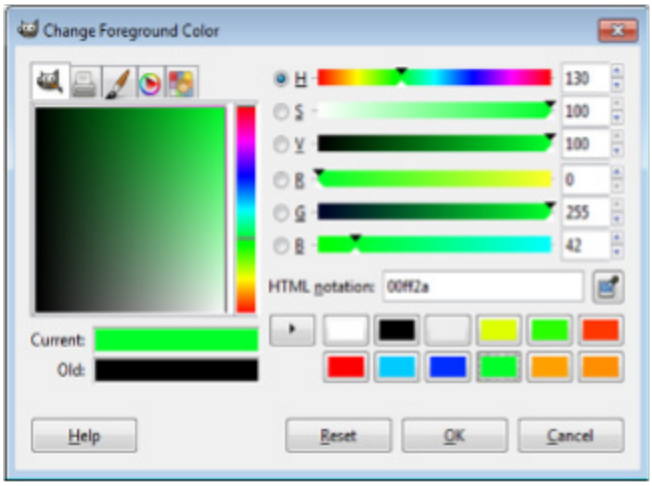

"After a certain high level of technical skill is achieved, science and art tend to coalesce in esthetics, plasticity, and form. The greatest scientists are always artists as well."

—Albert Einstein

According to Seaman, "satellite imagery is a synergy between art and science." RGB composites, he said "take advantage of the way color is presented on a computer monitor." Most modern computer displays are based on the "red-green-blue" (RGB) color model, which was developed from late-19th Century research on how the human eye responds to color. Varying amounts of red, green and blue light emissions provide the spectrum of color that anyone who

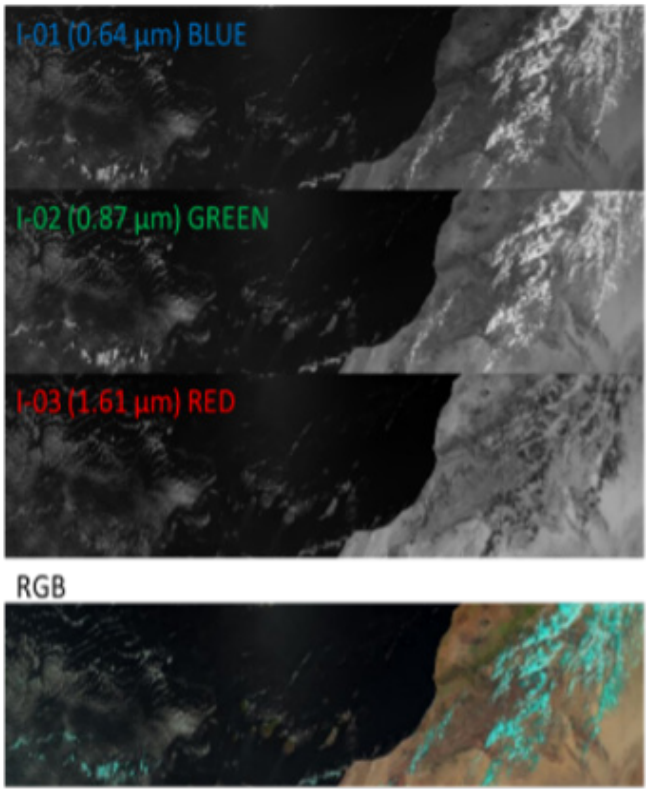

has used a color monitor or a color television set is familiar with. RGB composites take three different values, for example, data from individual spectral channels, channel differences, or any other mathematical manipulation desired, and these three values are assigned to the red, green or blue components of the resulting image as illustrated with the VIIRS bands shown at the bottom of the previous page: I-01; 0.64 µm (blue), I-02; 0.87 µm (green), and I-03; 1.6 µm (red). Put simply, three different images may be combined to produce a color image that provides a lot more information than any of the individual components can provide by themselves.

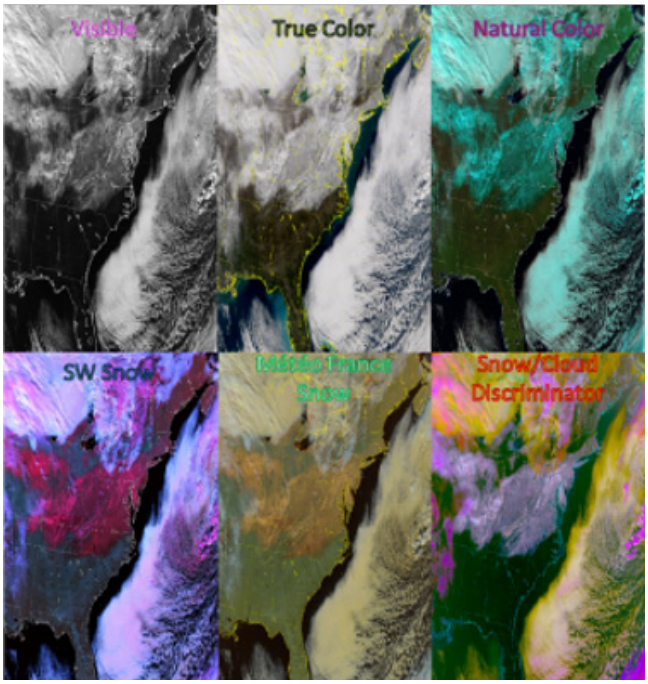

Seaman cautions that due to subjectivity, the qualitative interpretation of the data usually boils down to personal preference. For example, above are several VIIRS imagery products, which show various ways to try to discriminate snow and ice from features such as clouds. He explained that there are a few guidelines, which, if followed, make the delicate balance between art and science easier to manage and make the product choice a lot more meaningful.

The guidelines are discussed in the following section.

First, the amount of information to be presented has to be maximized.

Maximizing Information

To illustrate why maximizing information matters, Seaman presented two VIIRS Day/Night Band (DNB) images shown below. These images were created using the same data, but with different techniques. The image on the left uses a simple linear scaling of the DNB radiance values between the maximum and minimum values within the scene. The image on the right utilizes an improved technique, referred to as ERF-scaling, which he developed with Steve Miller (CIRA). These images are from a VIIRS nighttime overpass over Northern California at a time when many large wildfires were actively burning.

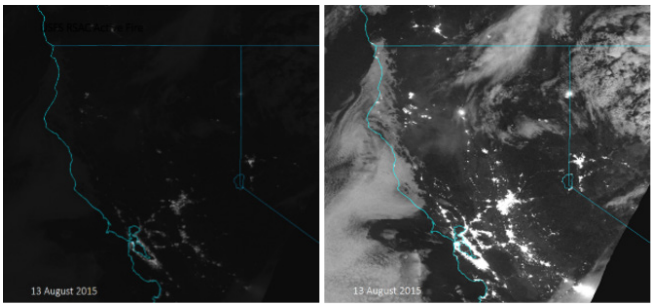

Compared to the above image on the left, the ERF-scaling technique (above right) makes the fires easier to spot and also shows evidence of smoke from the fires. It also reveals many more cities and towns, as well as clouds. In the coastal ranges, low clouds and valley fog are revealed.

This is valuable information, which can aid fire managers in decision making, especially when racing against the clock. For example, Seaman said that this kind of information can trigger important questions such as “is that fog going to make it to where the fires are? Is it going to be a visibility hazard for the air or ground crews? Is the increase in humidity going to suppress fire activity? What about the smoke, is that going to be a health hazard? Is it going to affect visibility?” He emphasized that this information is not present in the poorly scaled image.

Easy to Digest

The second guideline is to provide information that is, “easy to digest. You want it displayed in an intuitive manner.” For example, the VIIRS

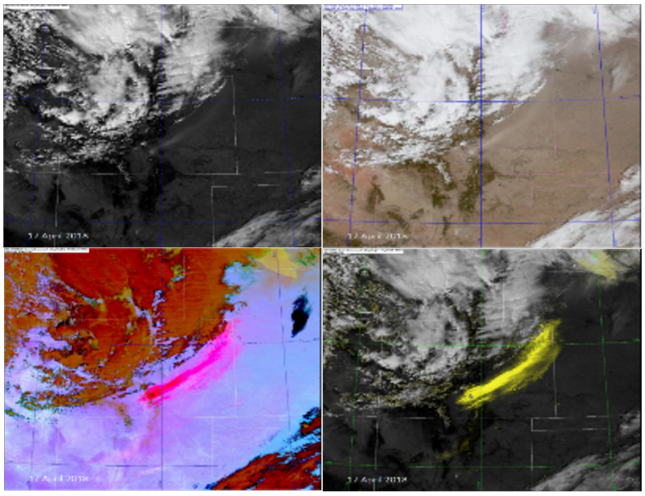

Top: Standard visible image (left), True Color image (right). Bottom: Dust RGB image (left), DEBRA Dust image (right). Credit Steve Mller (CIRA)

instrument captured the image above. It shows dust lofted from the Great Sand Dunes over the Eastern Plains of Colorado. While one can see the plume in the standard visible black-and-white image (top left), it's difficult to discern whether it is dust or smoke. The dust becomes more recognizable in the VIIRS true color image (top right), which displays the plume in a brown coloration that is indicative of dust. Smoke would have a grey or black coloration in a true color image, he explained. "However, it can be difficult to distinguish the lofted dust from the background land surface which is also light brown," he adds. This is where products such as a false color RGB composite—in this case, the dust RGB (bottom left), which makes the dust much more prominent against the background surface—come into play.

The disadvantage with false color RGBs is that they "are not intuitive, as knowledge of the features being displayed is predicated on knowledge of the channels used to create the RGB," Seaman said. Which is why he and his colleagues at CIRA also developed the "Dynamic Enhancement Background Reduction Algorithm, or DEBRA," which "uses a number of different spectral tests for dust to come up with a dust confidence factor, from which a final image is created." The DEBRA example where the dust confidence factor is displayed in varying shades of yellow, is shown in the image in the quadrant on the bottom right.

THE JOURNEY TO VIIRS: FROM TIROS-1 AND IN BETWEEN

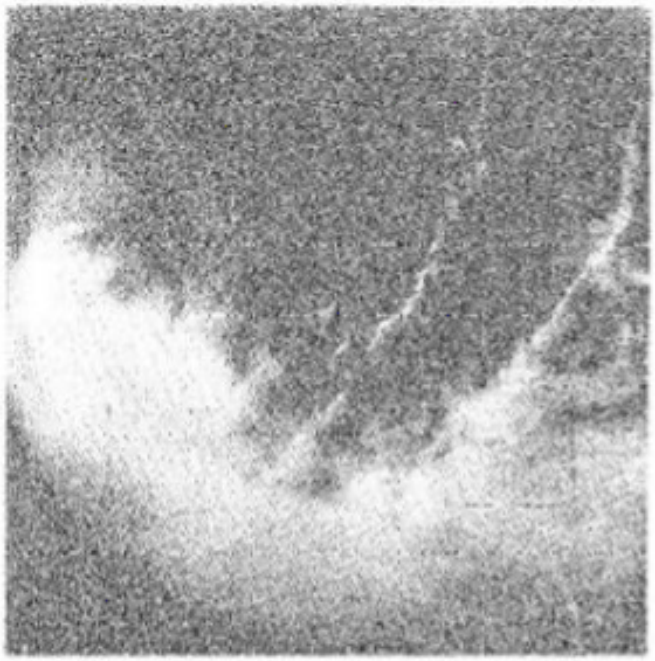

The ability to observe weather systems using space assets was one of the significant breakthroughs of 1960, which had its share of technological firsts. In April, images of cloud systems, albeit fuzzy, were transmitted from space following the launch of the first meteorological satellite—Television InfraRed Observation Satellite (TIROS-1). A few days after sending the cloud images, TIROS-1 uncovered a tropical cyclone, which had previously gone unnoticed, near New Zealand as shown by NOAA's Hurricane Research Division (HRD, 2015). Since then weather satellites have gone on to become important tools used to monitor the Earth's surface, oceans and atmosphere. TIROS-1 paved the way for many imagers including the Defense Meteorological Satellite Program (DMSP) Operational Linescan System (OLS), Advanced Very High Resolution Radiometer (AVHRR), Moderate Resolution Imaging Spectrometer (MODIS), and VIIRS.

The VIIRS instrument combines the best of, and where possible improves upon, its predecessors the OLS, AVHRR, and MODIS. Seaman points out that VIIRS comes with -22 channels, and a much higher spatial resolution compared to its predecessors. Seaman explained that TIROS-1,

AVHRR v3

Central Wavelength (μm)	Band Explanation	Spatial Resolution (m) @ nadir
0.630	Visible	1.1 km
0.862	Near IR	
1.61	Shortwave IR	
3.74	Midwave IR	
10.8	Longwave IR	
12.0		

VIIRS

VIIRS Band	Central Wavelength (μm)	Band Explanation	Spatial Resolution (m) @ nadir
M1	0.412	Visible/ Reflective	750 m
M2	0.445		
M3	0.488		
M4	0.555		
M5	0.672		
M6	0.746	Near IR	
M7	0.865		
M8	1.240	Shortwave IR	
M9	1.378		
M10	1.61		
M11	2.25		
M12	3.7	Medium-wave IR	
M13	4.05		
M14	8.55	Longwave IR	
M15	10.76		
M16	12.01		
DNB	0.7	Visible / Reflective	750 m across full scan
I1	0.64	Visible / Reflective	375 m
I2	0.87	Near IR	
I3	1.61	Shortwave IR	
I4	3.74	Medium-wave IR	
I5	11.45	Longwave IR	

for example, “had a single visible channel, and really didn’t look at the Earth for more than half the time because it wasn’t spin stabilized.” And AVHRR, depending on the model, had either five or six channels. What’s more, VIIRS comes equipped with nighttime visible imagery from a Day/Night Band (DNB), which provides unique information that is not available from other satellites. What VIIRS can “see” today is a quantum leap from TIROS-1 six decades ago.

Some of the differences between VIIRS and its predecessors include a pixel aggregation scheme that constrains pixel growth out toward the edge of scan (NOAA Technical Report, 2017) resulting in improved spatial resolution out to the edge of the data swath. Due to instrument optics, viewing geometry and the curvature

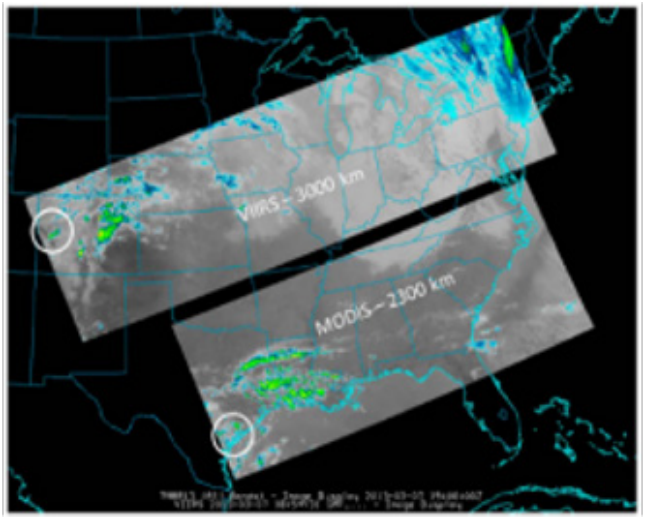

of the Earth, the spatial resolution of all polar-orbiting imaging instruments varies across the swath in what is known as the “bowtie effect.” Pixels near the edges of the swath have relatively coarse resolution compared to nadir (directly underneath the satellite), where resolution is the highest. Therefore, each scan of the instrument produces a strip of data roughly in the shape of a bowtie. For a MODIS 0.5 km resolution channel, a pixel at nadir represents 0.25 km^2 of surface area, whereas at the edges of the swath these pixels grow to 2.4 km^2. In contrast, a pixel from a VIIRS 375 m resolution channel represents 0.14 km^2 at nadir and 0.64 km^2 at swath edge, which is a significant improvement.

VIIRS also has a wider swath than MODIS, which prevents gaps near the equator as illustrated by the images below.

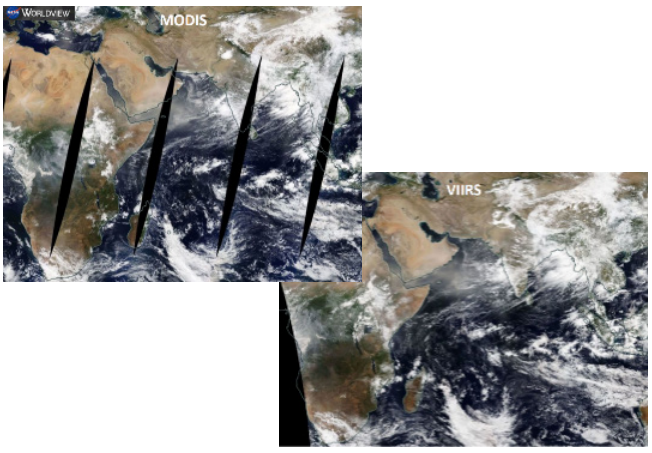

Daily global composite MODIS and VIIRS images from NASA’s worldview website. In the VIIRS image, which was taken the same day, there are no gaps at the equator. Credit: NASA Worldview.

SECOND TO NONE

The Day-Night Band

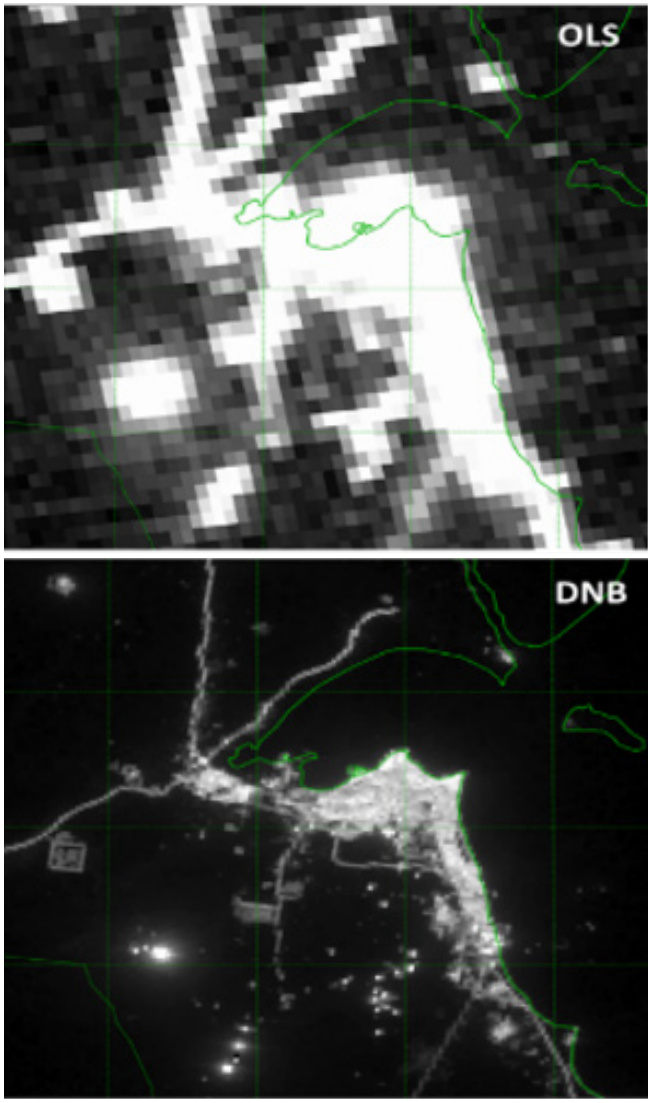

Image Credit: Steve Miller.

While the unique capability to generate imagery with the visible band at night began with the DMSP OLS, when it comes to spatial resolution, radiometric resolution, and sensitivity to low levels of light, VIIRS by far outmatches the OLS. As the two images above illustrate, the OLS cannot compete with the DNB. What's more, Seaman said that unlike its predecessor, "the DNB doesn't saturate and, most importantly, it provides well calibrated radiance data, enabling quantitative applications with the DNB that could never be done with the OLS."

For example, renegade icebergs floating around in the Arctic Ocean north of Alaska, are visible in the DNB image shown on the left on the next page, and are much harder to spot in the longwave IR imagery shown on the right. This ability to see patches of ice at night is useful to agencies such as the Alaska Sea Ice Program, which has utilized this imagery to rescue ships that got into trouble in icy waters. For more information, please read "Alaska Sea Ice Program (ASIP) used DNB in ship rescue," https://uaf-accap.org/event/vaws-november2020/.

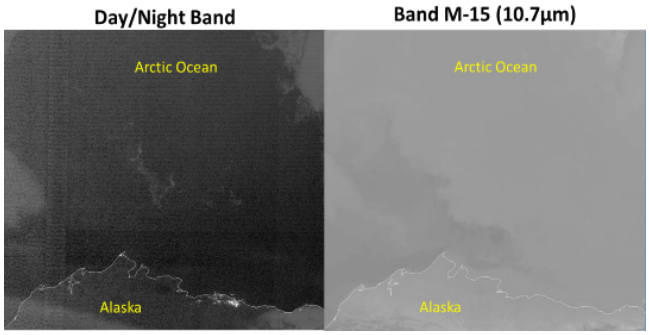

Filaments of Arctic Ice, October 4, 2018.

Can you spot the ice in the longwave IR? How about the clouds? You can clearly see them in the DNB!

Other examples of things that are possible with the DNB include the ability to track the movement of smoke plumes at night (with sufficient moonlight). In the examples below, the VIIRS DNB acquired images of smoke emanating from several fires in central Russia. The DNB also captured valley fog, which is visible in the same scene (see image below on the left). Neither the smoke nor fog are visible in the longwave IR imagery, as shown in the image on the right.

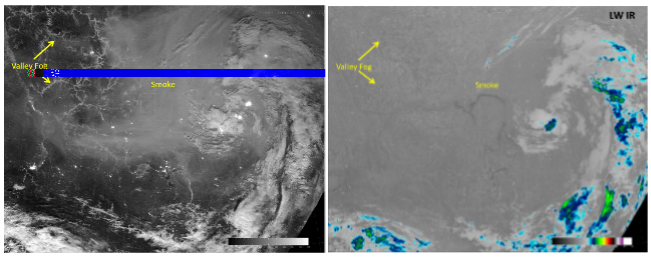

This ability to detect low clouds at night has also revolutionized tropical cyclone forecasting, almost eliminating what forecasters at the National Hurricane Center (NHC) refer to as the "sunrise surprise" because the IR imagery at night

may mislead forecasters into thinking the center of the storm was elsewhere when compared to what visible imagery revealed right after sunrise.

In the example below, a relatively weak tropical system was being monitored by the Joint Typhoon Warning Center (JTWC) between Madagascar and Mozambique. If one relied entirely on longwave IR imagery, they would more than likely assume the center of the storm to be underneath all the deep convection. However, the DNB's increased sensitivity to low clouds shows quite clearly that the low level circulation center is exposed and it's offset from the deepest convection. Knowing the location of the center of circulation is key to forecasting where a storm is headed. The DNB information has been instrumental in improving tropical cyclone forecasts and subsequently saving lives! The DNB helps identify the low-level center of tropical cyclones when the IR view is ambiguous.

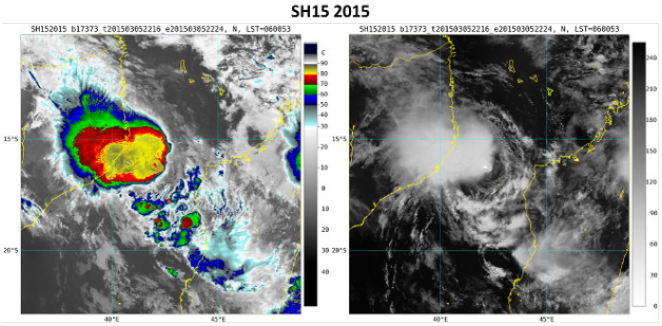

VIIRS longwave infrared (left) and Day/Night Band (right) images of Southern Hemisphere Tropical Cyclone 15 over the Indian Ocean's Mozambique Channel, between Madagascar and Mozambique. Credit: Galina Chirokova.

Improving Cloud Masks at Night

In another application area, the 10.7 µm – 3.9 µm BTD is used to detect low clouds at night. Hoping to build off this capability, a research team led by Seaman's colleague, Dr. Steve Miller, conducted some tests to find out whether the DNB's ability to detect clouds at night could also benefit the VIIRS Cloud Mask. Instead of what they expected—that the DNB would detect clouds the VIIRS cloud mask had missed—they sometimes found the reverse situation; the operational cloud mask appeared to show clouds where the DNB did not detect any. Turns out, the atmosphere still has a couple of tricks up its sleeve.

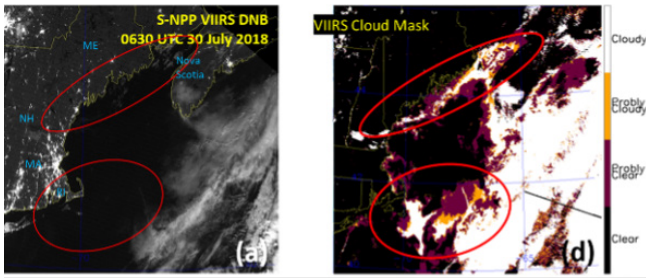

Credit: Yoo-Jeong Noh, Steve Miller.

To demonstrate the atmosphere's illusory trick, Seaman explained that the primary way to detect clouds at night is using the brightness temperature difference (BTD) between the longwave IR (e.g., 10.4 µm) and midwave IR (e.g., 3.9 µm) spectral bands. Due to differences in cloud emissivity, low clouds at night generally appear warmer at 10.4 µm than at 3.9 µm, resulting in positive values of the 10.4 – 3.9 BTD. However, this same BTD can result in false low cloud signatures under special circumstances. Because the 3.9 µm channel is less sensitive to the atmosphere, it sees emissions primarily from the surface. The 10.4 µm, in contrast, receives radiation from both the surface and lower atmospheric water vapor emissions, as shown in the plot below. For the clear-sky scenario of a warm and moist (red arrow) lower atmosphere over a cool (blue arrow) ocean surface, the scene will appear warmer at 10.4 µm compared to 3.9 µm, creating a positive 10.4 – 3.9 BTD and effectively tricking the VIIRS Cloud Mask into "thinking" that a low cloud is present. The team is studying the various physical mechanisms for this atmospheric foolery, with hopes of introducing new methods for overcoming the problem and potentially improving the fidelity of other products that are downstream of the cloud mask, such as sea surface temperature retrievals. The research team expects to report its findings in scientific journals in the near future.

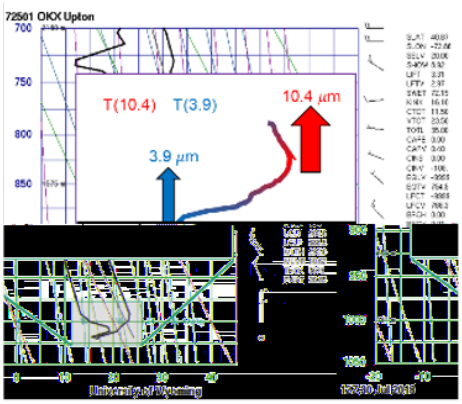

VIIRS 1.24µm Attributes and Resolutions

VIIRS Band	Central Wavelength (µm)	Type	Spatial Resolution	Temporal Resolution	Data Latency
M-8	1.24	Near-infrared	750-m	**CONUS:** ~2x / day per polar-orbiting satellite **Alaska:** more frequent overpasses near the poles	**Direct Broadcast (DB):** ~30-min **Satellite Broadcast Network (SBN):** 1 to 1 ½ h

The 1.24 µm (VIIRS Moderate Band 8 [M-8])

The 1.24 µm band is highly sensitive to snow and ice properties. It is unique in that it is not included on any existing geostationary satellite.

In the image below from a winter event that occurred on 30 December 2020, the "Snowmelt RGB," is used to discriminate between varying characteristics of snow and ice cover. The Snowmelt RGB (M-5, M-8, M-10), which Seaman developed combines the 1.6 µm (red), 1.24 µm (green), and 0.64 µm (blue) bands from VIIRS to provide information on surface snow/ice characteristics, including: wet vs. dry snow; fresh vs. old snow; sleet accumulation; and freezing rain accumulation. This new RGB is now being used by National Weather Service River Forecast Centers (RFCs) to identify regions where rapid snowmelt may lead to flooding.

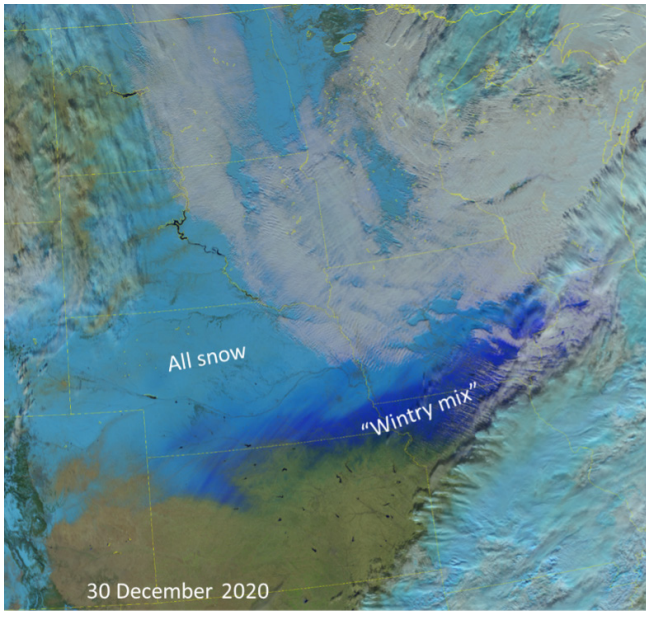

EMERGING APPLICATIONS

Beyond weather applications, the DNB has underscored its significance in many other areas, including light detection from cities, towns and other objects with lighting such as boats. In 2017, when Hurricane Maria made landfall on Puerto Rico as a category-5 hurricane, DNB imagery taken during and in the immediate aftermath was used to assess damages, including how much power was lost as a result of the hurricane. The imagery was also helpful in tracking and monitoring restoration efforts weeks and months after the storm passed.

Impacts of COVID-19 (March 2020)

It is this application of the DNB that is now being evaluated to determine what these observations revealed about the socio-economic behaviors and impacts of the COVID-19 pandemic, which impacted the globe in 2020. For example, many locations in the U.S. issued stay-at-home orders in March 2020 and many businesses shuttered their stores and turned off the lights. The DNB image shown below is an example of a Power Outage RGB—the difference between current DNB imagery and a background reference image—to monitor a loss of light emissions from cities as a result of outages or, in this case, shutdowns. This RGB highlights a loss of light in red, while stable light sources appear gold. The image below was created by comparing the monthly average light output of Las Vegas between March 2020 with February 2020 as seen by the DNB. Significant reductions in light were noted along the Las Vegas Strip, and at the Las Vegas Motor Speedway, suggesting these locations were greatly impacted by the

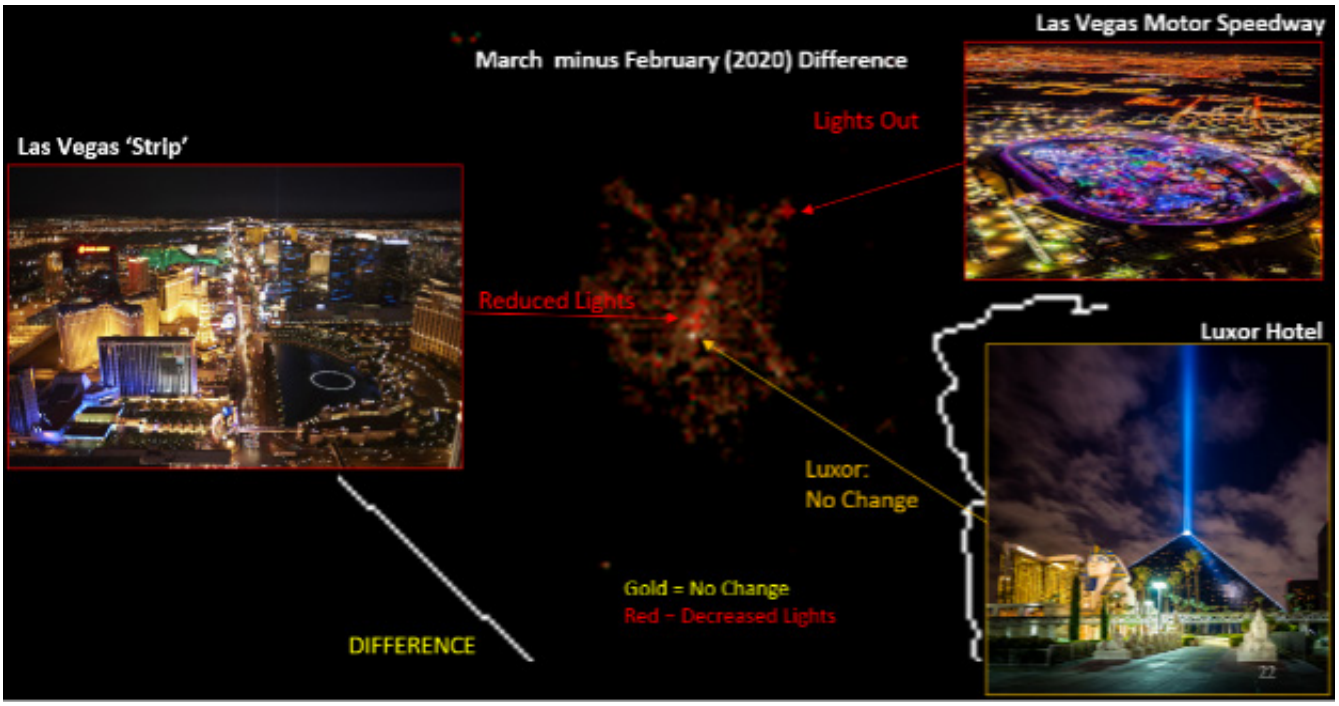

Image credit: Steve Miller (CIRA)

shutdown. The Luxor Hotel, however, which is home to one of the brightest human-made light sources today, did not shut off its lights during the pandemic and appears as a stable light source in the DNB imagery. Dr. Seaman is a member of a team of researchers addressing how this information relates to the actual economic impacts of the COVID-19 pandemic.

SUMMARY AND FUTURE WORK

In 1960, TIROS-1 transmitted a grainy image of clouds, which opened the doors to a new era of viewing cloud systems from space. Since then, imagery from weather satellites have become staples of weather and climate applications.

Since coming online, Earth observation satellites have captured many iconic images of the Earth. However, their imagery are more than simply pretty three-dimensional environmental observations of the Earth's surface. They serve as specialized mapping and monitoring tools that provide information on places and phenomena on the Earth's surface. They are resources for change detection in things such as land cover, sea ice, weather patterns, and many more. They help to validate quantitative retrievals, and they can also save lives and protect property during natural disasters such as wildfires and tropical storms.

Of note are two unique bands on VIIRS—the DNB and 1.24 µm band, which provide valuable information not available on any existing geostationary satellite. Imagery from the DNB has revolutionized many environmental nighttime applications from tracking wildfires, tropical cyclones, dense fog, ice packs, smoke and other aerosols, and many more. The 1.24 µm band is highly sensitive to snow and ice properties and provides valuable information on surface snow/ice characteristics. It has proved valuable in monitoring the Earth's ice sheets. ❖

Story Source

Materials obtained from JPSS June Science Seminar titled “The Value of VIIRS Imagery.”

References

Miller, S. D., Schmit, T. L., Seaman, C. J., Lindsey, D. T., Gunshor, M. M., Kohrs, R. A., Sumida, Y., & Hillger, D. (2016). A Sight for Sore Eyes: The Return of True Color to Geostationary Satellites, Bulletin of the American Meteorological Society, 97(10), 1803-1816. Retrieved Aug 24, 2021, from https://journals.ametsoc.org/view/journals/bams/97/10/bams-d-15-00154.1.xml

Cao, C., et al. (2017). Visible Infrared Imaging Radiometer Suite (VIIRS) Sensor Data Record (SDR) User’s Guide. Washington, D.C., https://ncc.nesdis.noaa.gov/documents/documentation/viirs-users-guide-tech-report-142a-v1.3.pdf.

NOAA. (2015). 55th Anniversary of the Launch of the First Weather Satellite. Accessed 2 August 2021, https://noaahrd.wordpress.com/2015/04/01/55th-anniversary-of-the-launch-of-the-first-weather-satellite/

NOAA. (2021). JPSS Satellites View A New Iceberg. Accessed 2 August 2021, https://www.nesdis.noaa.gov/content/jpss-satellites-view-new-iceberg

THE EVOLUTION OF THE CLIMATE PREDICTION CENTER MORPHING TECHNIQUE

The information in this article is based, in part, on the July 19, 2021, JPSS science seminar presented by Pingping Xie, NOAA Climate Prediction Center. With contributions from Robert Joyce, Shaorong Wu, Bert Katz, and Li Ren.

Clouds from Hurricane Sandy tower over Brighton Beach in New York, August 2012.

A FLASH BACK: CMORPH1

Two decades ago, scientists at the National Oceanic and Atmospheric Administration (NOAA) Climate Prediction Center (CPC), developed a technique to estimate global precipitation by fusing retrievals from passive microwave (PMW) and infrared (IR) measurements from multiple satellites in the low Earth orbit (LEO) and geosynchronous equatorial orbit (GEO) platforms (Joyce et.al., 2004).

The idea was to use satellite microwave data because the instruments can probe through most clouds and collect measurements day and night, regardless of cloud cover. In areas with persistent cloud cover where optical data is not helpful, microwave sensors provide a way to monitor precipitation. Examples include, the Advanced Technology Microwave Sounder (ATMS), Advanced Microwave Scanning Radiometer-Earth Observing System (AMSR-E), Advanced Microwave Sounding Unit (AMSU), and Special Sensor Microwave/ Imager (SSM/I), which fly onboard satellites in the "low Earth orbit," or LEO. Satellites in the LEO do not hover over the same spot on Earth, and therefore cannot provide continuous viewing. LEO satellites view each area only twice per day, except for the poles, which receive more passes. Geostationary satellites are positioned more than 20,000 miles above the equator. They orbit at the same speed that the Earth spins, and therefore seem to hover above a single point on the Earth's surface, thus a providing continuous view. But they do not have microwave sensors. CMORPH takes advantages of the continuous observations from GEO IR channels to derived cloud motion vectors that are utilized to propagate the PMW retrievals from LEO and their respective measurement times to the target analysis time.

Dr. Pingping Xie, a CPC scientist, and one of the developers of CMORPH, says that it was one of several satellite-based precipitation products being tested in meteorology, hydrometeorology, and hydrology research and applications. The first-generation CMORPH precipitation data extends all the way back to 1998, providing a record of more than two decades and continuing. To date, CMORPH1 is still used widely in operations, services, as well as in research and development. It generates 30-minute interval estimates on an 8-kilometer latitude/longitude grid (at the equator) from 60°S-60°N and two-hour time delayed updates.

SHORTCOMINGS

As has been the case for many weather, climate and hydrological applications, the combination of data from multiple satellites and instruments was a win-win for CMORPH1. But, Dr. Xie said, there were some problems. First, it only covers latitudes up to 60°S–60°N. Therefore, it provides incomplete global coverage as there are no precipitation estimates over the polar regions. Second, CMORPH1 does not represent cold season precipitation and orographic rainfall very well. And third, it is unable to take full advantage of GEO observations to fill in the gaps when and where PMW retrievals are not available.

A LEAP AHEAD TO THE SECOND GENERATION CMORPH

According to Xie, the second-generation CMORPH, like its predecessor, was designed with the notion to build a high-quality, high-resolution precipitation analysis over the globe by integrating information from satellite observations as well as in situ measurements and model simulations—something which was not part of CMORPH1. But, it will offer some clear improvements over CMORPH1 including a spatial resolution of 0.05° lat/lon (roughly about five kilometers over the tropics and sub tropics) over the entire globe (90°S–90°N); a 30-min interval at a production latency of no more than one hour for the initial production and refreshed at least once an hour until 12-hour latency—a move which further advances real time monitoring applications. Finally, an ongoing retrospective processing effort is expected to generate a historical record dating back to 1991, which will complement the existing time series, or long-term records of precipitation data to facilitate the quantitative application in climate analysis and monitoring.

Approach

The integration algorithm of CMORPH2 is an enhancement of that of the CMORPH1. Xie explains that PMW retrievals of precipitation from all satellites are first calibrated against a common reference standard, the retrievals from the GPM Microwave Imager (GMI) and combined locally into inter-calibrated multi-satellite PMW retrievals, called MWCOMB. Similarly, snowfall rate (SFR) retrievals generated by Meng et al. (2011) from five PMW sensor carrying satellites are also inter-calibrated and combined into composite PMW SFR retrievals (SFCOMB). The MWCOMB and SFCOMB are then blended locally to form a composite of all-precipitation retrieval combined global fields, named APCOMB. IR based precipitation estimates (LPE) are used to fill in the PMW retrievals over PMW field of views (FOVs) for which PMW retrievals are not available due to complicated underlying surface condition.

Information Integration

Meanwhile, motion vectors of precipitating clouds are derived from consecutive images of GEO IR based precipitation estimates from 60°S to 60°N and from the NCEP Global Forecast System (GFS) hourly precipitation forecasts over high latitudes. These motion vectors are then applied to propagate the retrievals of instantaneous precipitation rates recorded in APCOMB from their respective measurement times to the target analysis time to form satellite-based precipitation estimates (the raw CMORPH2) over the entire globe. A kalman filter-based technique is applied to promote the retrievals and define the final raw CMORPH2.

Bias Removal

Since biases exist in the raw CMORPH2, a second part of the algorithm is developed to remove the biases through calibration against independent sources. Xie says over land, this is done through comparison against the CPC daily gauge analysis, while over ocean, the raw CMORPHs are adjusted against the GPCP monthly merged analysis V3.1 which is a long-term record on a much coarser time and space resolution (monthly/0.5°lat lon). He notes that the bias correction algorithm has been developed offline and as of November 2021 has not been installed in the production system.

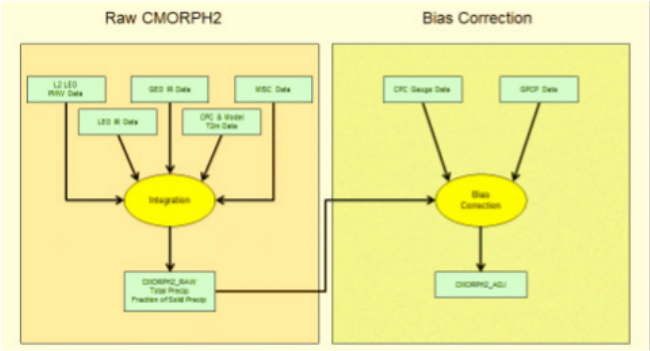

Presently, a processing system has been installed and is running on Linux stations at the CPC. In addition, there are several developments taking place: a migration to a supercomputer system as well as a sub-system, called Production Monitoring System (PMS), to monitor the real-time production of CMORPH2 time so that any problems/issues that are detected are solved as early as possible.

TESTING THE UPGRADES

To help them discern how CMORPH2 real-time production performs, and their next steps, Xie and his team performed several comprehensive tests in which they compared it against several independent datasets including models forecasts and ground observations. Some examples from these experiments are provided in the comparison and verifications section.

COMPARISON & VERIFICATIONS

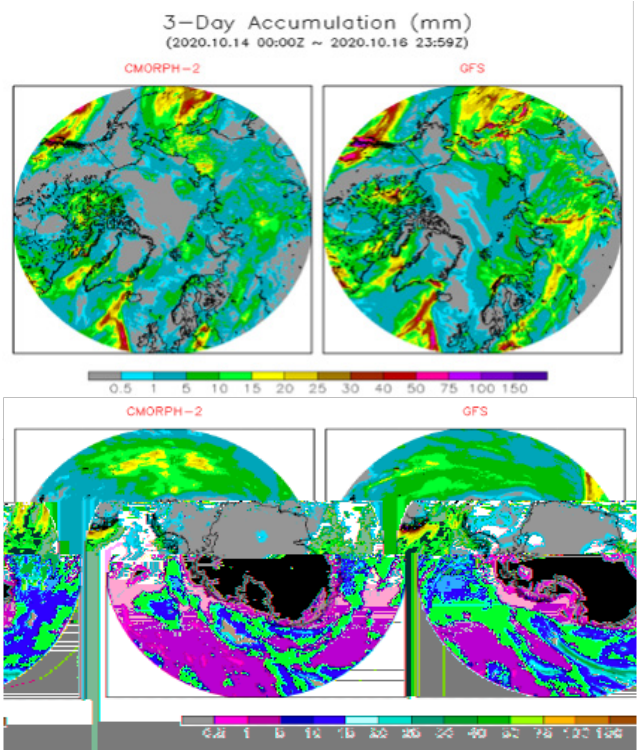

Comparison with GFS over Polar Caps

"Numerical models of modern era perform quite good in capturing precipitation over high latitudes. As a result, comparison against model precipitation provides information on the quality of CMORPH2," Xie says.

The upper and bottom panels in the figure on the left show three-day accumulated precipitation from CMORPH2 (left) and GFS (right) over Northern/Southern polar caps.

"Overall, both display very similar spatial patterns. However, there are differences in smaller scale features and magnitude that need to be examined in the future against ground observations," Xie says.

Verifications Against Ground Observations

For ground observation, Xie and his team look at:

- **Global land**

This experiment covered comparisons against CPC daily gauge analysis for a 24-month period from July 2018 to June 2020, using daily gauge analysis on 0.25° lat/lon grid over global land.

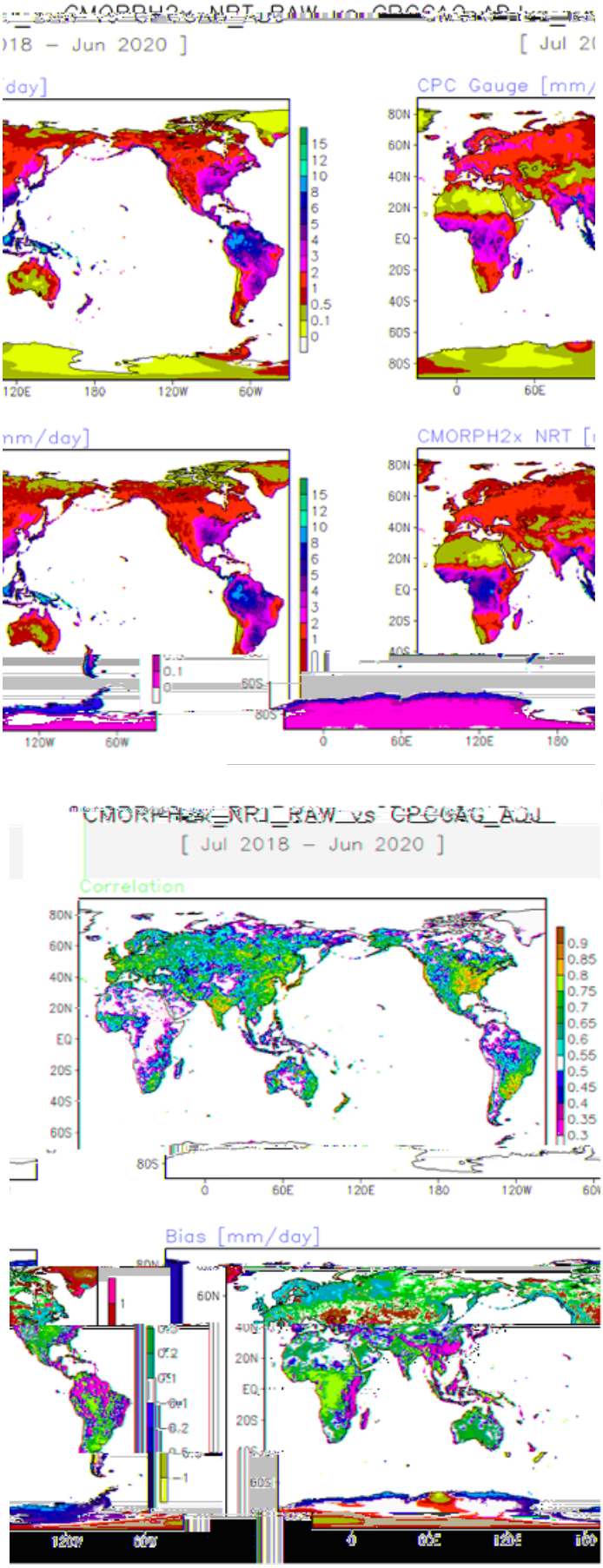

They found that CMORPH2 showed comparable spatial distribution patterns of mean precipitation but exhibited bias (over-/under-estimation over the tropics/extra-tropics. There was a high correlation (>0.7) for daily precipitation on a 0.25°lat/lon grid box, and a low correlation over some areas (e.g. equatorial Africa, NW corner of S. America) attributable to poor gauge analysis.

- **Multi Radar–Multi Sensor Estimates over CONUS**

This experiment covered comparisons against Multi Radar–Multi Sensor (MRMS) radar estimates for the July 2018 to June 2020 period, for 30-min, hourly and daily precipitation over 0.05°, 0.10°, and 0.25°lat/lon grids over and adjacent to the mainland U.S.

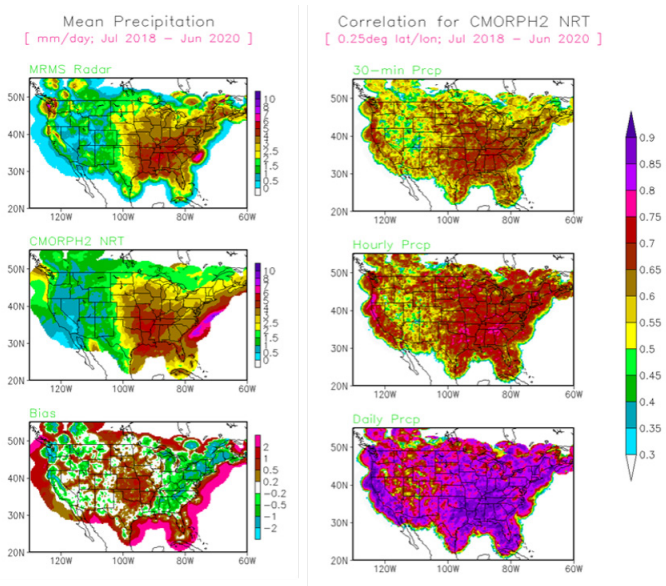

Here they found that CMORPH2 reproduced the precipitation observed by the MRMS gauge-corrected radar precipitation quite well. In addition, it captured the temporal variations of precipitation well with very high correlation over most of the CONUS except the western mountainous regions. CMORPH2 tends to over-/under-estimate precipitation over central CONUS/other regions.

- **Stage IV precip analysis (gauge only) over Alaska**

For this experiment, CMORPH2 was compared against Stage IV precipitation (gauge-only) for a three-month period from June–August 2019, for 6-hourly precipitation over 0.25°lat/lon grids over Alaska.

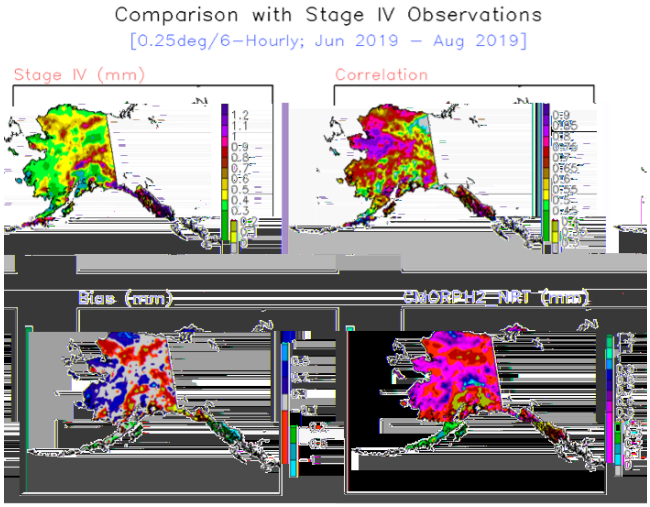

Here, they observed that while CMORPH2 tended to underestimate over the majority of the domain, there was very good correlation over most of the state.

- **Taiwan radar estimates**

For this experiment CMORPH2 was compared against Taiwanese Central Weather Bureau (CWB) radar precipitation estimates for the same 24-month period of coverage used for global land and MRMS radar estimates for 30-min, hourly and daily precipitation over 0.05°, 0.10°, and 0.25°lat/lon grids over and adjacent to the Taiwan Island.

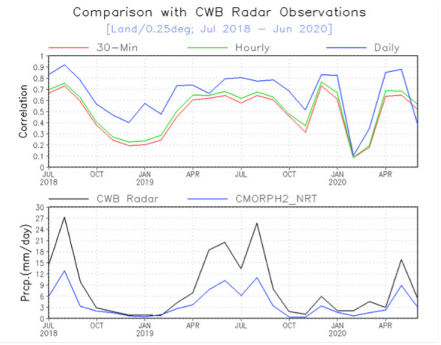

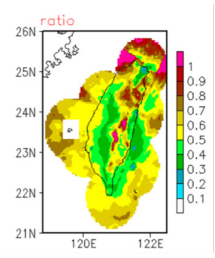

Ratio between CMORPH2_RT and CWB radar estimates

In the experiments done over Taiwan, the team observed that unsatisfactory retrievals of orographic effects largely caused underestimation. Nonetheless they found that the correlation was quite high for most of the seasons with rainfall.

GROUND TO COVER

Nearly a decade after unveiling CMORPH, the CPC began working on the next generation. So far, the second-generation CMORPH has demonstrated substantial improvements in detecting and quantifying precipitation over extra-tropics and during cold seasons. What's more, unlike its predecessor, CMORPH2 comes with a better spatial resolution, which is roughly about five kilometers over the tropics and sub tropics, over the entire globe (90°S–90°N). CMORPH2 also has a very short latency of one hour and refreshed once an hour (to be reduced to 30 minutes soon).

Two pieces of work underway right now are to install the bias correction procedures into the production system and to migrate the real-time production system to the NWS Weather and Climate Operational Supercomputing System (WCOSS), pending approval from the NCEP Central Operation (NCO). The former, Xia says, is expected to greatly improve the quantitative accuracy of the CMORPH2 for key applications like hydrometeorological prediction and global water cycle quantification. The latter will improve the production stability and further reduce the real-time production latency. Studies are also planned to experiment with the inclusion of PMW retrievals from the direct broadcast (DB) to further improve the quality of CMORPH2 for very short latencies. Currently CMORPH2 are mostly filled with GEO IR based precipitation estimates (GPE) before the formal version of PMW retrievals are available.

Additionally, a retrospective analysis to construct a 30-year record of CMORPH2 dating back to 1991 has also begun.

And last, but certainly not least, is the development of CMOPRH through user feedback, which "is important to its sustained

and successful use in field operations at the National Weather Service (NWS)," Xie says. Assessments of CMORPH's impact in field operations provide a valuable feedback loop between end users and developers, as it gives the developer "a better understanding of the end-user's needs for CMORPH2. It also enables the developer to provide products to end users in the form they need," Xie says. For example, several past enhancements were the result of interactions between the CMORPH developers and various centers and field offices including the NWS in Alaska.

SUMMARY AND FUTURE WORK

The JPSS funded CMORPH2 is constructed by integrating information from multiple sources, including PMW retrievals of rainfall and snowfall from more than 10 LEO satellites, IR-based precipitation estimates from multiple LEO platforms and five GEO satellites, precipitation forecasts from NCEP GFS global models, CPC daily gauge analysis, and the GPCP merged analysis of global monthly precipitation analysis.

It provides estimates of 30-minute precipitation over a very fine spatial resolution of 0.05°lat/lon grid over the entire globe and presents much improved skills upon its predecessor, CMORPH1, especially in detecting and quantifying cold season precipitation over mid- and high-latitudes. CMORPH2 is generated on a near real-time basis at a very short latency of one hour and a very high refresh rate of once an hour for improved operational applications. ❖

Story Source

Materials obtained from JPSS July Science Seminar titled "Real-Time Production of the Second Generation CMORPH."

References

Joyce RJ, Janowiak JE, Arkin PA, and Xie P (2004) CMORPH: A method that produces global precipitation estimates from passive microwave and infrared data at high spatial and temporal resolution. Journal of Hydrometeorology, Vol 5, pp 487-503.

National Center for Atmospheric Research Staff (Eds). Last modified 03 Aug 2020. "The Climate Data Guide: Precipitation Data Sets: Overview & Comparison table." Retrieved from https://climatedataguide.ucar.edu/climate-data/precipitation-data-sets-overview-comparison-table.

SATELLITE DATA:

HELPS SCIENTISTS MONITOR & UNDERSTAND THE OZONE LAYER AND EVALUATE ITS RECOVERY

The information in this article is based, in part, on the August 23, 2021, JPSS science seminar presented by Lawrence E. Flynn (NOAA/NESDIS/STAR). It features contributions from Zhihua Zhang (IMSG), Eric Beach (IMSG), Chunhui Pan (UMD), Irina Petropavlovskikh (NOAA), C. Trevor Beck (NOAA/NESDIS/STAR), Ding Liang (GSTI) and figures created by Colin Seftor (SSAI), Paut Newman (NASA GSFC), Craig Long (NOAA), and Nancy Kang (NASA GISS).

Over the centuries, there have been significant events, which have occurred and shaped the world in one way or another. Among these were technological innovations in the 19th century, which were prompted by industrialization, and the creation of space-based rockets in the 20th century, which led to many advances including the use of space-based cameras in weather observations. In 1960, there was a landmark moment in weather history when the Television InfraRed Observational Satellite, or TIROS 1, relayed images of cloud systems, demonstrating that they could be viewed from space.

The 1970s introduced technologically more advanced satellites, which would carry on the work of TIROS 1, and establish a groundwork for future satellites such as the U.S. Joint Polar Satellite System (JPSS) Suomi National Polar-orbiting Partnership (Suomi NPP) and NOAA-20. Some, like the National Aeronautics and Space Administration's (NASA) Nimbus satellites, came with instruments such as microwave radiometers, ultraviolet radiometers, and atmospheric sounders that the agency says would "produce many firsts." For example, the Backscattering Ultraviolet instrument (BUV) on the Nimbus-4 satellite provided a way to measure atmospheric ozone columns and profiles from space. The BUV would lead the way for other instruments including the Total

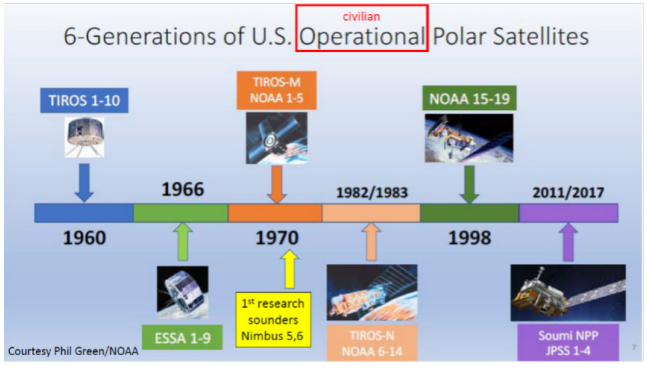

Ozone Mapping Spectrometer (TOMS), the Solar Backscatter Ultraviolet spectrometer (SBUV), Limb Infrared Monitor of the Stratosphere (LIMS), Stratospheric Aerosol and Gas Experiment (SAGE), and NOAA's SBUV/2 that would also provide measurements of atmospheric trace gases such as Ozone (O_3) and Sulfur Dioxide (SO_2), and other atmospheric constituents such as aerosols. It was also in the 1970s that theories began to be developed about chlorofluorocarbons (CFCs)—inert nontoxic compounds albeit long lived—potentially causing damage to ozone in the middle and upper parts of the stratosphere (Molina, M and Rowland, S., 1974). Data from these satellite instruments would help scientists to better monitor and understand the Ozone Layer, and advance our understanding on the threat that CFCs posed to the atmosphere. At the time, CFCs were ubiquitous. They were used in numerous products ranging from packing materials, hairsprays and other aerosol sprays, to refrigerators, and air conditioners.

By the mid-1980s, even more instruments had come on the scene. Among these were the HALogen Occultation Experiment (HALOE) aboard the Upper Atmosphere Research Satellite (UARS) and the Microwave Limb Sounder (MLS), as well as SAGE II and III. In the mid-1980s, researchers encountered a hole in the ozone layer over Antarctica. This was produced by ozone destruction in the lower stratosphere. But what was even more significant was the cause, as it was something that had not been considered before—a second type of halogen chemistry on ice particles in the lower stratosphere (Salawitch, R.J., et al, 1988). In 1989, theories began to be refined and tested focusing on a third mechanism for ozone destruction. This involved halogen chemistry on sulfate aerosols in the lower stratosphere and could cause major ozone loss especially following strong volcanic eruptions (Hofmann, D.J., and Solomon, S., 1989). Following this, the U.S. Naval Research Laboratory (NRL) launched the Polar Ozone and Aerosol Measurement (POAM II 1993, III 1998) missions to study trace constituents in the stratosphere.

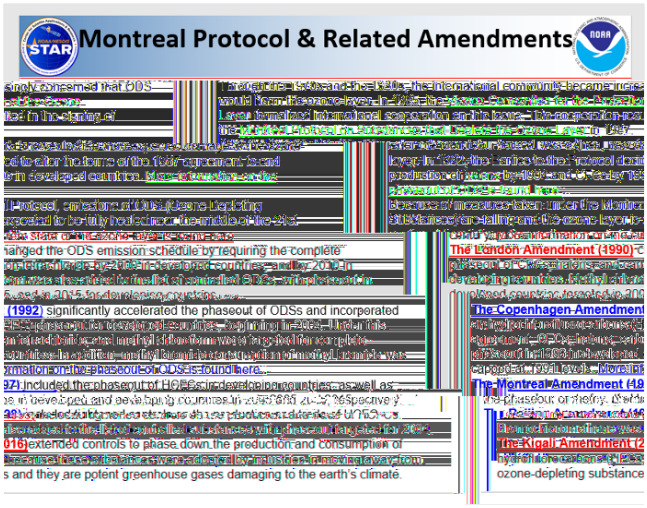

The scientific discoveries from the 1970s and 1980s would spur countries to act and work together to help protect the Earth's ozone layer. They would also lead to a paradigm shift in the production and consumption of ozone depleting substances (ODS) such as CFCs. There was the Vienna Convention for protection of ozone, which formalized the agreements to cooperate, and from that cooperation came the Montreal protocol in 1987, which set deadlines for phasing out ODS such as halons and CFCs. Seeing a need for more measures, several amendments were introduced including the London amendment, the Copenhagen amendment, the Montreal amendment, the Beijing amendment and the Kigali amendment. There were more changes and lessons to be learned ahead including new information on other substances that contain chlorine and bromine and other additions such as methyl chloroform, which was phased out in 2005.

"With global adherence to the Montreal protocol and related amendments, the ozone layer recovery is expected, but interactions between ozone and climate change, while also expected, are not fully understood," says Dr. Lawrence Flynn, a research scientist at NOAA's Center for Satellite Applications and Research (STAR), whose areas of expertise include research and analysis for validation, algorithm development, and calibration of existing and next generation satellite-based ozone sensors. In August 2021, Flynn gave a talk on the ozone layer in which he traced the sequence of advances in

recognizing and understanding the destruction of atmospheric ozone, and in the progression of quantifying the problem using remote sensing methods and records.

SPACE-BASED OBSERVATIONS OF ATMOSPHERIC OZONE: THE BASICS

Flynn explains that remote sensing measurements of the Earth's atmosphere from space can be classified in various ways including the wavelength of the measured radiation, the source of the radiation, the viewing geometry and physical path of the radiation, and the orbit of the spacecraft.

The measurements made by satellite instruments usually provide indirect information on the atmospheric parameters of interest. They measure the electromagnetic radiation that was impacted by the atmosphere in some ways, which enables them to reveal information about its constituents. Estimates of the parameters are often obtained from an inverse retrieval algorithm.

Electromagnetic Spectrum

The first consideration is the electromagnetic spectrum, which is classified into several wavelength regions. He says visible radiation is the most recognized because "our eyes can see in the visible and distinguish colors. So we can directly observe how different wavelengths—different colors—interact with the atmosphere. We see that the sky above us is blue, and at sunset, it turns red. These are physical manifestations of how the different wavelengths of visible light interact with the neutral atmosphere mainly nitrogen (N_2), but also with its various components."

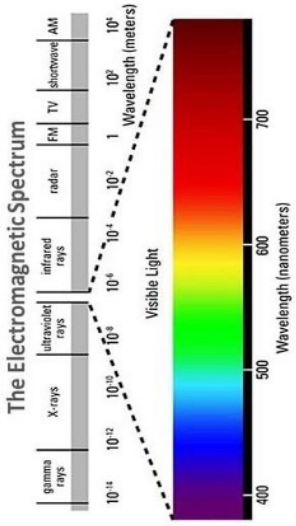

The wavelength intervals range from visible light, to infrared in the longer wavelengths, and beyond to even longer wavelengths and lower energy photons such as microwaves and radio waves. In the shorter wavelength range there is an interval classified as ultraviolet radiation. Continuing beyond these to even shorter wavelengths and higher energy photons come X-rays and then gamma rays. As shown in the figure on the next page, each wavelength range, e. g., ultraviolet, visible and infrared, behaves differently when interacting with different components of the atmosphere.

For more details please visit:
https://coralreefwatch.noaa.gov/product/5km/tutorial/crw03c_em_spectrum.php

For example, ozone strongly absorbs some ultraviolet wavelengths and carbon dioxide and water vapor both strongly emit/absorb some Infrared wavelengths.

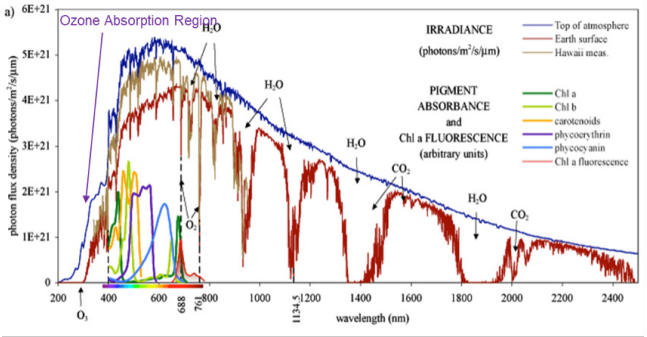

Ultraviolet, Visible and Near-Infrared Atmospheric Transmittance
Source: https://www.giss.nasa.gov/research/briefs/2007_kiang_01

Signal Sources

To view the atmosphere from space, sensors need to have a source of radiation. These include passive methods, which use existing natural sources, and active methods, which use human-made sources. Passive sources include direct, scattered or reflected sunlight, moonlight or starlight in the UV/visible or near-infrared, and radiative emission in the infrared and microwave. And active sources include GPS radio waves, UV/visible and infrared lasers (for LIDARs), and microwave transmitters.

Viewing Geometries and Physical Path of Radiation

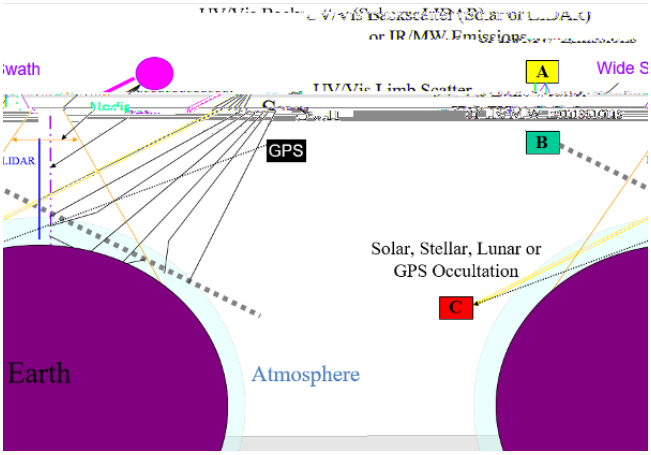

There are several ways to observe radiation from space. A schematic of these remote sensing observing strategies and geometries is shown above.

Flynn explains that the most common atmospheric observations are obtained by looking down from a satellite through the atmosphere with the Earth in the background, either directly down (Nadir) or with a range of angles (Wide Swath).

He says there's a second viewing geometry, which senses the attenuation of an extra-atmospheric source as it passes through the atmosphere (called Occultation). And, a third viewing geometry, which looks at the atmosphere but at angles without the Earth or a source in the background (Limb Viewing). The latter two geometries, Flynn says, can provide the highest vertical resolution for retrieving atmospheric profiles.

Spacecraft Orbital Paths

The orbital paths of space-based sensors provide a way to measure the atmosphere in different places and with different time sampling. Most operational instruments are located on platforms either with near-polar Sun-synchronous orbits or with geostationary orbits.

Satellites in near-polar Sun-synchronous orbits complete a revolution in approximately 100 minutes. They are designed to cross the equator

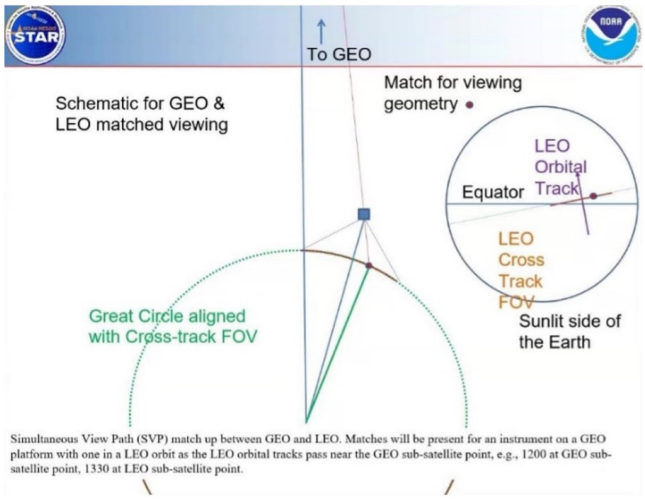

at the same local solar time orbit after orbit. For example, a 1:00 p.m. Sun-synchronous orbit would pass over 14 different equatorial locations spaced around the globe at 1:00 p.m. on a given day. On the other hand, satellites in geostationary orbits have an orbital period close to 24 hours. They are stationed above the equator at a height of approximately 36,000 kilometers and travel at the same rate as the Earth, which makes them appear to hover above a fixed point.

There are times when satellites in the Low-Earth orbits (LEO), for example those in near-polar Sun-synchronous orbits, fly under satellites in geostationary orbits (GEO). These situations provide opportunities for match ups in the line of sight. They also make it possible to perform comparisons and cross calibrations of measurements from instruments on the different platforms.

PRESENT DAY

The number and variety of instruments that are contributing data on atmospheric ozone continues to rise. Flynn says that the data records from these instruments have helped increase our understanding of ozone chemistry for all three major loss mechanisms. For example, the European Organisation for the Exploitation of Meteorological Satellites (EUMETSAT) has the Global Ozone Monitoring Experiment-2 (GOME-2) onboard the Meteorological operational satellite-C (MetOp-C) and the TROPOspheric Monitoring Instrument

(TROPOMI) on board the Copernicus Sentinel-5 Precursor (S5P) satellite. However, Flynn says that while the GOME-2 instrument's spectral resolution allows for multiple atmospheric trace gases to be estimated, these instruments are nadir-viewing, so the vertical resolution of their ozone profile retrievals are limited. There are measurements available from other, limb-viewing instruments, such as the JPSS Ozone Mapping and Profiler Suite (OMPS) Limb Profile, that can provide high vertical resolution ozone profiles. A brief lineage of instruments/ measurements with a focus on U.S. missions is provided in the box below.

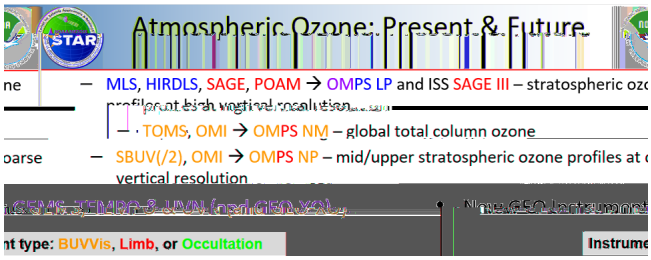

Some current and future atmospheric Ozone remote sensing instruments with a focus on U.S. instrument series. Slide courtesy Lawrence Flynn, August 2021 JPSS Science Seminar.

MORE THAN FOUR DECADES OF TOTAL OZONE RECORDS: THE STORY IN A THOUSAND WORDS

In what he calls "a picture worth 1000 words," Flynn describes total ozone anomalies observed from 1978 through 2020. The anomaly plot (shown below) in which the average annual cycle is removed, shows the percent differences of monthly averages with respect to the average annual cycle for the full record. The values are plotted for 10° latitude zonal means for latitudes from 80°S to 80°N beginning in 1980 and extending until 2020. It reveals year to year dynamics, general trends in ozone and their latitude and seasonal dependencies for all three types of ozone destruction.

The Viewing System

Flynn said the plot revealed many things, one being that the "satellite record isn't perfect." Something which is obvious from the appearance of black lines in a month or periods of months that had no values. He explained that there are also other places with missing data. The values were retrieved by using measurements of backscattered solar ultraviolet, which came from the SBUV/2 and the OMPS nadir profiler instruments, and as a result had places, for example, in the northern or the southern hemispheres with missing data during polar nights. The increased size of these missing areas in the early mid 1990s is caused by drifting orbits. The equator crossing times moved further from noon for the satellite flying the SBUV/2 instrument, so the satellite flew over more nighttime regions in the winter hemisphere.

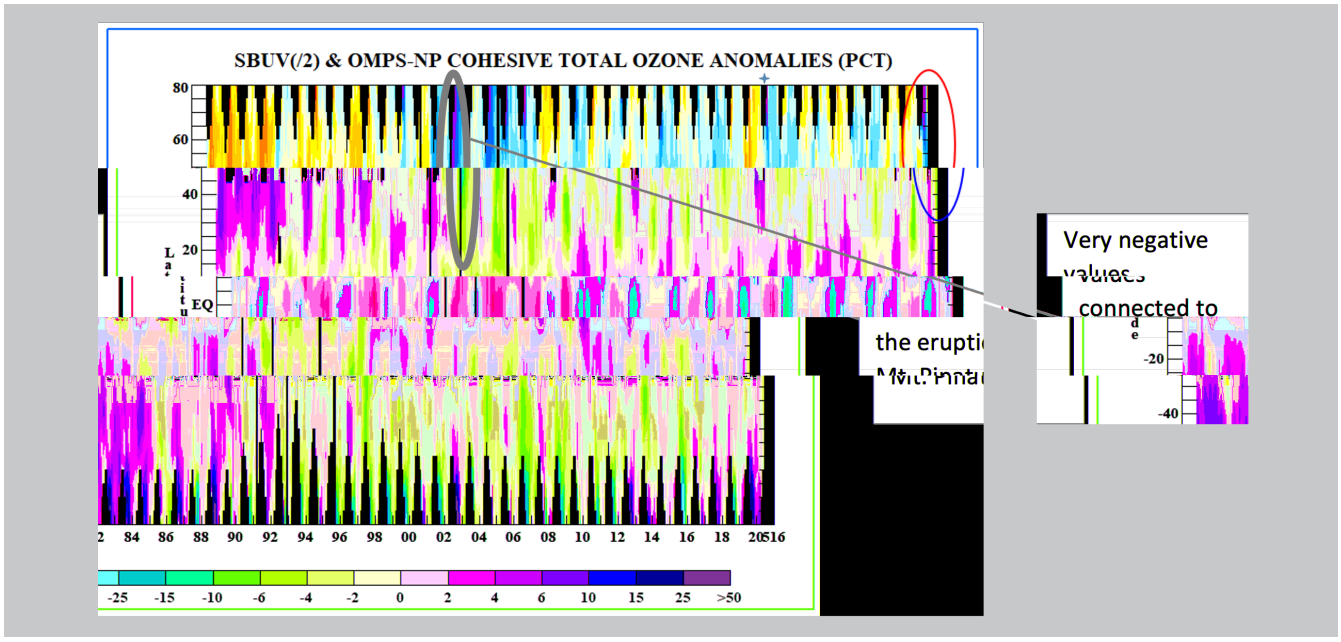

What's Going on With Ozone?

The plot shows a positive range of anomalies at the beginning of the record – brown, orange and red areas. The values then dip close to zero or negative during the mid 1990s—blue areas—before beginning to come back toward the positive range. At the mid-latitudes, this is primarily caused by the first type of ozone depletion. Overall variations are noted from year to year, and at the equator, ups and downs are noted about every two and a half years, which Flynn says is due to a phenomenon in the atmospheric dynamics known as the quasi biennial oscillation (QBO). "There are changes in the winds and changes in the rising and falling at the atmosphere at the equator and this turns into variations in the ozone," he said. The plot also shows that there does seem to be still some seasonality especially in the higher mid-latitudes where the values go down more than at the equator. This is produced by seasonality in the ozone depletion and recovery trends influenced by the seasonal variations in temperature of the atmosphere and its influence on ozone destruction. (Every four years, NOAA and the World Meteorological Organisation collaborate to generate an Ozone Layer Assessment. Flynn recommends that interested readers take a look at the Executive Summary and Twenty Questions components of the latest report at https://csl.noaa.gov/assessments/ozone/2018/ for more details on ozone trends and the state of the Ozone Layer.)

Ozone events

One ozone event is highlighted by the high negative values shown around 1993. The blue values, which are shown in the gray oval in the plot, indicate that there was great destruction to the ozone layer. They correlate with elevated aerosol levels in the atmosphere following the eruption of mount Pinatubo in 1991. When the stratospheric aerosols from the eruption reached the northern hemisphere and encountered colder temperatures, the result was greater ozone destruction. This is an example of the third type of ozone destruction on sulphate aerosols.

Another ozone event, Flynn said, focused on the ozone dropping off in the northern hemisphere, which is highlighted by the red oval in the upper right-hand corner of the plot. Flynn said that this was an unusual event during the northern hemisphere winter of 2019/2020 (NOAA Climate Prediction Center, 2020), the ozone hole type of chemistry that is mostly seen above the Antarctic in the Southern Hemisphere Spring—purple and pink regions between 60°S and 80°S—(the second type of ozone destruction) took place. There was enough isolated air to cause temperatures to fall low enough to create the conditions that formed a "mini" ozone hole in the Northern hemisphere. Because of mixing of the atmosphere and greater wave activity going on in the atmosphere in the northern hemisphere compared to the isolated polar vortex in the southern hemisphere over Antarctica, such low ozone events are rare in the Arctic.

OBSERVATIONS FROM OMPS

Satellite instruments provide comprehensive measurements of the ozone layer. The figure below, for example, helps show the set of information gained from a one-day snapshot from the OMPS' nadir mapper and limb profiler instruments. The figure shows a false-color map of total ozone over Antarctica. Flynn explained

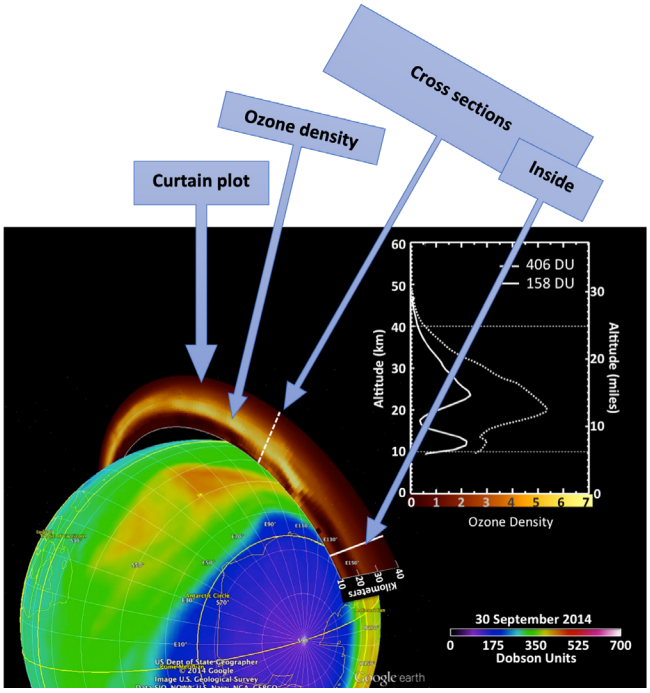

Figure from Colin Seftor SSAI for NASA GSFC.

that the blue region is at levels considered to be ozone hole conditions. He added that the figure also shows limb profiler retrievals of ozone profiles in a curtain plot. The curtain plot, he said, "is exaggerating how big the atmosphere is to show the profiles retrieved from the limb. The ozone density is given by different coloring." He continued to describe the figure in more detail, noting that it also shows one cross section for one particular retrieval inside the ozone hole (solid line), and another for one outside the ozone hole (dotted line). "Almost all of the ozone in the 15 to 20 km range has been destroyed for the profile inside the ozone hole region," he says.

From the figure, we see the ozone column amounts from 400 Dobson units to about 150 Dobson units. To put this in perspective, Flynn gives an example of what 300 Dobson units would look like if it was collected from the full atmosphere and brought down to sea level. He says if it was all isolated out of the atmosphere and brought down to standard temperature, the layer would be about the height of a pile of three dimes. The ozone layer that protects us from harmful UV radiation is a very small component of the total atmosphere.

TREND MODELS AND STUDIES

The figure below is a schematic showing the success of the Montreal Protocol and additional amendments in controlling the production and release of ozone depleting substances. It converts the different chemicals to similar units based on how effective the different compounds are in destroying ozone. Below are some of Dr. Flynn's takeaways from the figure:

1. Starting in the 1960s and 1970s, manmade releases of ODS increased at a rapid pace.
2. Beginning in the 1990s we begin to see some lessening in the growth of the ODS in the stratosphere in response to the limits on their production in the Montreal Protocol and amendments.
3. Since these ODS have long lifetimes in the atmosphere, and can be released from old equipment, the values do fall as quickly as one might expect given the reductions in

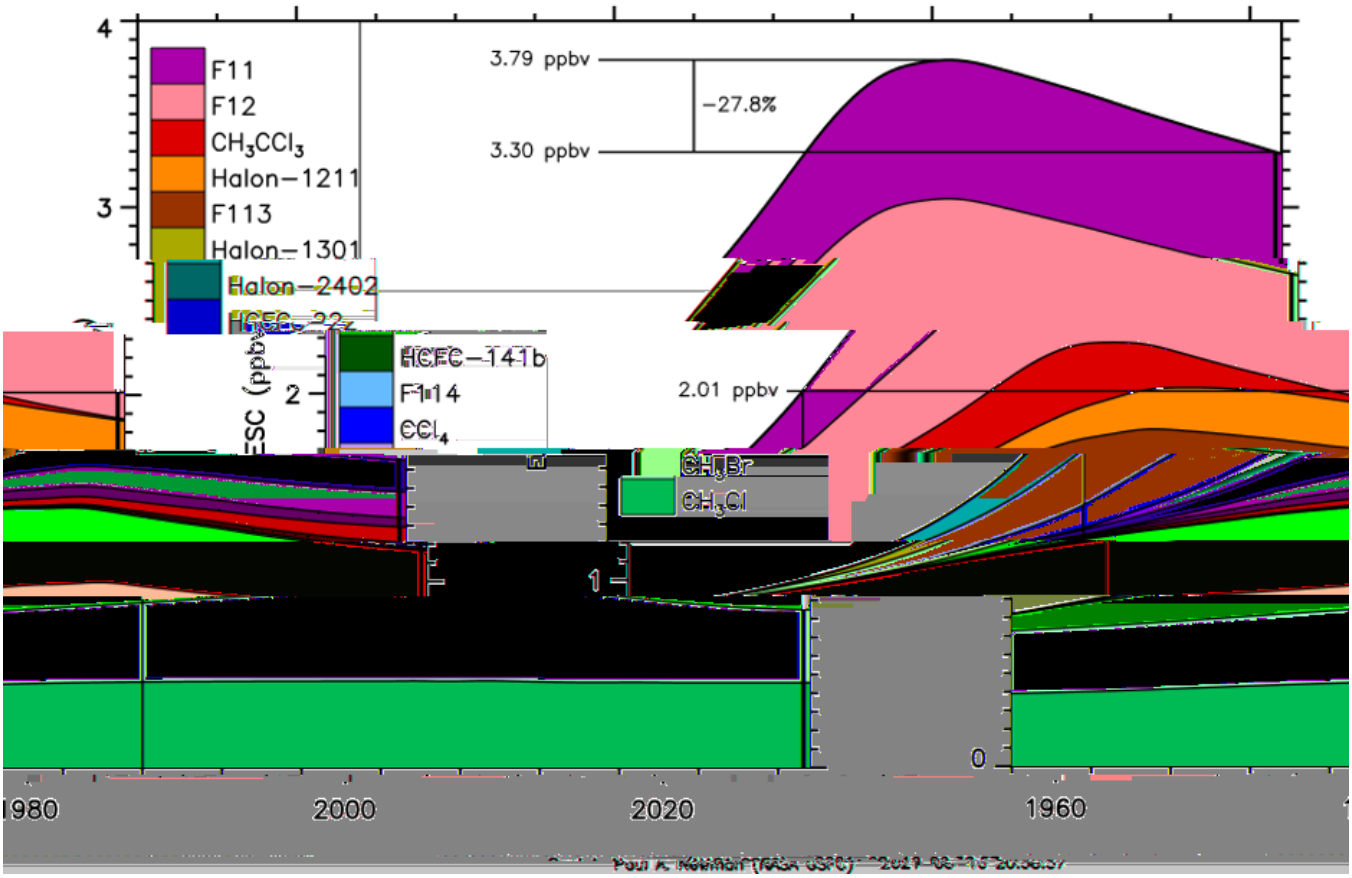

production. Even so, the peak ozone net ozone destruction potential for the ODS peaked around the year 2000.

4. The slope of the decline is not anywhere as big as the slope of its increase. This is because these compounds are fairly stable. Natural degradation does not destroy them easily—it takes a long time.

5. The cumulative levels of ODS over time are consistent with the ozone anomalies in the "1,000 Words" figure. Ozone depletion increased during the 1980s, 1990s and began to turnaround at the start of the 21st century. Even so, the atmospheric levels since the maximum have only returned approximately 1/4 of the way back (~27.8%) to the levels in 1980. This means that we will have ozone holes and ozone depletion with us for several more decades.

SUMMARY AND FUTURE WORK

Since coming on the scene, Earth observation satellites have produced data and imagery, which have provided valuable insights of our planet. They have revolutionized many remote sensing applications including in weather prediction and environmental hazard prediction. Moreover, their long-term data of the Earth's surface including the land and oceans as well as its atmosphere have contributed greatly to the scientific understanding of changes in climate. For example, long-term data from various satellite instruments have helped scientists discover the ozone chemistry for all three mechanisms of ozone destruction.

Dr. Flynn continues to do his part in using satellite data to monitor, and understand the ozone layer, and evaluate its recovery. Presently, he says he "is hard at work extending and validating ozone climate data records for use in the WMO 2022 Ozone Assessment." And for interested readers, he recommends that they take a look at the Executive Summary and Twenty Questions components of the latest report at https://csl.noaa.gov/assessments/ozone/2018/ for more details on ozone trends and the state of the ozone layer. ❖

Story Source

Materials obtained from JPSS August Science Seminar titled "Monitoring the Recovery of the Ozone Layer."

References

L. Flynn, et al., "Performance of the Ozone Mapping and Profiler Suite (OMPS) products", J. Geophys. Res. Atmos., 119(10), 6181-6195 (2014) https://doi:10.1002/2013JD020467.

Molina, M., Rowland, F. Stratospheric sink for chlorofluoromethanes: chlorine atom-catalysed. destruction of ozone. Nature 249, 810–812 (1974). https://doi.org/10.1038/249810a0

Hofmann, D.J., Solomon, S., 1989. Ozone destruction through heterogeneous chemistry following the eruption of El Chichon. J. Geophys. Res., 94, 5029-5041. https://agupubs.onlinelibrary.wiley.com/doi/abs/10.1029/JD094iD04p05029.

NOAA Climate Prediction Center, April 21, 2020. "Spring 2020 brings rare ozone "hole" to the Arctic." https://ww8B5 ozone

GLOBAL TEMPERATURE:

THROUGH THE LOOKING GLASS OF THREE SATELLITE MICROWAVE SOUNDER GENERATIONS

The information in this article is based, in part, on the September 29, 2021, JPSS science seminar presented by Cheng-Zhi Zou of NOAA/STAR with contributions from the University of Maryland's Hui Xu and Xianjun Hao, and University of Washington's Qiang Fu.

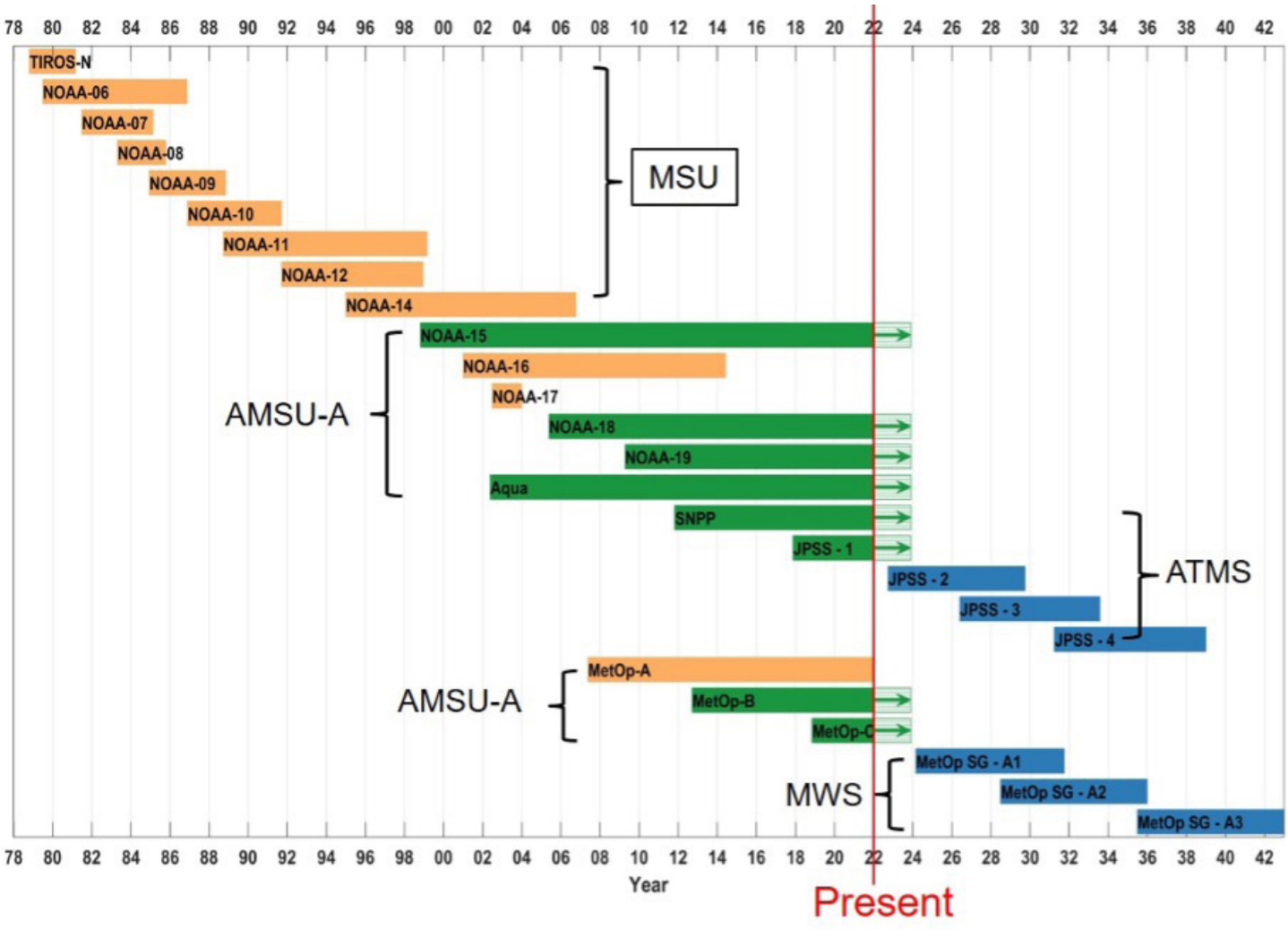

Figure above: Plot showing satellites and instruments used in CDR development. Orange: Decommissioned; Green: Currently operational; Blue: Future satellites.

Temperatures from the Earth's surface to the upper stratosphere are essential climate variables in the Global Climate Observing System (GCOS/WMO 2010). Changes in these temperatures provide clues on the Earth's changing climate for both short-term events and long-term trends. The long-term surface and tropospheric warming trends and stratospheric cooling trends are both indicators of human-induced global climate changes. It is critical to measure the atmospheric temperature profile and its long-term changes from the surface to the upper stratosphere for a complete monitoring and understanding of the global climate changes.

El Niño events in two- to three-year cycles cause global temperature anomalies on the surface and in the troposphere, which affects regional precipitation and flooding. Spikes in stratospheric temperatures lasting about two years occur in response to volcanic eruptions (Hansen et al. 1978). Solar cycle causes decadal variability in the upper stratospheric temperature time series (Randel et al. 2009). Increasing carbon dioxide and other greenhouse gases in the atmosphere cause warming trends on the surface and in the troposphere. However, the same increasing carbon dioxide causes cooling trends in the stratosphere (Manabe and Wetherald 1967, Zou and Qian 2016).

Scientists use various tools to study the Earth's climate and its changes. Among these are airborne, spaceborne, land and the ocean surface observations from airplanes, satellites, ground instruments, ships, buoys, etc. Data from NOAA observing systems in space and on the ground are used along with other climate-related data from NOAA and its

partners to construct long-term records and provide information on climate variability and trends on scales that run the spectrum from local to global. Some recorded observations, for example, the surface temperature, go as far back as the late 1800s, while others, such as records from the space age, span a much shorter period. Still, space borne sensors "provide the only means available to measure global temperatures from the surface and troposphere to the stratosphere," says NOAA scientist, Dr. Cheng-Zhi Zou. Dr. Zou is a satellite climatologist with the NOAA/Center for Satellite Applications and Research, working on the development of the satellite-based temperature data record and has used the data for climate trend monitoring for nearly 20 years.

The satellite record includes observations—covering over four decades—from three generations of microwave sounders onboard polar orbiting satellites from the National Oceanic and Atmospheric Administration (NOAA), the National Aeronautics and Space Administration (NASA), and the European series of Meteorological Operational satellites (MetOp). The instruments include Microwave Sounding Units (MSUs) that were onboard TIROS-N to NOAA-14 from 1978 to 2006, Advanced Microwave Sounding Units (AMSUs), for example AMSU-A onboard NOAA-15 to NOAA-19, NASA Aqua and MetOp series, and the current generation's Advanced Technology Microwave Sounders (ATMS) onboard the Suomi National Polar-orbiting Partnership (Suomi NPP) and NOAA-20 satellites in the Joint Polar Satellite System (JPSS). These instruments have provided observations, which while primarily for weather, due to their continuity and global coverage, have generated Climate Data Records (CDRs), which according to Zou "are widely used for climate change monitoring and to support national and international climate change assessments such as the Intergovernmental Panel on Climate Change (IPCC) and climate reports such as the annual Bulletin of the American Meteorological Society (BAMS)."

SATELLITE GENERATIONS: WHY DO THEY MATTER?

According to Dr. Zou, there are two key ingredients needed to develop a CDR for long-term monitoring, inter-satellite calibration and satellite merging. However, several factors can impact this development, including significant changes in instrumentation and technology, observing system biases, satellite orbital drift, system calibration, degraded sensors, etc., and therein lies the challenge.

Channels

According to Zou, MSUs had a total of four channels (50.30, 53.74, 54.96, and 57.95 GHz), but only one—the 57.95 GHz was designed to measure temperatures in the lower stratosphere. He says the nadir view brightness temperatures of channels two, three and four on MSU represent temperatures of the mid-troposphere (TMT), upper-troposphere (TUT), and lower-stratosphere (TLS). AMSU-A has 15 channels from the surface to the upper stratosphere; Its channel five is the companion channel for MSU channel two, while channel six on the 22 channel ATMS is the companion channel for channel five on AMSU-A, as their channel frequencies are identical. His talk focused on the mid-troposphere, and more specifically, channel two on the MSU and its companion channels on AMSU-A and ATMS.

AMSUs such as AMSU-A onboard NOAA-15 to NOAA-19, Aqua and MetOp series, replaced MSUs since 1998. AMSU was followed by ATMS, the third and current generation onboard the Suomi National Polar-orbiting Partnership (Suomi NPP) and NOAA-20 satellites in the Joint Polar Satellite System (JPSS).

Scanning Patterns

Aside from channels, Zou said that the three satellite generations also differed in their scanning patterns. At 11, the MSU had the fewest scan positions per scanline along with a beam width of 7.5° and nadir view resolution of 110 km, while AMSU-A has 30 scan positions per scanline, with a beam width of 3.33° and

nadir view resolution of 45 km. Whereas ATMS has 96 scan positions per scanline with a beam width of 2.2° and nadir view resolution of 31 km for temperature sounding channels.

To develop CDRs from different sensors with different scanning patterns, swath radiance data were converted into gridded data with 2.5° by 2.5° latitude/longitude resolution for each sensor. This allows consistent merging across different sensors with different scanning patterns within the same gridded format. In addition, a limb-adjustment needed to be conducted in which radiances at off-nadir view angles were adjusted to those at the nadir direction. This adjustment allows use of the off-nadir footprints in the same way as the nadir observations to increase observational samples and reduce noise and sampling-related biases in CDR development. Simulations from the Community Radiative Transfer Model (CRTM) developed by the NOAA/Center for Satellite Applications and Research (STAR) were used to derive the limb-adjustment.

Orbital Drift

NOAA satellites before NOAA-19 had all incurred orbital drift with satellite aging caused by constant gravitational attraction from Earth. Satellite orbital drifts cause changes in local observation time, or so-called diurnal sampling drifting effect. The temperature diurnal differences due to different observation times can become aliased with the long-term satellite time series, causing spurious trends in the merged satellite observations. Its effect is particularly large for TMT over land where diurnal amplitude is large.

Techniques for removing the diurnal drift biases were to adjust the scene brightness temperatures at different observation times from all different satellites to a common local time before satellite merging. The diurnal anomaly used for such an adjustment is a function of time and geolocation, which was accomplished by developing an accurate physical model to represent the diurnal anomalies.

Degraded sensors

As an example, for more than 20 years, NOAA-15 has orbited the Earth from 520 miles above Earth, 14 times daily and is operational to present day. However, Zou says, data quality problems manifested as a large non-climate seasonal variability in radiances have occurred since 2016 due to sensor degradation (see lines for before recalibration in figure below). Large calibration drifts in NOAA-15 were also found throughout its observational period, he says, and for many other legacy POES satellites.

To use these satellites in CDR development, recalibration and reprocessing are needed to remove the calibration drifting errors and minimize instrument temperature signals in these observations.

—Cheng-Zhi Zou

Recalibration, in older satellites, such as NOAA-15 as well as other legacy satellites, can largely remove calibration drifting errors to make them more consistent with each other for satellite merging (see results for after recalibration in the figure below). But still, after 2018, the quality of the NOAA-15 data was degraded to the extent that it could not be mitigated by recalibration and reprocessing. Therefore, the NOAA-15 data after 2018, he says, are not useful for climate studies and excluded from the CDR development (as shown in the figure below). Zou notes that such recalibration and quality control needs to be conducted for each legacy satellite to ensure that the final CDR use data of good quality and without calibration drifting errors.

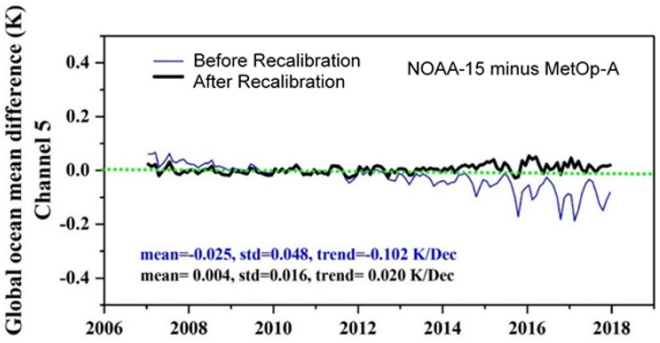

Figure showing Global mean inter-satellite differences between NOAA-15 and MetOp-A for before and after recalibration.

DEVELOPMENT OF REFERENCE CDR USING ATMS AND AMSU-A MICROWAVE SOUNDERS

Satellite microwave sounders measure brightness temperatures (BTs) which have seasonal cycles in them. In climate change studies, these seasonal cycles appear as noise and have to be filtered out. Zou says the seasonal cycles are removed by treating the original BT time series with a yearly mean seasonal climatology, which creates an anomaly time series that is used to calculate climate trends. The panels shown below give examples of the BT and its anomaly time series. His discussion focused on anomaly time series.

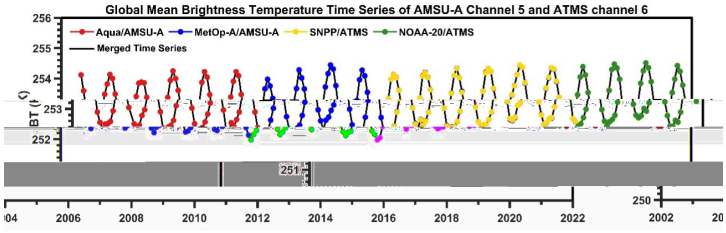

Figure showing Brightness Temperature Time Series Measured by AMSU-A/ATMS channels. The data periods used in the plot are 08/2002–12/2009 for Aqua, 01/2008–12/2017 for MetOp-A, 01/2012–10/2021 for S-NPP,and 01/2018–10/2021 for NOAA-20. Earlier satellites were overlaid by the later satellites during their overlapping periods.

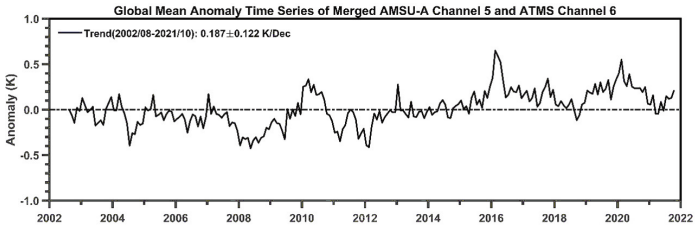

Figure showing Deseasonalized BT anomaly time series from the AMSU-A/ATMS channels.

Just as satellite instruments vary, so do the approaches that are used to create the datasets. For example, several datasets including NOAA/STAR, Remote Sensing Systems (RSS), and University of Alabama at Huntsville (UAH), as well as the University of Washington (UW), which only produces TMT over the Tropics, use what is known as a forward merging approach. With this approach, the record begins with datasets from MSU and extends to AMSU-A. Another approach, which Dr. Zou and his colleagues are exploring, is referred to as backward merging. With this approach, he says, the POES microwave sounder CDR will start with the most recent microwave instrument, in this case, ATMS, and extend backward to MSU. The backward merging approach uses the recent ATMS observations as an anchor (reference) because it has high radiometric stability, and then adjusts and merges the earlier satellites, which had lower radiometric stability, to the reference. Such an approach removes calibration drifting errors in legacy satellites and produces a CDR with high accuracy in trend detection. For example, the total trend from 1979 to present from the backward merging approach is much more accurate than the earlier versions of the CDRs, providing high confidence for the datasets to be used in climate change monitoring and verifying climate model simulations.

Radiometric Stability in Microwave Sounder Observations

Zou says that there are several things to consider prior to merging a record. One of these is establishing the radiometric stability of the sensors whose records are to be merged. This, he explains, is because measurement stability is the primary requirement for climate change detection. But this is not a trivial task since, for most POES satellites, calibration drifting errors had mixed with orbital drifts. This error mixing had prohibited a clear definition and evaluation of radiometric stability. In 2018, Zou and his colleagues evaluated radiometric stability for satellite microwave sounders only in stable Sun-synchronous orbits, including the Suomi NPP/ATMS, Aqua/AMSU-A, and MetOp-A/AMSU-A (Zou et al. 2018). Because there were no orbital drifts for satellites in stable orbits, Zou and his colleagues were able to determine that these satellite microwave sounder observations had achieved a high radiometric stability of 0.04K/decade. Once these satellites are merged together, the accuracy in trend detection in the merged time series is even higher, achieving 0.01K/Decade (Zou et al. 2021). He says that according to the Global Climate Observing System (GCOS)—an organization that aspires for accurate and sustained climate observations, and free and open access to climate data—the

required accuracy in trend detection for the merged time series: 0.02K/Decade (GCOS, 2016). Because the accuracy in trend detection in the merged time series with sensors in stable orbits is higher than the GCOS requirement, the time series qualified their use as reference observations. He explained that to date, he and his colleagues have developed a reference temperature mid-troposphere (RFTMT) CDR stretching back to 2002 using satellites in stable orbits with an accuracy of 0.01K/Dec in trend Development of CDR from the Earliest MSU to the Recent ATMS.

With the RFTMT developed for 2002 to present, a few more steps were conducted by Zou and his colleagues to complete a CDR dataset covering the entire period of satellite microwave sounder observations from late 1978 to present, spanning three generations of microwave sounders.

Recalibrate MSU/AMSU satellites to remove calibration drifting errors: The team developed an Integrated Microwave Inter-Calibration Approach (IMICA) to remove calibration drifting errors in legacy satellites. The IMICA method used simultaneous nadir overpass matchups between satellite pairs and global mean differences to derive optimal and accurate instrument calibration coefficients. The optimal calibration coefficients derived from the IMICA method resulted in consistent level-1 radiances across satellites, which helps to generate a consistent satellite merging for high accuracy in trend detection.

Removing viewing angle differences: Limb-adjustment was implemented to adjust observations at off-nadir view angles to those at the nadir direction. Simulations from the Community Radiative Transfer Model were used to derive the limb-adjustment, which was the CRTM simulated differences for each scan position between those with off-nadir and zero scan angles. Off-nadir biases were only in the range of 0.1 K after limb-adjustment, compared to nearly 10 K before the limb-adjustment.

Removing channel frequency differences: The frequency adjustment was based on CRTM simulations where adjustments were simulated differences between those with channel frequency inputs taken from the AMSU-A and MSU, respectively. The simulation was for each scan position for the NOAA-14 MSU channel 2 using NASA MERRA2 reanalysis as inputs. After the adjustment, MSU channel 2 observations for NOAA-14 to TIROS-N became equivalent AMSU-A channel 5 observations.

Removing diurnal sampling drifting errors: Zou and his colleagues developed an observational-based physical model to remove diurnal sampling drifting errors. The physical model used cosine function to accurately represent diurnal cycles in the atmospheric temperature. Diurnal sampling drifting errors were assumed to be proportional to cosine of the satellite orbital drifts. The magnitudes and phases of the cosine diurnal cycles were obtained using satellite overlapping observations. Application of such a physical model largely removed the diurnal drifting errors for all satellites.

Removing instrument blackbody temperature effect: A blackbody warm target was used to calibrate the MSU and AMSU-A raw counts observations to obtain level-1 radiances. The warm target temperature was measured by the Platinum Resistance Thermometer embedded on the blackbody. This temperature incurred a large seasonal variability and long-term trends for most MSU and earlier AMSU-A satellites due to solar heating on the instrument that were correlated to seasonal and long-term changes in satellite solar angles (Zou and Wang 2011). These variability and trends were mostly removed by the recalibration procedure with the IMICA approach. However, small residual variability and biases still exist due to imperfect calibration. These small residual biases need to be further removed before satellite merging. Christy et al. (2000) developed an empirical algorithm to remove the radiance errors due to this warm target effect. This approach finds a best fitting empirical relationship between the correction term and warm target temperatures and then removes the best fit from the unadjusted time series. After applications of this algorithm, warm target effects were removed for all legacy satellites.

Dealing with biases due to short overlaps: NOAA-9 and NOAA-10 had only 3 months of overlaps. Since their overlap did not cover a full annual cycle, mismatches in seasonal cycles between the two satellites caused by instrument anomalies could largely affect merging accuracy. To overcome the problem, the team developed an algorithm to merge the two satellites in the anomaly time series and to consider long-term trends of both satellites during the merging. Such an approach had avoided the impact of seasonal cycles on the merging accuracy and achieved a best merging for the two satellites.

Stratospheric Cooling Adjustments: TMT has a significant weight from the lower stratosphere and its contribution to the TMT trend needs to be corrected to derive the real tropospheric temperature trend. The lower stratospheric contribution can be removed by using the lower-stratospheric temperature (TLS) time series observed by the MSU channel four (Fu et al. 2004; Fu and Johanson, 2005). Based on the characteristics of their weighting functions, TMT and TLS were combined together to provide an adjusted mid-tropospheric temperature time series which accurately removed the stratospheric cooling effect in TMT.

Mid-Tropospheric Temperature Trends from the Newly Developed STAR V5.0 Dataset

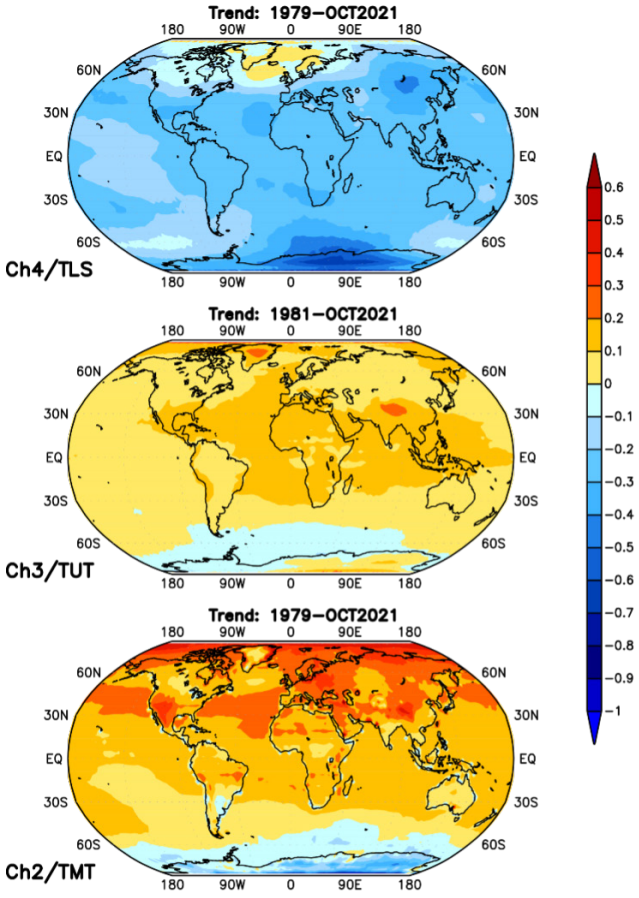

Spatial trend patterns from NOAA/STAR MSU/AMSU-A Version 3.0 monthly gridded time series for layer temperatures of mid-troposphere (TMT), upper-troposphere (TUT), and lower-stratosphere (TLS) for 1979 to Oct 2021.

WHY IS THIS RELEVANT?

Global warming has two major indicators: warming trends at the Earth's surface and troposphere and cooling trends in the stratosphere. Fossil fuel burning emits greenhouse gases into the atmosphere, including the troposphere and stratosphere. Increasing greenhouse gases in the troposphere absorb more radiation emitted by the surface and then emit it back to the surface, trapping the energy within the surface and tropospheric layers. This is the so-called greenhouse effect that causes the warming trends at the surface and troposphere. In contrast, increasing greenhouse gases in the stratosphere emit more radiation to the outer space and thus causes net energy loss in the stratosphere. This energy loss results in a stratospheric cooling trend. In addition, ozone depletion in the stratosphere results in less absorption of the solar ultraviolet radiation, which also causes a cooling trend in the stratosphere. These are well-known predictions from human-induced global warming theory based on climate modeling physics (Manabe and Wetherald 1967). The global TMT and TLS observations from the satellite microwave sounders and upper-stratospheric temperature observations from the Stratospheric Sounding Unit (SSU, Zou and Qian 2016) are unique datasets that can provide verifications on the human-induced global warming theory (Snater 2019).

Zou says that the climate trend in the layer from the surface to about 10 km above from 1979 to present is 0.15°/Dec, based on the newly developed STAR V5.0 TMT dataset.

This trend translates to a total warming of 0.63K during the past 42 years from 1979 to present. The IPCC recommends limiting the global warming to be within 1.5°C above the pre-industrial level for sustained economic and social activities. With the added warming of 0.63°C during the last 42 years, global warming appears to be approaching the IPCC suggested threshold level. In addition, this total warming is associated with smaller warming during the first half and larger warming during the latter half of the whole period, suggesting that tropospheric warming is accelerating. The figure shown in the previous page, on the left (https://www.star.nesdis.noaa.gov/smcd/emb/mscat/) shows how trends of TMT, TUT, and TLS distribute over the globe. These plots are from an early version of the STAR datasets. They will be updated by STAR Version 5.0 when TUT and TLS are all completed.

SUMMARY AND PERSPECTIVE

Three generations of satellite microwave sounders have provided more than 40 years of atmospheric temperature observations. Although these instruments were designed primarily for weather observations, due to their continuity and global coverage, together they are the basis for an indispensable long-term and high-quality global climate data record (CDR) in support of the climate research communities as well as service providers and users to monitor historical atmospheric temperature changes. To make these observations as CDRs for climate change monitoring, inter-satellite calibration and reprocessing are needed to remove instrument bias and drifting errors arise from instrument degradation and satellite orbital drifts. In these aspects, Zou and his colleagues developed STAR V5.0 TMT CDR from 1979 to present using a backward merging approach with RFTMT as a reference. Such an approach allows the CDR to inherit the high radiometric stability in the newest generation of satellite microwave sounders and achieve high accuracy in trend detection for the entire observation period.

Looking ahead, Dr. Zou and his team will use the backward merging method to develop merged MSU, AMSU, and ATMS temperatures of the upper-troposphere (TUT) and lower-stratosphere (TLS) CDRs. Furthermore, the team will extend the method to develop merged SSU, AMSU, and ATMS temperatures of mid-stratosphere (TMS), upper-stratosphere (TUS), and top-stratosphere (TTS) CDRs. This bundle of CDRs will provide global temperature trend monitoring from the lower troposphere all the way to the upper stratosphere spanning the period from 1979 to present. These CDRs bring benefits for the users from the National and international climate assessment programs (i.e., IPCC, WCRP), climate modelers, and satellite cal/val programs that can use the CDRs as reference. Zou says the most important benefit of these CDRs is they can be used to verify global warming trends predicted by the climate modeling physics due to fossil fuel burning, which provides confidence on climate modeling physics and their guidance on climate change mitigation and adaptation policies. ❖

Story Source

Materials obtained from JPSS September Science Seminar titled “Extending the POES Microwave Sounder Climate Data Record with ATMS for Climate Change Monitoring.”

References

Christy, J. R., R. W. Spencer, W. D. Braswell, 2000. MSU tropospheric temperatures: Dataset construction and radiosonde comparisons. J. Atmos. Oceanic Technol. 17, 1153–1170.

Fu, Q., C. M. Johanson, S. G. Warren, D. J. Seidel, 2004. Contribution of stratospheric cooling to satellite-inferred tropospheric trends. Nature 429, 55–58.

Fu, Q., and C.M. Johanson, 2005. Satellite-derived vertical dependence of tropical tropospheric temperature trends. Geophys. Res. Lett., 32, L10703, doi:10.1029/2004GL022266.

GCOS/WMO, 2016. The Global Observing System for Climate: Implementation needs, GCOS- 200 (GOOS-214) (p. 341). Switzerland: World Meteorological Organization.

Hansen J. E. , W. C. Wang, A. A. Lacis, 1978. Mount Agung eruption provides test of aglobal climatic perturbation. Science, 199, 1065–1068.

Randel, W. J., and Coauthors, 2009. An update of observed stratospheric temperature trends. J. Geophys. Res., 114, D02107, doi:10.1029/2008JD010421.

WMO, 2010. Implementation plan for the global observing system for climate in support of the UNFCCC (2010 update). GCOS-138, GOOS-184, GTOS-76, WMO/TD-1523, 180 pp. [Available online at http://www.wmo.int/pages/prog/gcos/Publications/gcos-138.pdf.]

Zou, C.-Z. and W. Wang, 2011. Inter-satellite calibration of AMSU-A observations for weather and climate applications, J. Geophys. Res., Vol. 116, D23113, DOI:10.1029/2011JD016205

Zou, C.-Z., and H. Qian, 2016. Stratospheric Temperature Climate Data Record from Merged SSU and AMSU-A Observations, J. Atmos. Oceanic Technol., Vol. 33, 1967-1984, doi:10.1175/JTECH-D-16-0018.1.

Zou, C.-Z., M. Goldberg, and X. Hao, 2018. New generation of U.S. satellite microwave sounder achieves high radiometric stability performance for reliable climate change detection, Science Advances, 4(10), eaau0049, doi: 10.1126/sciadv.aau0049.

Zou, C.-Z., Xu, H., Hao, X., & Fu, Q., 2021. Post-millennium atmospheric temperature trends observed from satellites in stable orbits. Geophysical Research Letters, 48, e2021GL093291. https://doi.org/10.1029/2021GL093291

Santer, B, C Bonfils, Q Fu, J Fyfe, G Hegerl, C Mears, J Painter, et al. 2019. “Celebrating the Anniversary of Three Key Events in Climate Change Science.” Nature Climate Change 9(3): 180-182. https://doi.org/10.1038/s41558-019-0424-x.

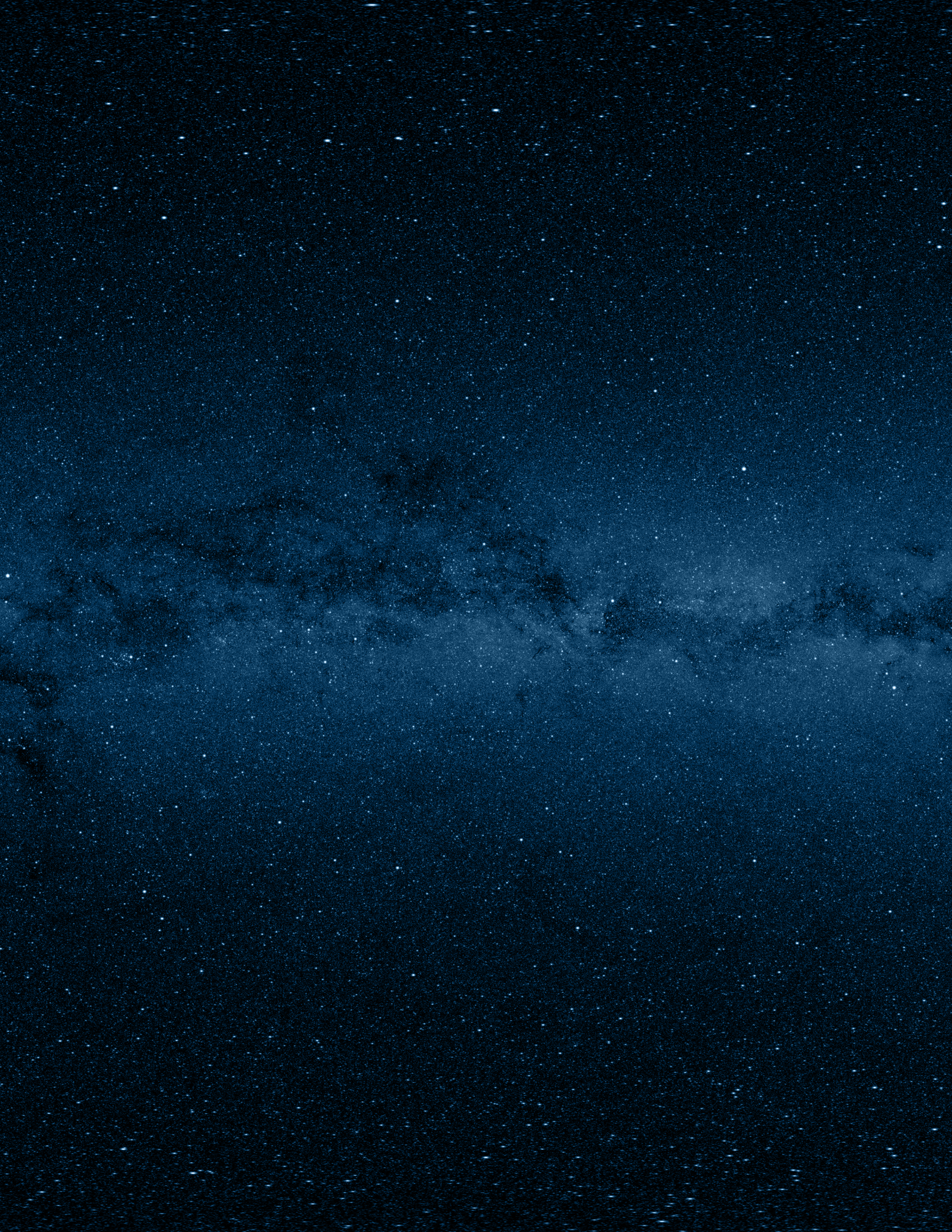

WEB FEATURES

WEB FEATURE: JANUARY 8, 2021

A MODEL THAT PREDICTS THE SPREAD OF WILDFIRE SMOKE BECOMES OPERATIONAL

Jenny Marder
Senior Science Writer, Joint Polar Satellite System
NASA Goddard Space Flight Center

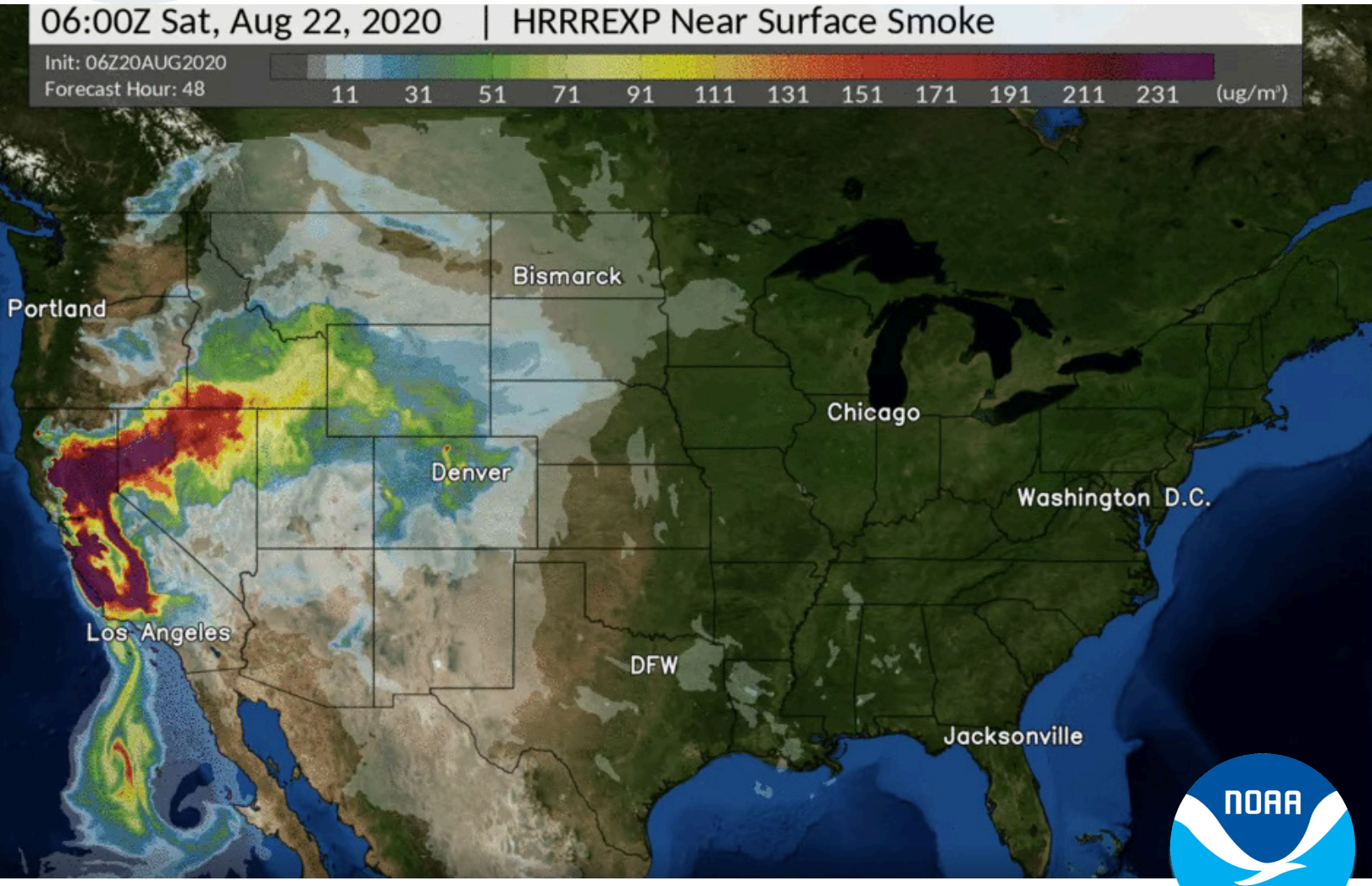

The near-surface smoke forecast for August 20–22, 2020, by HRRR-Smoke. The animation shows the heavy smoke transport from the wildfires in the western U.S. affecting air quality for millions of people around the country. Credit: NOAA Global Systems Laboratory.

A weather model that maps the height and thickness of wildfire smoke and predicts its movement has become operational at NOAA's National Centers for Environmental Prediction. HRRR-Smoke is the first weather forecast model in the U.S. to include smoke's impact on weather, and it has become a vital resource for fire crews, air traffic controllers, local forecasters, and even school administrators.

On September 9, San Francisco woke to eerie orange skies. Smoke from the massive August complex wildfire, which ultimately burned more than a million acres in Northern California, was choking the city, blocking out the sun and creating a dystopian gloom.

Bay Area residents anxious to know when the smoke would lift and when it would feel safer to go outside turned to their local forecasters who shared regular updates from a weather forecasting model called the High-Resolution Rapid Refresh Smoke model, or HRRR-Smoke.

During wildfires, first responders and air traffic controllers rely on HRRR-Smoke for visibility. Fire crews consult it when deciding where to pitch base camps or to stage resources. And after a fire passes through, EPA crew workers use it to determine whether the smoke has lifted enough to travel to burned areas to clean up hazardous waste.

HRRR-Smoke is the first weather forecast model in the U.S. to include smoke's impact on weather, and it has been operating experimentally out of NOAA's Global Systems Laboratory in Colorado since 2016. Earlier this month, after more than a year of rigorous testing, HRRR's smoke forecasting capabilities were transitioned to NOAA's National Centers for Environmental Prediction, where thousands of computer processors power a fleet of weather models. There, HRRR-smoke now runs around the clock, producing a new weather and smoke forecast every hour.

The model ingests real-time data from the NOAA-20 and Suomi-NPP satellites, as well as NASA's Terra and Aqua satellites. It relies on a metric called fire radiative power, which measures the amount of heat released by a fire in megawatts. The model also uses observations of wind speed, rain and atmospheric temperatures, and combines that with vegetation maps to incorporate what's burning. All of these measurements are mapped to a three-dimensional grid that extends nearly 12.5 miles into the atmosphere, producing detailed updates of the amount of smoke produced, the plume height and the direction the smoke is expected to move. It also provides forecasts up to 48 hours into the future.

Jeff McQueen, the air quality modeling team leader for the National Weather Service, said that when HRRR-Smoke first emerged, it surprised forecasters with its ability to provide local information on wildfire smoke at a resolution four times greater than what they were accustomed to with other weather models. HRRR-Smoke sees smoke at a spatial resolution of nearly 2 miles by 2 miles per pixel.

"It was kind of revolutionary the first time we saw smoke forecasts at that resolution," McQueen said. For the first time, he said, they were seeing how smoke interacted with sea breezes or with air flows east of the Rocky Mountains. "Before this product, smoke would get trapped against the mountains, and we'd miss the true impact of smoke stuck in the valleys," he said.

As weather drives the behavior of smoke, smoke in turn influences the weather. Smoke that's blocking incoming radiation can affect both wind speed and temperatures, said Mike Staudenmaier, division chief of the National Weather Service's Western Region Science and Technology Infusion Division.

"And it can be on the orders of several degrees of temperature differences," he said. "That's the exciting thing with this, it's showing how back and forth engagement between chemistry and atmospheric models can provide a more accurate forecast."

The recent move to NCEP operations means a more reliable dataset for users, Staudenmaier said.

"When something is experimental, we're at the whims of bandwidth, availability, that kind of thing," he said. "If a server or computer system goes belly up, that data is not available. Now that it's operational, it has a requirement to be available at least 99 percent of the time."

It will also free up Ravan Ahmadov and his coworkers to separately focus on research and future updates. Ahmadov, a CIRES scientist working in the Global Systems Laboratory, is the main developer of HRRR-Smoke.

Ahmadov said his hope in future models is to better characterize and forecast the rapid changes in fire intensity, in part by bringing in new satellite data from the GOES-16 satellite and the future JPSS-2 satellite, which is slated to launch in 2022.

"Over the next several years, there will be two systems," Ahmadov said. "One is fully operational and won't change much. Another experimental system will be changing and improving." ❖

WEB FEATURE: MARCH 1, 2021

IN A FIRST FOR NESDIS, JPSS GROUND PROGRAM MOVES ITS DATA TO THE CLOUD

Jenny Marder
Senior Science Writer, Joint Polar Satellite System
NASA Goddard Space Flight Center

One of the JPSS program's system of ground stations is located in Norway's remote Svalbard islands. Antennas at the station here collect data from satellites as they fly over the North Pole. Credit: KSAT.

This month, NOAA's Joint Polar Satellite System shifted part of its operational data processing ground system to cloud computing. This makes the program the first of NOAA's National Environmental Satellite, Data, and Information Service (NESDIS) major ground systems to make this transition.

This new system will replace "racks and racks of computers" at the NOAA Satellite Operations Facility, or NSOF, in Suitland, MD. In the previous system, raw data collected from the satellite instruments and received through a system of antennas was then consolidated at NSOF, where it was processed into data products that are used by scientists and assimilated into weather prediction models.

Now, data will instead be processed in the Amazon Web Services GovCloud. The transition has reduced the JPSS footprint of hardware at NSOF and the NOAA Consolidated Back-Up (CBU) facility in West Virginia by 40 percent, said Heather Kilcoyne, JPSS Ground Segment Project Manager.

Each day, the JPSS satellites receive about 400 gigabytes and deliver more than seven terabytes of data to customers.

For NESDIS, this marks the first time the agency has taken a mission operations function at a high security level, and moved it to the cloud, said Irene Parker, Chief Information Officer for NESDIS. “That’s huge for us,” she said.

And the move had to be done without any impact to availability or integrity, Parker said.

“It can’t ever go down, and we have to ensure our data stream is accurate, because if it’s not accurate, lives and property can be damaged.” The transition, she added, “has been seamless to the user community. That was one of the key goals.”

This move by JPSS is the first step in a bigger vision for NESDIS, which plans to shift the bulk of its ground systems to cloud computing. That will include data processing, distribution and archive of ground operations—nearly all but the actual commanding of the satellites.

The move to cloud has a number of benefits. Among them, significant long-term cost savings, flexibility to upgrade and faster deployment for science products, Kilcoyne said.

“We want to invest in mission capabilities rather than hardware,” she said. “And if we discover something new and find a better way to create one of our data products, deployment is easier in the cloud. You don’t have to physically install new hardware on the system and make sure it’s running correctly, you just start a parallel set of cloud services, deploy the updated software, and start testing.”

The transition was not without its challenges. The program was in a race to complete all testing, verification, and security measures on a tight two-year deadline, before the existing hardware, which was nearing the end of its lifetime, stopped working. Learning to use new technology and finding the best tools for the system without sacrificing processing speed or security meant a steep learning curve for the engineers on the 120-member team.

“Everybody worked extremely hard on this,” said Marge Ripley, the data product management and services lead for JPSS. “It took lots of long hours to pull it off. But we had a team that was willing to learn in order to pave the way.”

A collaboration between NOAA and NASA, JPSS is the United States’ most advanced series of polar-orbiting environmental satellites. It provides significant technological and scientific advancements for severe weather prediction and environmental monitoring. These data are critical to the timeliness and accuracy of forecasts three to seven days in advance of a severe weather event. ❖

WEB FEATURE: AUGUST 20 , 2021

HOW SATELLITE MAPS HELP PREVENT ANOTHER 'GREAT GRAIN ROBBERY'

Jenny Marder
Senior Science Writer, Joint Polar Satellite System
NASA Goddard Space Flight Center

Banner image: Left: Dr. Forrest Hall accepts a medal in 1978 for outstanding scientific achievement.

Mid-June in Utah usually marks the tail end of the most fertile time of year for crops. In a typical year, snowmelt in April and May wets the soil, resulting in a burst of blooming flowers and crop growth.

"Usually we have a beautiful, green landscape right now," said Dr. Jon Meyer, a research climatologist with the Utah Climate Center. "It's one of my favorite times of year because we get green for six weeks—and then we go back to brown for the rest of the year."

Not so this year. Drought has gripped the American West, and in Utah, more than 92 percent of the state meets the criteria for "extreme drought," fueled by what Dr. Meyer described as "a deadly combination of record heat and record dry." In a recent presentation on drought in the Southwest, Meyer showed a collection of grim indicators: high temperatures, little rainfall, low soil moisture, and finally, poor vegetative health.

This last indicator has become an important metric for climate scientists and meteorologists trying to understand how weather and temperature impact the health of crops, and as an extension, food security, food prices and the global agricultural market.

TRACKING CROP HEALTH

This week in the U.S., 216 million acres of crops are experiencing drought conditions and 76 million people are affected by drought, according to the National Integrated Drought Information System. Globally, more than 1 billion people, nearly one-sixth of the world's population, suffer from chronic hunger and malnutrition, and drought is a major factor.

NASA and National Oceanic and Atmospheric Administration (NOAA) scientists have spent decades developing tools to help state and government officials plan for drought and food shortages. One of them is the Vegetation Health Index, or VHI. Using data from the JPSS program's VIIRS instrument, first on the joint NASA-NOAA Suomi-NPP satellite and now on NOAA-20, the product shows crop health across the globe represented in color-coded maps. Green and blue indicate lush, healthy growth; red shows areas that are dry and sparse.

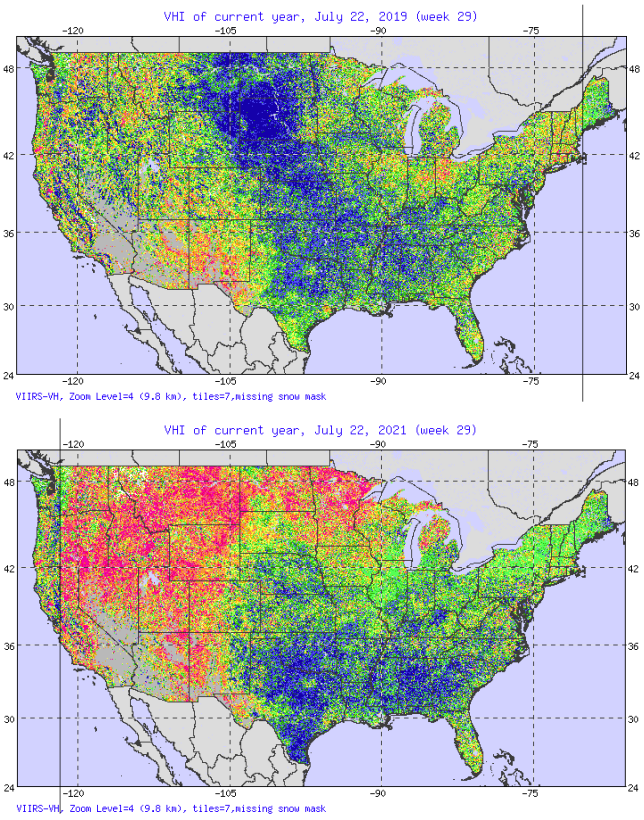

This Vegetation Health Index map from mid-August, 2021 shows how regions globally are being impacted by thermal, or heat stress. Credit: NOAA STAR Vegetation Health Index.

The Vegetation Health Index was created in the mid-1990s by a research scientist in NOAA's meteorology and climatology division named Dr. Felix Kogan. In the past decade, the number of people using this product has jumped from about 2,400 in 2010 to about 69,000 in 2020, Kogan said.

Laura Haskell of the Utah Division of Water Resources coordinates the state of Utah's official recommendation to the U.S. Drought Monitor map, which shows the drought status for each region of the United States, and plays an important role in decision-making involving agricultural reimbursements and other government assistance. Data from the Vegetation Health Index informs that recommendation, she said.

And it has a bigger role to play in what Eric Luebehusen, a meteorologist at the U.S. Department of Agriculture, calls "crop intelligence." The USDA has a small but mighty team of meteorologists engaged in a major effort to develop estimates of crop production in more than 120 growing regions, covering 35 countries. They do this for major row crops, such as corn, wheat, sunflowers, soybeans, barley, cotton and rapeseed—and they rely on the VHI to help create these yield estimates.

What's more, the research the VHI informs just might be protecting the price of your groceries. Knowing how crops are faring in other countries informs decisions about planting, food prices and foreign market exports, said Mark Brusberg, chief meteorologist for the USDA.

For example, said Brusberg, who monitors crops in Brazil, "if an area of the Southern Hemisphere is experiencing drought and there's going to be a shortage of corn, it might impact prices in the U.S. as well, and farmers might decide to plant more corn here."

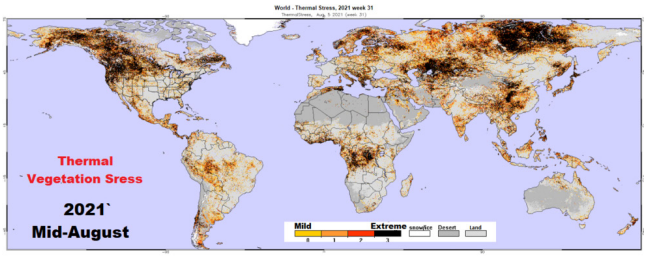

This Vegetation Health Index map from mid-August, 2021 shows how regions globally are being impacted by thermal, or heat stress. Credit: NOAA STAR Vegetation Health Index.

These estimates go into a monthly report that forecasts supply and demand for major crops called the World Agricultural Supply and Demand Estimates.

"The balance sheets maintained by the USDA that track production and trade not only help the market establish prices," Brusberg said, "but they also provide valuable information to U.S. producers for decision making at the farm and ranch level."

THE GREAT GRAIN ROBBERY

The need for crop intelligence dates back to 1972. In July of that year, the Soviet Union purchased 15 million tons of wheat, corn, soybeans and barley from the United States at low subsidized prices. Russia was experiencing severe drought and needed foreign grain. But the massive purchase, which took the United

States by surprise, depleted the country's grain stocks and caused wheat prices to soar, resulting in a domestic food crisis.

Later nicknamed The Great Grain Robbery by congressional leaders, the event highlighted the need for global agricultural monitoring, and it just happened to coincide with a satellite that could provide just that: NASA's Landsat 1.

Landsat 1 launched into space that same month, allowing for the first-ever view of drought and crop conditions from space. This convergence of events prompted NASA to team up with the U.S. Department of Agriculture (USDA) and NOAA to develop, in 1974, the first satellite crop production forecast: The Large Area Crop Inventory Experiment, or LACIE.

Dr. Forrest Hall was a project scientist for LACIE at NASA's Johnson Space Center, and one of LACIE's creators.

In the early days of Landsat 1, Hall's team would print out gray-scale satellite maps of the world, tape them as a mosaic to the wall of the conference room and study them, drawing squares to locate fields. They trained algorithms to distinguish between the radiometric signatures of individual crops in the satellite data. Then they validated the maps themselves, tromping through corn, wheat and soybean fields in Ohio and Indiana to see if the crops were indeed growing as the models said.

It was a couple of years later that the LACIE program, an effort to provide global estimates of crop yields, began. This was considered a high-priority project by the U.S. government and the data highly sensitive. When they overestimated or underestimated, it showed up in the markets.

"We briefed President Ford at one point on the Russian wheat crop," Hall said.

It was an exciting time, Hall added, and a lot of work. "We spent a lot of hours away from our families."

Dr. Kogan was also well suited to the task of monitoring vegetation from space. He had been making crop predictions in the Soviet Union, using precipitation and temperature models. In fact, he correctly predicted in 1972 that the grain yield would be well under the amount needed to meet consumption needs. He moved to the United States because he wanted to do similar work, but globally, and incorporate data from satellites.

As the years passed and more satellites launched, the ability to do this kind of agricultural monitoring became increasingly important and vegetation health products increasingly advanced.

OBSERVING CROPS AS THEY GROW

Like other vegetation maps, Kogan's Vegetation Health Index uses a formula called Normalized Difference Vegetation Index, or NDVI. NDVI is calculated by measuring both the visible and near-infrared light that bounces off vegetation. Chlorophyll in a plant absorbs visible light but reflects near-infrared light. If the reflected radiation is greater in the near-infrared wavelengths than in the visible, then the vegetation in that particular pixel is likely to be greener and more lush.

But the VHI is unique in that it combines NDVI with temperature. Temperature gives insight into extreme heat or freezes that might damage crops. Because of this, VHI and other satellite-based indices also allow scientists to monitor different stages of the crops as they grow, which makes the resulting crop yield predictions more accurate.

Crops need certain ambient air temperatures for growth. Spring wheat, for example, needs a daily average temperature of at least 41 degrees Fahrenheit to grow, corn needs at least 50 degrees Fahrenheit, and cotton won't grow until the daily average is closer to 60 degrees.

In 2017, Luebehusen found that he could apply the VHI formula to the crop stage for a particular area in order to model the yield: corn in the silking stage in the Ukraine, for example. It was a game changer, he said.

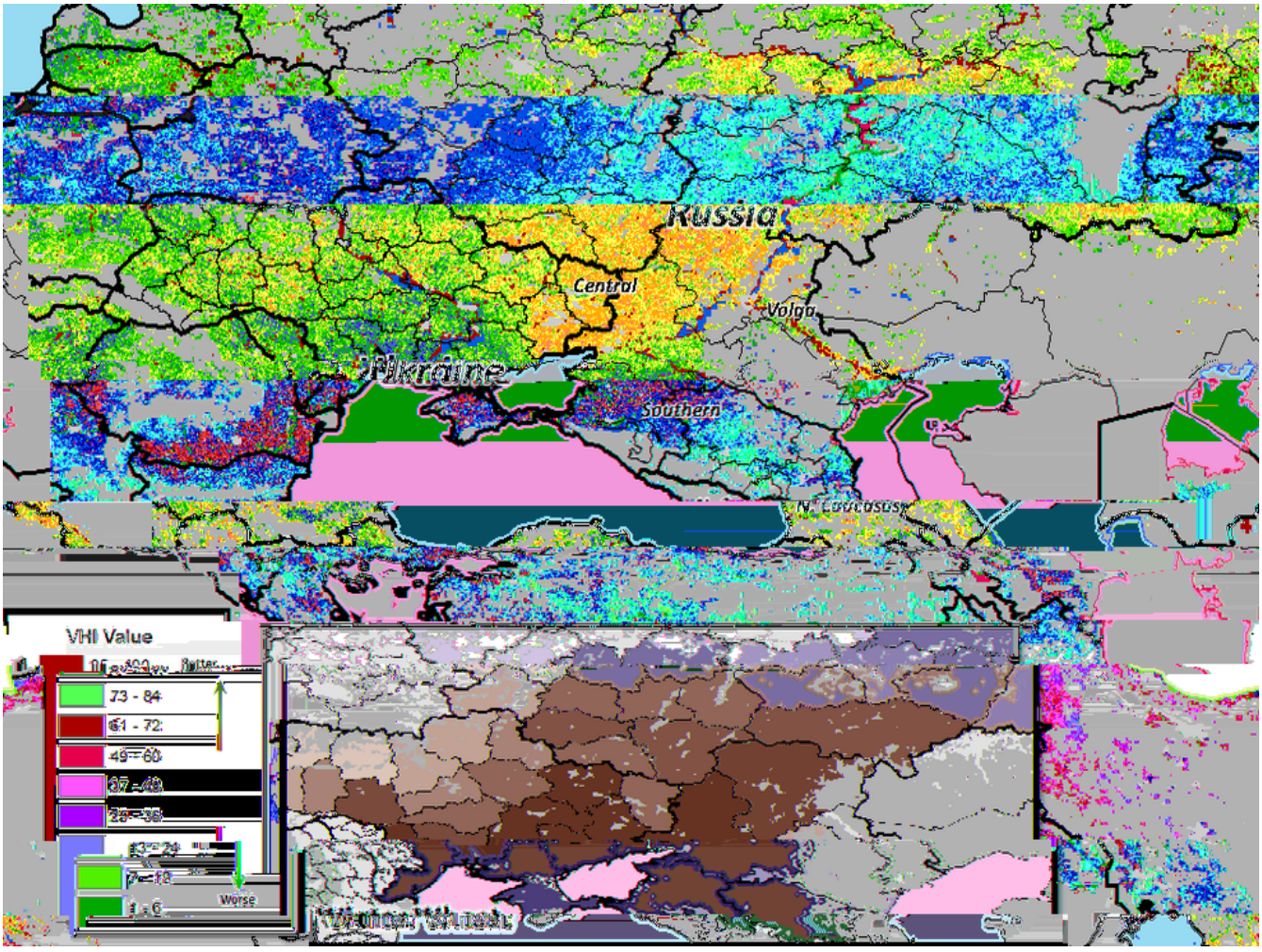

In Russia, lingering impacts from the Autumn drought on the winter wheat crop were evident in early Spring. This map shows the Vegetation Health Index in Russia on May 1, 2021. Credit: Agricultural Weather Assessments Group (USDA/OCE/World Agricultural Outlook Board).

"As long as you know when the crop was put in the ground, roughly, you can now estimate with a good degree of accuracy when the crop enters the key stages of development where weather matters the most," Luebehusen said.

From the early days of the LACIE program, these global yield estimates grew out of an important interagency partnership between NASA, NOAA and the USDA. This partnership continues with the VHI product, as NOAA and NASA work together to launch and build the next satellite that will carry the VIIRS instrument, JPSS-2, which is slated to launch in 2022.

"If we didn't have the VHI data, we'd be hosed," Luebehusen said. "It's become an integral part of our operations." ❖

Read on mobile.

Read online.
jpss.noaa.gov
or
repository.library.noaa.gov
DOI: 10.25923/4mpp-k509

JPSS.PROGRAM

JPSSPROGRAM